Potential Impact of Climate and Land Use Changes on the Water Resources of the upper Blue Nile Basin

Michael Menker Girma

Freie University of Berlin

6/19/2012

Department of Earth Sciences

Institute for Geographical Sciences, Physical Geography

Potential Impact of Climate and Land Use Changes on the Water Resources of the Upper Blue Nile Basin

A Dissertation

Submitted in fulfillment of the requirements for the degree of Dr. rer.nat to the Freie Universität Berlin

by

MICHAEL MENKER GIRMA

Berlin, June 2012

Supervisor: Univ.-Prof. Dr. Brigitta Schütt

Second examiner: Jun.-Prof. Dr. Wiebke Bebermeier

Date of the viva voce/defense: June 19, 2012

DEDICATION

This is dedicated to WUBET ZEWDU

ACKNOWLEDGEMENTS

I would like to thank my advisor Prof. Brigitta Schütt for her constructive comments and suggestions on the draft of this dissertation and for providing professional support and space during the whole period of the research. This research was supported by the Deutscher Akademischer Austauschdienst (DAAD) through a study grant. The field work was sponsored by the International Water Management Institute (IWMI) as part of its research project, Rethinking Water Storage for Climate Change Adaptation.

Dr. Seleshi Bekele, Dr. Matthew McCartney, and Dr. Fred Hatterman provided technical assistance during the implementation of this research project and deserve special thanks. I want to express my appreciation to Dr. Amare Haileslassie for his encouragement and cooperation in providing useful information for the research at the start of this research project.

I want to acknowledge the assistance of the Ethiopian Meteorological Agency, the Ethiopian Ministry of Water Resources, the Ethiopian Electric Power Corporation and the Potsdam Institute for Climate Impact Research (PIK) in providing data for the research.

I would like to express my appreciation to Pasquale Borelli, Maik Blättermann, Marlen Schlöffel, Zyliad and Steffen Schneider from Freie University of Berlin; Tobias Vater from PIK and Yordanos Abel from Berlin for their friendship and/or for their assistance while I was having personal difficulties in Germany. Solomon Bokasa from the Metahara sugar state and Tesfaye Dejene from the International Livestock Research Institute played significant role during the field work of this research project.

Finally special thanks go to Dr. med. Holger Mellerowicz from the Emil von Behring Krankenhaus, Berlin, Dr. Axel Panzer from the DRK-Kliniken Westend, Berlin, my wife Elsabeth Demissie and my daughter Hermela Michael. This PhD work wouldn't have been a reality without their kindness and unreserved assistance.

Michael Menker Girma

TABLE OF CONTENTS

Pages

LIST OF TABLES

Pages

LIST OF FIGURES

Pages

ACRONYMS AND ABBREVIATIONS

AOGCM	Coupled Atmosphere-Ocean GCM
CCLM	COSMO model in CLimate Mode
CRU	Climate Research Unit university of East Anglia
DKRZ	German Climate Computing Center
DWD	German Weather Service
ECHAM	Climate model developed by EC*MWF* at HAMburg
EM	Europa Model
ENSO	El Niño-Southern Oscillation
FAO	Food and Agriculture Organization of the United Nations
GCM	Global Climate Model
GRIB	GRIdded Binary
HadGEM2	Hadley Centre Global Environmental Model, version 2
IPCC	International Panel on Climate Change
IWMI	International Water Management Institute
MW	Mega Watt
MWR	Ministry of Water Resources of Ethiopia
NBI	Nile Basin Initiative
NCEP	National Center for Environment Prediction
NCAR	National Center for Atmospheric Research
NetCDF	Network Common Data Form
PIK	Potsdam Institute for Climate Impact Research
REMO	REgional atmosphere MOdel
SCS	Soil Conservation Service of United States Department of Agriculture
SDSM	Statistical Down Scaling Model
SRES	Special Report on Emission Scenarios
SWAT	Soil and Water Assessment Tool
UBN	Upper Blue Nile
UCAR	University Cooperation for Atmospheric Research

ABSTRACT

Potential Impact of Climate and Land-use Changes on the Water Resources of the upper Blue Nile basin

The upper Blue Nile basin is the major crop production area of Ethiopia with about 6 million hectares of cultivated land. It supplies surplus food to the national market. The basin contributes about 763 MW of hydroelectricity to the national grid at present. Additional 6000 MW of hydroelectricity is expected from the renaissance dam in the near future.

The major effect of climate change in the basin is through its effect on crop production and hydropower generation. The droughts of the 1960s, 70s and 80s have led to crop failure in the basin and the country at large and led to famine and death of several people and livestock. The recent droughts in 2008 and 2009 reduced water levels at many dams and caused below normal power generation and frequent blackouts. Expansion of large scale irrigation, upland area afforestation and expansion of private large scale irrigation schemes through foreign direct investment are the major land use changes expected. The objective of this study was to study the potential impact of climate and land use changes on the discharge of the upper Blue Nile River using climate change and formulated future land use change scenarios.

Statistical downscaling of climate change scenarios, bias correction of regionally downscaled climate change scenarios and hydrological modeling were used in this study. Statistical downscaling approach was used to downscale monthly rainfall at five stations in the basin using six downscaling domains. Predictors were synthesized based on correlation analysis between large scale climate predictors and observed station data (rainfall). Area averaged monthly predictors were used to establish a regression model between the predictors and observed rainfall from the five meteorological stations. The regression models were validated against observed station data and were used to generate downscaled future rainfall. Data for future scenario were extracted from the ECHAM5 A1B run.

Regional climate change projections of ECHAM5-A1B downscaled by the REMO and CCLM models were obtained and compared to observed climate. Raw REMO data was bias corrected using a probabilistic approach called CDF-transform. Bias corrected CCLM data was obtained from the Potsdam Institute for Climate Impact Research. Difference and ratios were used to bias correct temperature and rainfall. A future time land use change scenarios was developed in consultation with soil and water experts, review of project documents, discussion with small holder farmers, considering foreign direct investment and past trends.

The Soil and Water Assessment Tool (SWAT2009) was used to study the hydrological impact of climate and land use change. The model was calibrated and validated using measured stream flow measured at El Diem. The impacts for two future periods (i.e. 2041-2070 and 2071-2100) were obtained by running the calibrated model with climate and land use change scenarios.

The results of statistical downscaling of rainfall data showed a decrease in rainfall by 6-12% during the short rainy season in the basin but mixed results in the main rainy season. Future research in downscaling rainfall should consider different IPCC emission scenarios and use

of multiple GCMs. In addition the effect of domain size on model performance, uncertainties in the statistical downscaling and the data used should be evaluated.

Average annual projected runoff changes for the basin from the CCLM were 9.2% and -10.0% relative to the historical flow for 2041-2070 and 2071-2100 respectively. It showed consistent increase by 102.8% and 141.4% during the same period for REMO. Although there is some agreement on the direction of future runoff change, the discrepancy in the magnitude of change between the two downscaling models highlights the need for better understanding the uncertainties in downscaling. There is a need for further studies to better understand the reasons for contrasting results in the regional models in simulating rainfall.

Projected future land use change in the basin resulted in a decline in runoff by 1%. As the large size and complex hydrology of the basin might mask the effect on the runoff, it is recommended to carry out calibration of the hydrological model at sub basin level in order to capture the change in runoff as a result of land use change in the basin.

ZUSAMMENFASSUNG

DER POTENTIELLE EINFLUSS VON KLIMA- UND LANDNUTZUNGSWANDEL AUF DIE WASSERRESSOURCEN IM OBEREN BECKEN DES BLAUEN NILS

Das Obere Becken des Blauen Nils ist mit ca. sechs Millionen Hektar Anbaufläche Äthiopiens Hauptanbaugebiet für landwirtschaftliche Produkte. Der hier erzielte Produktionsüberschuss wird in den nationalen Markt eingebracht. Die Wasserkraftwerke des Beckens speisen bereits jetzt ca. 763 MW in das nationale Stromnetz ein; der im Bau befindliche Renaissance-Damm soll zukünftig weitere 6000 MW an hydroelektrischer Energie liefern.

Der Klimawandel wirkt sich im Becken insbesondere auf die Landwirtschaft und die Wasserkraftgewinnung aus. Die Trockenperioden der 1960er, 70er und 80er haben zu Ernteausfällen, Hungersnöten und dem Tod zahlreicher Menschen und Tiere geführt. Die Dürren der Jahre 2008 und 2009 hatten niedrige Pegelstände vieler Reservoirs zur Folge und damit einhergehend eine unterdurchschnittliche Energiegewinnung bis hin zu Stromausfällen. Die zunehmende Ausbreitung von großflächigen staatlichen und privaten Bewässerungssystemen, finanziert durch direkte Auslandsinvestitionen, sowie die Aufforstung von Hochlandbereichen sind die wichtigsten zu erwartenden Landnutzungsänderungen. Das Ziel der vorliegenden Untersuchung ist es, ausgehend von modellierten Szenarien, den potentiellen Einfluss von Klima- und Landnutzungswandel auf den Abfluss des Oberlaufs des Blauen Nils zu untersuchen.

In der vorliegenden Studie wurden Daten des globalen Klimawandelmodells ECHAM5 (Emissionsszenario A1B) zunächst durch downscaling auf regionale Maßstäbe heruntergerechnet und anschließend biaskorrigiert. Darauf basierend wurde eine hydrologische Modellierung durchgeführt. Der downscaling-Ansatz unter Verwendung von sechs downscaling domains wurde zur Berechnung der zukünftigen monatlichen Niederschläge von fünf bestehenden Messstationen im Oberen Becken des Blauen Nils herangezogen. Ein kombinierter Prädiktor wurde erstellt, resultierend aus einer Korrelationsanalyse zwischen den großmaßstäblichen Klimaprädiktoren des ECHAM5-Models und den regionalen Niederschlagsmesswerten der fünf meteorologischen Stationen. Flächengemittelte monatliche Prädiktoren fanden bei der Erstellung eines Regressionsmodells zwischen den Prädiktoren und dem an den fünf Messstationen gemessenen Niederschlag Anwendung. Die Regressionsmodelle wurden mit Messdaten validiert und durch downscaling für die Berechnung des zukünftigen Niederschlags verwendet.

CHAPTER 1 INTRODUCTION

1.1 Hydrological impact of climate and land use change in the upper Blue Nile basin

With the advent of Global Climate Models (GCMs) it is becoming increasingly possible for researchers to study the impact of projected climate change on water resources (Randall et al., 2007). Hydrological models require future projections of climate variables such as precipitation and temperature to simulate future flows. However, future projections from GCMs have a coarse spatial resolution (typically 2.5^{o}) and so cannot be used directly for hydrological modeling, which is usually performed at a catchment scale. Downscaling using dynamical and statistical approaches is commonly used to bypass the scale mismatch (Fowler et al., 2007).

Statistical downscaling is based on the view that the regional climate is conditioned by large scale climatic state and local physiographic features. Local climate information is derived by first determining a statistical model which relates large-scale climate variables (or "predictors") to local variables (or "predictands"). Then the large-scale output of a GCM simulation is fed into this statistical model to estimate the corresponding local and regional climate characteristics (Wilby et al., 2004). One of the primary advantages of these techniques is that they are computationally inexpensive and thus can be easily applied to output from different GCM experiments. Generally downscaling of climatic variables in the tropics is challenging, both because there is strong ocean atmosphere coupling and because the relationships between large scale predictors and local variables vary strongly within the annual cycle (Wilby et al., 2004). Due to these difficulties and the limited availability of long time series of observed and high resolution climate data, few downscaling models have been developed for the tropics.

Dynamical downscaling is preferred by many researchers over statistical downscaling because of the assumption of temporal stationarity in statistical downscaling. Statistical downscaling uses transfer functions validated under historical or present climate that may become invalid under future climate conditions (Wilby et al., 2004). Dynamical downscaling uses a high-resolution regional climate model (RCM) driven by boundary conditions from a GCM to produce higher resolution information. RCMs generally have a resolution of about

50 km (Rockel, 2008; Jacob, 2001) and incorporate model components such as terrain height and cloud physics. There is a need for a systematic assessment of current regional climate model outputs in order to establish a level of confidence in regional climate model simulations for impact assessment.

Changes in land cover and land use have significant impacts on the regional hydrology by affecting the amount of runoff, soil moisture and ground water recharge. In the upper Blue Nile basin changes in land cover and land use are expected through expansion of large scale irrigation following the tributaries of the upper Blue Nile particularly Beles, Koga, Fincha, Rib and Birr; upland area afforestation particularly near existing or proposed dam locations and expansion of private large scale irrigation schemes in the lowlands through foreign direct investment. A distributed hydrological modeling approach using SWAT was used utilized to evaluate hydrological impacts.

This research project was proposed with the objective of studying the potential impact of climate and land use changes on the discharge of the upper Blue Nile basin using climate change and formulated land use change scenarios.

1.2 Implications of climate change in the upper Blue Nile basin

The demand for fresh water resources already exceeds the supply in many parts of the Earth (World Resources Institute, 2000). In addition, it is very likely that the climate of the Earth is changing (IPCC, 2007). The management of water resources under such circumstances is a complex task and should consider future climate scenarios in addition to plans for existing and projected water demand.

Climate change affects human kind in several ways. Drought and flooding are among the main effects of climate change which significantly affect the livelihood of the people. The capacity to respond to climate change depends largely on the development level of a country. According to the IPCC report “Africa is the continent most vulnerable to the impacts of projected climate changes because widespread poverty limits adaptation capabilities” (Downing et al., 1997). In developing countries like Ethiopia where rainfed agriculture dominates the rural economy, the effects of climate change are enormous.

The implications of climate change in Ethiopia mainly focus on its effects on crop production and hydropower generation. Despite sufficient average annual rainfall and overall favorable environmental conditions for agriculture, the performance of rainfed crop production is very poor. The national yield of major cereals oscillates around one ton per hectare. The low performance is usually attributed to high temporal and spatial variability in rainfall. Due to gradual and prolonged variability and decline in rainfall over the highlands since the 1960's coupled with the droughts of the 1960's, 1970's and 1980's several people have raised concern about the impact of climate change on water resources in Ethiopia. Climate impact on the water resources of the upper Blue Nile basin will have an impact on the food security in overall Ethiopia as the upper Blue Nile basin, which covers about 14 percent of the total land area of Ethiopia, is the major crop production area of the country. With about 6 million ha (MWR, 1998c) of cultivated land, the Upper Blue Nile basin is known for the supply of surplus food production to the national market. The major crops are cereals such as teff, wheat, maize and sorghum and pulses such as lentil, chickpea and beans.

Ethiopian power supply heavily relies on hydropower. During drought years, the hydropower generation is significantly affected due to shortage of water in the dams for power generation. In 2008 and 2009, severe drought reduced water levels at many dams in the country, causing below normal power generation and frequent power black outs. The consequence of power shortage was significant in affecting the economy of the country (ERG, 2009). In 2009 the Ethiopian electric and power corporation was forced to rent two 31 mega Watt diesel generators in order to supplement the hydroelectric supply of the country for the first time in the corporation history (Single, 2009).

Although the Blue Nile is the largest river in volume of discharge and has suitable topography for power generation in Ethiopia, it development for hydropower generation was very low. The reason for the low level of investment in hydro dams in the upper Blue Nile basin emanates from the lack of capital on the part of the Ethiopian governments and dependence of Sudan and Egypt on the Nile, which makes it difficult for the international financial institutions to fund unilateral projects in the basin (Arsano and Tamrat, 2005)Until May 2010, there were only three small hydro dams namely Fincha, Tis Isat I and II producing

a total of 228 MW in the basin (EEPCo, 2012).Recently, the Beles dams started operation with the capacity of 435 mega Watt. The Amerti Nesh project is finalized in 2011 and start production of an additional 100 mega Watt. This makes the contribution of the basin to a maximum of 763 mega Watt if Tis Abay I and II power station continued producing hydroelectricity (EEPCo, 2012) In mid 2011 the government of Ethiopia announced inauguration of the construction of a major hydro power dam at the out let of the upper Blue Nile basin in anticipation of increasing the power generation capacity and export market. This huge structure is expected to store large amount of water and generate 6000 MW of electricity (EEPCo, 2012). How climate variability and change will affect the performance of this structure is an interesting issue.

On the other hand recent flooding in 2006, affected many people in the upper Blue Nile basin and other parts of Ethiopia. In the Omo valley and in the Dire Dawa the effect was severe with thousands of people killed and displayed because of the flooding (IFRCRCS, 2006). In Lake Tana basin, which is the one of the origins of the Nile, more than 15,000 people evacuated their homes as a result of flooding (IFRCRC, 2006). In the Upper Blue Nile basin, flooding is common in low land areas such as the Lake Tana basin particularly the Fogera plains, and in the lowlands of Beles, Didesa and Dabus river basins.

CHAPTER 2 STATE OF THE ART

2.1 Global circulation models and climate scenarios

The most widely used approach to study the hydrological impacts of climate change is to combine the outputs of the general circulation models (GCMs) with a hydrological model. The common outputs of GCMs used as inputs into the hydrological models are temperature and rainfall (Randall et al., 2007).

GCMs are numerical models representing the physical processes in the atmosphere, ocean, cryosphere and land surface (Roeckner et al., 2006). The coupled atmosphere-ocean GCMs (AOGCMs) combine atmospheric and oceanic GCMs and are basis for model predictions of future climate. The current GCMs (e.g. ECHAM5, HADGEM2) have a horizontal resolution of about 200km extending 40-80 km height in the atmosphere (Collins et al., 2008). Even if the horizontal resolution of the current GCMs is far better than the first generation GCMs, which was about 1000 km, the resolution is still quite coarse for the use in impact assessment which usually requires inputs at the scale of a watershed. Besides the coarse resolution, the current GCMs might lack the capacity to simulate ENSO driven tropical precipitation, water vapor, temperature and outgoing long wave radiation. In addition many physical processes which occur at smaller scale such as clouds cannot be properly modeled due to the use of average value over the larger scales (Conway, 2009; Hulme et al., 2001).

To bypass the scale problems higher resolution climate models are nested into GCMs or empirical relationships between large-scale circulation patterns and regional climate are derived. These two methods are referred as ‘dynamical downscaling’ and ‘statistical downscaling’ techniques (Fowler et al., 2007; Wilby et al., 2004).

2.2 Climate change scenarios

Due to the complexity of the climate system of the globe and limited knowledge of the same, it is not yet possible to predict climate change. As a result climate change scenarios are commonly used by climatologists to specify a number of future climates (IPCC, 2007). Climate change scenarios are plausible representations of the future climate and are consistent with assumptions about future emissions of greenhouse gases and other

pollutants. They are based on today's understanding of the effects of increased atmospheric concentrations of these gases on the global climate. While formulating climate change scenarios assumptions on future trends in population, economy, technology, energy demand, and agriculture (land use) on emission of greenhouse gases over long time scales were used (IPCC, 2007).

The International Panel on Climate Change (IPCC, 2007) summarized future emission of greenhouse gases based on four scenarios called storylines labeled, which are labeled as A1, A2, B1 and B2. These storylines describe the relationship between the forces driving greenhouse gas and aerosol emissions and their evolution during the 21st century. Each storyline of the special report on emission scenarios (SRES) represents different demographic, social, economic, technological, and environmental developments. The four storylines combine two sets of divergent tendencie. One set varies between strong economic values (A1 and A2) and strong environment values (B1 and B2), the other set varies between increasing globalization (A1 and B1) and increasing regionalization (A2 and B2) (IPCC-TGICA, 2007).

After quantification of the driving forces affecting future emissions using integrated assessment models each of the storylines was converted to the corresponding scenario family. The scenario families were further subdivided into seven scenario groups, four for the A1 family, and one for each of the other scenario families. Each scenario group represents a quantitative interpretation of a particular qualitative scenario storyline with the help of one model. The models used to develop the scenarios were: Asian Pacific Integrated Model (AIM), Atmospheric Stabilization Framework Model (ASF), Integrated Model to Assess the Greenhouse Effect (IMAGE), Multiregional Approach for Resource and Industry Allocation (MARIA), Model for Energy supply Strategy Alternatives and their General Environmental Impact (MESSAGE) and the Mini Climate Assessment Model (MiniCAM) (IPCC, 2007).

The following is a detailed description of the basic assumptions used for the seven scenario groups. The information provided below is entirely based on IPCC (2007):

A1. The A1 storyline and scenario family describes a future world of very rapid economic growth, global population that peaks in mid-century and declines thereafter, and the rapid introduction of new and more efficient technologies. Major underlying themes are convergence among regions, capacity building and increased cultural and social interactions, with a substantial reduction in regional differences in per capita income. The A1 scenario family develops into three groups that describe alternative directions of technological change in the energy system. The three A1 groups are distinguished by their technological emphasis: fossil-intensive (A1FI), non-fossil energy sources (A1T) or a balance across all sources (A1B) (where balanced is defined as not relying too heavily on one particular energy source, on the assumption that similar improvement rates apply to all energy supply and end use technologies).

A2. The A2 storyline and scenario family describes a very heterogeneous world. The underlying theme is self-reliant and is based on preservation of local identities. Fertility patterns across regions converge very slowly, which results in continuously increasing population. Economic development is primarily regionally oriented and per capita economic growth and technological change is more fragmented and slower than other storylines.

B1. The B1 storyline and scenario family describes a convergent world with a global population that peaks in mid-century and declines thereafter, similar t the A1 storyline.Rapid change in economic structures toward a service and information economy, with reductions in material intensity and the introduction of clean and resource-efficient technologies is assumed. The emphasis is on global solutions to economic, social and environmental sustainability, including improved equity, but without additional climate initiatives.

B2. The B2 storyline and scenario family describes a world in which the emphasis is on local solutions to economic, social and environmental sustainability. It is a world with continuously increasing global population, at a rate lower than A2, intermediate levels of economic development, and less rapid and more diverse technological change than in the

B1 and A1 storylines. While the scenario is also oriented towards environmental protection and social equity, it focuses on local and regional levels.

Approximate carbon dioxide equivalent concentrations corresponding to the computed radiative forcing and due to anthropogenic greenhouse gases and aerosols in 2100 for the special report on emission scenarios B1, A1T, B2, A1B, A2 and A1FI illustrative marker scenarios are about 600, 700, 800, 850, 1250 and 1,550 parts per million respectively (Figure 1). Scenarios B1, A1B and A2 have been the focus of model intercomparison studies. Temperature and sea level rise ranges for the same scenarios are provided in table 1 (IPCC, 2007).

Table 1 Projected global average surface warming and sea level rise at the end of the 21st century.

	Temperature Change (°C at 2090-2099 relative to 1980-1999)		Sea Level Rise (m at 2090-2099 relative to 1980-1999)
Case	Best estimate	Likely range	Model-based range excluding future rapid dynamical changes in ice flow
Constant Year 2000 concentrations	0.6	0.3 – 0.9	Not available
B1 scenario	1.8	1.1 – 2.9	0.18 – 0.38
A1T scenario	2.4	1.4 – 3.8	0.20 – 0.45
B2 scenario	2.4	1.4 – 3.8	0.20 – 0.43
A1B scenario	2.8	1.7 – 4.4	0.21 – 0.48
A2 scenario	3.4	2.0 – 5.4	0.23 – 0.51
A1FI scenario	4.0	2.4 – 6.4	0.26 – 0.59

Source: IPCC (2007)

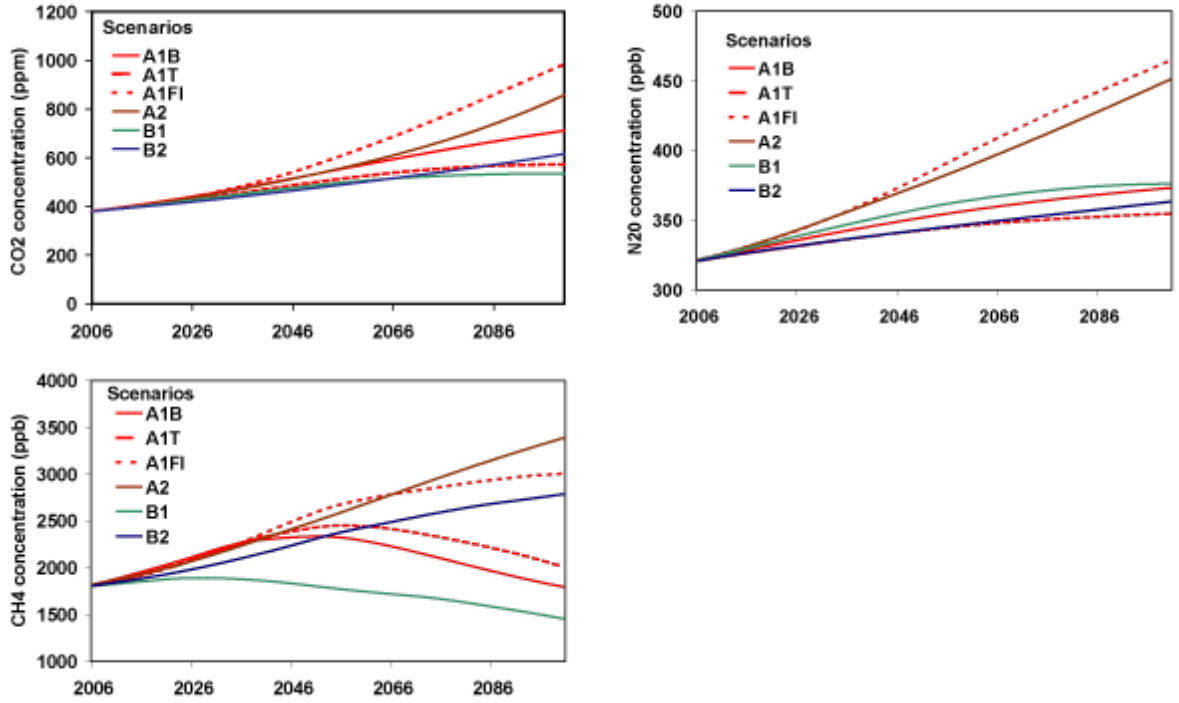

Fig. 1 Projected changes over the 21st century in the atmospheric concentrations of three green house gases: carbon dioxide (chemical formula: CO2), methane (CH4), and nitrous oxide (N2O). Copy from: US EPA, 2012.

2.3 Observed regional trends in temperature and rainfall in the Nile Basin

According to Wing et al., (2008), while there is generally no significant change detected in the annual rainfall in most of the Nile sub-basins (Wing et al., 2008), there appears to be decreasing seasonality in some key watersheds of the upper Nile in Ethiopia such as the southern Blue Nile and Baro-Akobo. Conway and Hulme (1993) also supported the idea that, except for Lake Victoria, all sub-basins of Nile experienced slightly-to-strongly decreasing trends in precipitation. However, a research work by the University of Oxford (2009) emphasizes that the strong inter-annual and inter-decadal variability in Ethiopia's rainfall makes it difficult to detect long term trend. According to the same source, there is no statistically significant trend in observed mean rainfall in any season in Ethiopia between 1960 and 2006 (University of Oxford, 2009). Decrease of July, August and September rainfall observed in the 1980s has shown recovery in the 1990s and 2000s (University of Oxford, 2009)

Mean annual temperature of Ethiopia has increased by 1.3 °C between 1960 and 2006 with an average rate of 0.28 °C per decade(University of Oxford, 2009) . The increase in temperature has been most rapid in June, August and September at a rate of 0.32 °C per decade. Daily temperature observations showed significantly increasing trends in the frequency of hot days and much large increasing trends in the frequency of hot nights (University of Oxford, 2009).

2.4 Climate change in the Nile basin

One of the earliest studies in Nile river basin that considered the implications of climate fluctuations for water resources was a study by Hulme (1994). In this study a range of climate scenarios from historical analogues, instrumental data and general circulation model experiments were constructed to study impact of climate change on the Nile and it concludes that there is no clear signal from the composite model scenario about the magnitude or extent of precipitation changes over the Blue Nile catchment or over the central Sudan. However, in the White Nile catchment, the author found a high probability for increased precipitation in both the summer and winter seasons (Hulme, 1994).

The same study points out that with an inevitable increase in evaportranspiration which would result from the higher surface air temperatures, the best scenario for greenhouse induced forcing of Nile discharge would be for reduced Blue Nile flows and constant or slightly increased White Nile flows. Hulme (1994) also warns that these scenarios remain highly uncertain until substantial improvements are made in combined Ocean-Atmosphere global climate models.

Based on three general circulation model climate scenarios, Conway and Hulme (1996) conclude that the mean annual Blue Nile flow for 2025 will be changed by +15, -9 and +1% using a wet, dry and composite cases respectively. The results from three equilibrium global circulation model experiments were used for the study. The geophysical fluid dynamics laboratory and the Goddard institute for space studies were chosen as examples of dry and wet cases to highlight the inter model differences in precipitation changes. The third case applied a composite scenario generated from seven different GCM experiments. The composite precipitation scenario was generated from a weighted mean of seven equilibrium

GCM change fields. Each GCM was given a weighting based on its ability to simulate current precipitation. The temperature changes were given equal weights in the composite scenario (Conway and Hulme, 1996).

Recent studies on climate change impact on the Nile river basin indicate generally an increasing trend in runoff. Soliman et al. (2009) find out that an annual average increase of 1.5% and a large increase (+10%) during the beginning of the flood season might occur. In the same study they indicate a decrease of runoff towards the end of the rainy season in October and November and during the dry season (Soliman et al, 2009).

According to Beyene et al. (2010) streamflow increases at high Aswan dam by 111, 92 and 84% for the near (2010-2039), mid (2040-2069), distant (2070-2099) future respectively of the A2 scenario. Applying the B1 scenario to the same period an increasing streamflow by 114, 93 and 87% occur. According to the same study, the Blue Nile River is expected to experience increases in stream flow early in the century due to increased precipitation (Beyene et al., 2010).

Taye et al. (2010) apply that of the IPCC third assessment report increasing mean runoff and extreme peak flows for Nyando catchment for the 2050s while trend for Lake Tana catchment for mean volumes and high/low flows remain unclear (Taye et al.,2010). Nyando and Lake Tana are located in the two source regions of the Nile River basin.

2.5 Land use change and the upper Blue Nile basin

The impact of land use/cover change on stream flow pattern in a typical watershed called Chemoga in the Blue Nile basin of Ethiopia was investigated by Bewket and Sterk (2004). The finding of the study was a decrease in stream flow at a rate of 1-7 mille meters per year between 1960 and 1999 which can be partially explained by changes in land cover/use and a degradation of the watershed that involves destruction of natural vegetative covers, expansion of croplands, overgrazing and increased area under eucalyptus plantations (Bewket and Sterk, 2004).

Hurni et al. (2005) studied the implications of changes in population, land use and land management on surface runoff in upper Blue Nile basin of Ethiopia in small test plots and micro-catchments. They conclude that population increase in the Ethiopian highlands caused increase inoverall runoff rates to lowland areas in earlier times. Additionally, Hurni et al. (2005) emphasize that while recent efforts to conserve watersheds might affect total runoff rates in catchments only in semiarid parts, but might not have effects on runoff in humid parts of the Ethiopian highlands.

CHAPTER 3 METHODS and DATA USED

This chapter provides an overview of the methods and data used. Detail information on the methods and data used are provided in chapters 5, 6 and 7.

3.1 Overall design

The potential impacts of climate and land use change on the water resources of upper Blue Nile were studied using global circulation model future scenarios and formulated land use change scenarios (Figure 2). Future daily climate data of ECHAM5 IPCC AR A1B scenario downscaled by the COSMO-Climate Limited-area Modelling (CCLM) and the REgional atmosphere MOdel (REMO) with the resolution of 50m X 50m were obtained from the Potsdam Institute for Climate Impact Research (PIK) (Hattermann, 2011). In addition statistical downscaling was on monthly time scale were performed to downscale rainfall outputs of ECHAM5 A1B climate scenarios.

The impact of land use change on the water resources of upper Blue Nile basin were studied by formulating future land use scenarios. The future land use scenarios were based on recent trends, historical land use information and anticipated future changes. Data on historical land use and near future (2015-2030) changes were collected from key informants through workshops and personal consultations during the field work at the upper Blue Nile basin. General data on emerging uses like bio fuel and leasing of land for foreign investors for production of export crops were also collected during the field work at the basin and in Addis Ababa (WWDSE, 2011, NBI, 2010).

The Soil and Water Assessment Tool hydrological model (SWAT) (Neitsch, 2002) was used to simulate future water resources of the basin based on global circulation model future climate (2041-2100) and land use (2015-2030) change scenarios. The model outputs particularly discharge, water yield, and evapotranspiration were compared against historical datasets to quantify the possible impacts of climate change on the hydrology of the basin.

3.2 Data used

In this study climate, hydrologic, soil and land use data were used to model the impact of climate and land use change on the water resources of the upper Blue Nile basin.

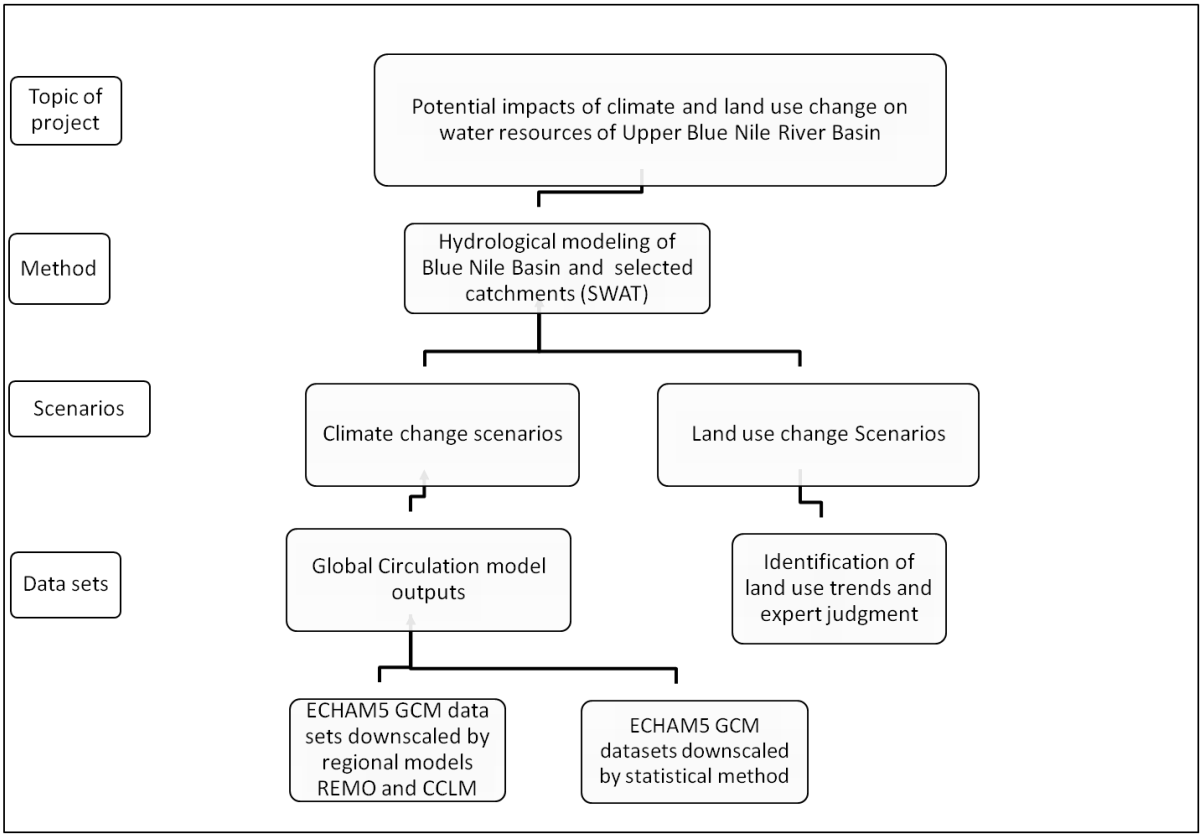

Fig. 2 Frame work of the research project

3.2.1 Observed climate data

Observed daily climate data for the period of 1961- 1990, from sixteen climate stations (Table 6) in the upper Blue Nile basin were provided by the Ethiopian Meteorological Agency. Data were used for the statistical downscaling and hydrological modeling. The climate variables include daily minimum temperature, maximum temperature, rainfall, humidity, sunshine hours, wind speed and evaporation (Figure 3). Figure 3 also shows the runoff gauging station, El Diem which is used for modeling the impact of climate and land use change.

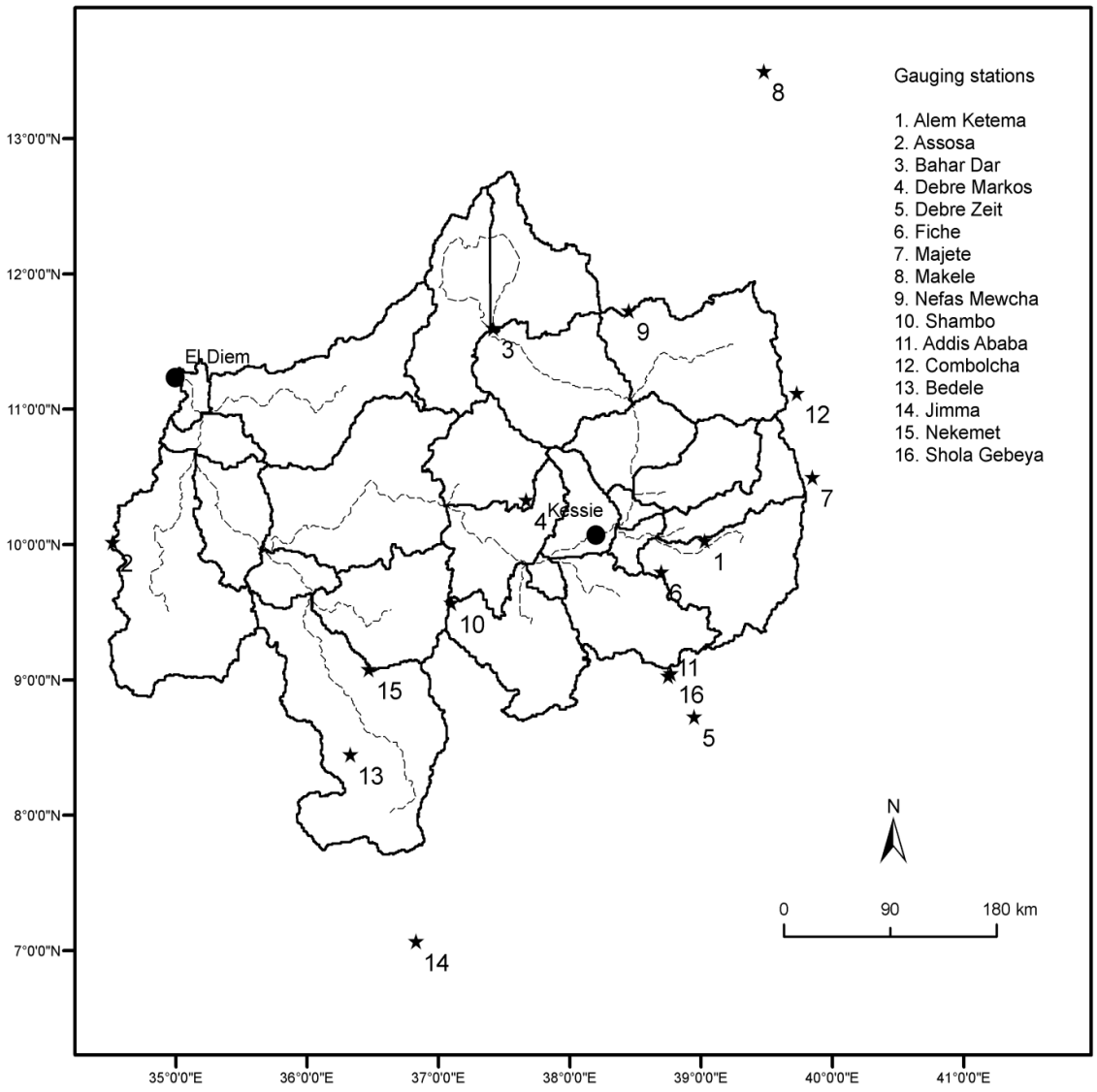

Fig. 3 Location of climate stations
(Data source: National Meteorology Agency of Ethiopia)

3.2.2 Monthly reanalysis data

Observed monthly data of the large scale predictor variables representing the current climatic conditions (1961-1990) were taken from the datasets of the National Centre for Environmental Prediction (NCEP) (Kalnay, 1996). These data are GCM-generated through assimilation of observations and have a spatial resolution of 2.5° latitude by 2.5° longitude. The data include surface and pressure label variables: geopotential height, relative humidity, specific humidity, zonal wind speed, meridional wind speed, mean sea level pressure, sea surface temperature and precipitable water.

3.2.3 Monthly global circulation model scenarios

Data for future climate change scenarios on monthly timescale which were used as predictor variables for the statistical downscaling were provided by the International Panel on Climate Change (IPCC) data distribution centre (Wegner, 2007). The data were extracted from the ECHAM5 run 2 simulations from the Max-Plank Institute of Meteorology following the IPCC SRES A1B scenario, with a spatial resolution of 1.9° latitude by 2.5° longitude.

3.2.4 Downscaled regional data

Dynamically downscaled temperature and rainfall time series of ECHAM5 global circulation model outputs based on the IPCC SRES-AR4 A1B scenario on daily timescale were used for hydrological impact assessment (Hattermann, 2011). Climate projections from CCLM and REMO were obtained in grids of 0.5° x 0.5° horizontal resolution. Future climate change scenarios for studying climate change impact were extracted by superimposing the locations of the eight stations used to simulate historical runoff over the grids of the regional models in the basin.

3.2.5 Land use soil and digital elevation model data

Digital and analogue soil parameter data such as soil depth, soil texture, hydraulic conductivity and bulk density which are required for the hydrological modeling were provided by the soil database of the Abay Master plan document (MWR, 1998d; MWR, 1999) and other project documents (WWDSE, 2011). Land use data with a scale of 1:250,000 which are required in simulation of runoff were extracted from the Ethiopian woody biomass land use database (WBISPP, 2004). SRTM digital elevation model with a horizontal resolution of 90m were used for the hydrological modeling (Jarvis et al., 2008). Detail information on land use, soil and relief is provided in chapter 4.

Field infiltration tests were conducted using the Decagon's handheld Mini-disk infiltrometer at 15 sites in different parts of the upper Blue Nile basin (Figure 4). As most of calculated values derived from the quick infiltration tests overestimate the hydraulic conductivity; only two of the data were used for the hydrological modeling

3.2.6 Hydrologic data

Dekad and monthly discharge data of the upper Blue Nile at El Diem and tributaries were obtained from the Ethiopian Ministry of Water Resources and through contact with water professionals. Most of the gauging stations are located either at the head waters of the tributaries or in the tributaries middle of the river course. Consequently it was not possible to calibrate the hydrological model at the outlet of each sub basin. This was only possible for Diem gauging station, which is located at the outlet of the upper Blue Nile, Data of El Diem gauging station were used for calibrating and validating the hydrological model.

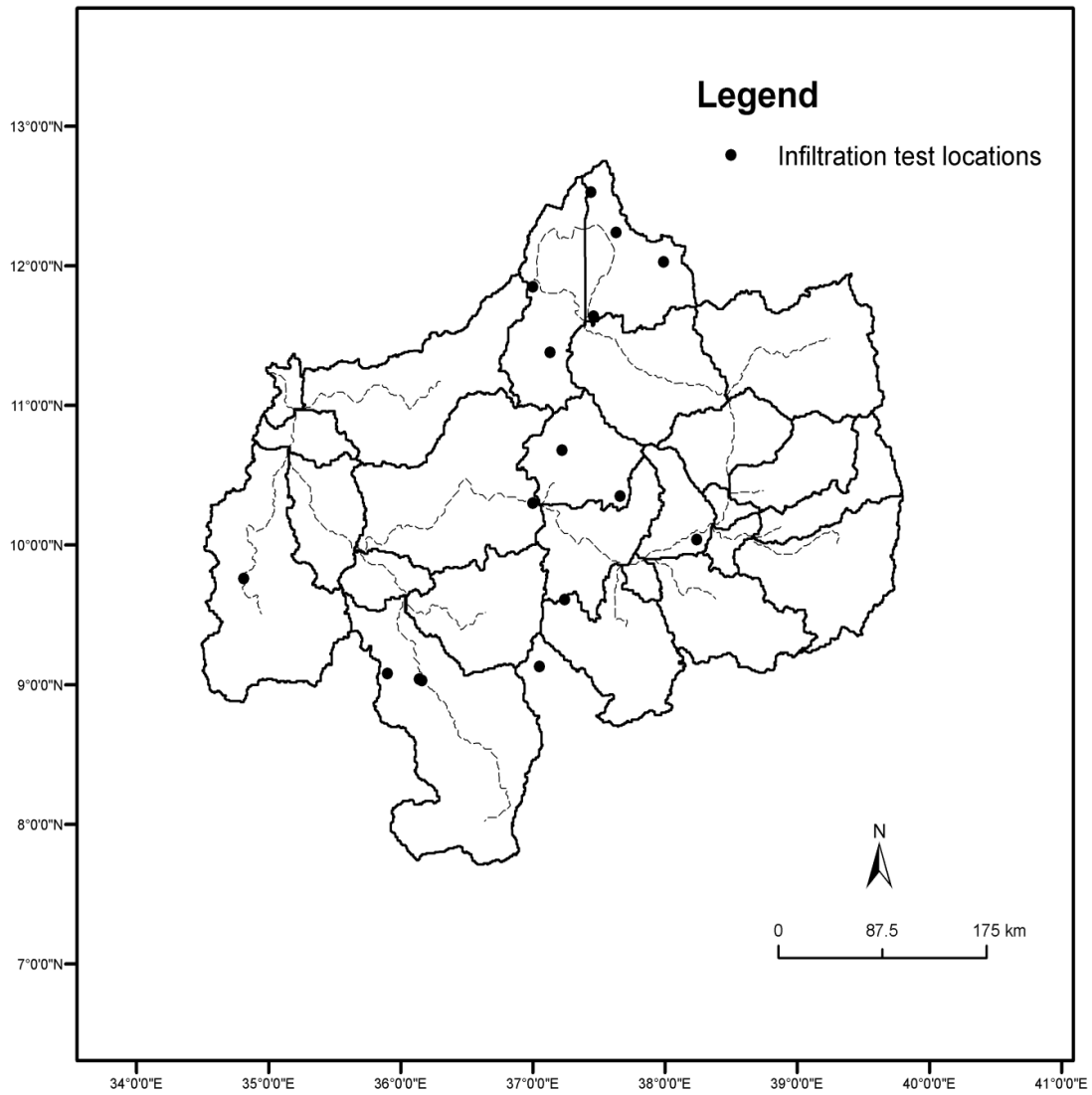

Fig. 4 Distribution of infiltration test locations in the upper Blue Nile (Source: Own analysis)

3.3 Software used

The statistical downscaling was accomplished under Linux environment using downscaling and climate data manipulation tools. These include Clim.pact (Rasmus, 2010), CDO (Schulzweida et al., 2009), Climate explorer (KNMI, 2010), R (John et al., 2010), GrADs (Doty and Kinter, 1992) and WGRIB (Ebisuzaki et al., 2005). Small programs where written in R for the preparation of the weather generator input data of SWAT. The programs read air temperature, rainfall, solar radiation, wind speed and relative humidity including missing values and prepared the 13 climate variables of SWAT weather generator files automatically. Shell scripts and R codes were prepared to be used for the statistical downscaling of ECHAM5 rainfall and temperature scenarios for selected climate stations.

3.4 Statistical analysis

Correlation analysis was used for screening of predictor variables for statistical downscaling of global circulation model climate scenarios. Multiple regression analysis was performed between observed climate and large scale predictors for selected stations in the upper Blue Nile basin during statistical downscaling. Other statistical tests were performed during bias correction of regional model outputs.

CHAPTER 4 STUDY AREA

4.1 The upper Blue Nile basin

The upper Blue Nile is the major tributary of the Nile and is located within the western and central part of Ethiopia between latitudes 7^{o} 45' and 12^{o} 45'N and longitudes 34^{o} 05' to 39^{o} 45'E. The upper Blue Nile consists of the major part of the Abay basin of Ethiopia and covers an area of 157,000km^2. It includes all sub-basins of the Abay except Rahad and Dinder which do not drain to Sudan through the main river system of the Abay. The upper Blue Nile drains towards Sudan on its western border and shares common boundaries with the Tekeze and Dinder basins to the north, the Omo Gibe basin to the south, the Awash basin to the east and south-east and the Baro-Akobo to the south-west. The basin is located within the Amhara, Oromiya and Benishangul-Gumuz regions of Ethiopia (Figure 5).

4.2 Climate

The climate of the upper Blue Nile basin is predominantly influenced by altitude and its proximity to the equatorial monsoonal systems. As a result the climate of the basin ranges from hot and semi-arid to high altitude cool alpine climates (MWR, 1998b). The basin has three mains seasons: a main rainy season which occurs between June and September (et. Kirmet); a dry season from October to January (et. Bega) and the short rain period which may occur between February and May (MWR, 1998b). Generally, temperature is cool and moderate in the highlands and it is warm and hot in the western lowlands.

The traditional Ethiopian classification of climate is based on elevation and recognizes three zones (Conway, 2000):

1. the Kolla zone below 1800 metres with mean annual temperatures of 20-28°C;
2. the Woina dega zone between 1800 and 2400 metres with mean annual temperatures of 16-20°C;
3. the Dega zone above 2400 metres with mean annual temperatures of 6-1 6°C.

According to Conway (2000), there is little variation in temperature through the year, roughly between 3 and 6°C from the warmest month to the coolest months (i.e. between November and February). In summer, peak temperatures are reduced because rainfall, cloudy conditions and energy use for evapotranspiration rather than sensible heat occur

when the highest temperatures would normally be expected (i.e. July and August). The hottest period is, therefore, March to May, before the onset of the major rains (Conway, 2000).

The South West Monsoon originating from the Atlantic Ocean and the south East Indian Ocean monsoon causes the major and minor rains respectively (MWR, 1998b). Mean annual rainfall of the basin varies from 800 - 2,000 mm and increases with altitude. In most parts of the basin the rainfall is unimodal. However, the eastern part of the discussed basin gets a substantial amount of rainfall during the short rainy period (MWR, 1998b). The head water of the Abay and the Didesa basin receives high rainfall which is usually greater than 2000 mm yr^{-1}

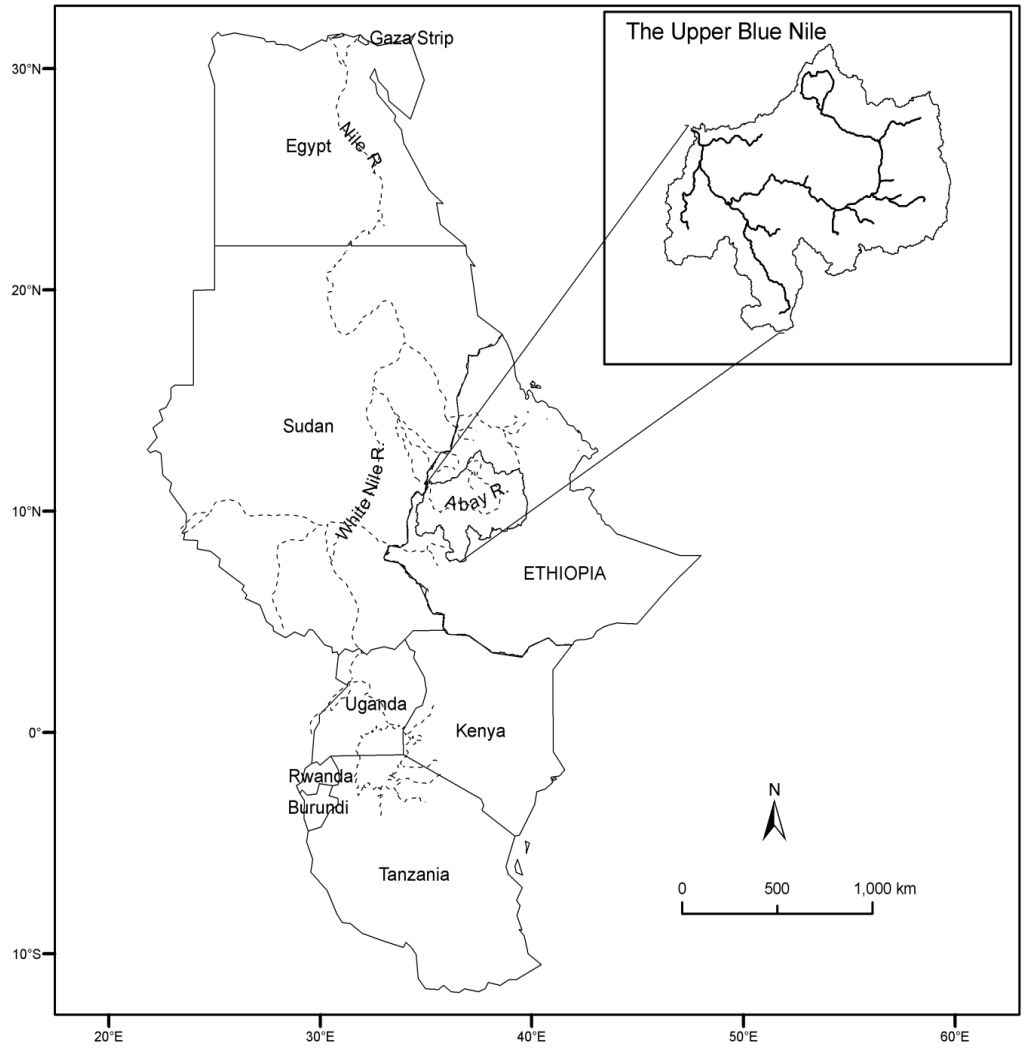

Fig. 5 location of the upper Blue Nile basin
(Source: Own analysis)

Annual average humidity in the upper Blue Nile basin varies between 47-88%. The humidity level is lower in the highlands as compared to the lowlands. In the highlands most of the months have humidity levels ranging from 45 to 65 %. The humidity increases to around 80% during the main rainy season (MWR, 1998b).

4.3 Relief

The upper Blue Nile basin has diverse land forms which include high mountains, rolling ridges, flat grassland areas and valleys. The elevation range from about 490 masl, where the Abay crosses the Sudan border to 4,247 masl in the eastern highlands. About 62% of the upper Blue Nile is above 1,500 masl. Three major relief units can be identified in the basin:

1. the plateau highlands in the central Ethiopian highlands with elevations ranging between 2,000–2,700 masl;
2. the plateau valleys in the eastern part of the basin which descend to the Abay canyon and contain the main tributaries of the Abay; and
3. the lower plains and hill lands in the western part of the basin close to the Sudanese border.

The head waters of the Abay, which are located in the central Ethiopian highlands and are situated between 2,000 to 3,000 masl, sloping downwards in westerly direction to the escarpment above the lowland plains and the valley of the Nile River (Figure 6) (MWR, 1998a).

4.4 Hydrology

The source of the upper Blue Nile River is the Gilgel Abay, which flows north towards Lake Tana (MWR, 1998a). After leaving Lake Tana, the upper Blue Nile River enters a deep canyon, the Abay gorge, which is 10–20 km wide and up to 1.3 km deep. In its descent towards Sudan, the upper Blue Nile River is joined by medium size tributaries from the Gojam highlands such as Abeya, Suha, Chemoga, Birr, Fettam and Dura and major tributaries from the left bank Beshilo, Welaka, Jemma, Muger, Guder, Finchaa, and Didessa. The Beles and Dabus rivers join the upper Blue Nile River in the lowlands before it enters the Sudan lowlands (Figure 7). During its passage from the source to the Sudan border the upper Blue Nile Rivers falls up to 1,300 m and travels for about 1000 km. The upper Blue Nile River has an average slope of 1.4 m km^{-1} and hence it is swift and turbid (MWR, 1998a).

The upper Blue Nile River has a mean annual discharge of 48 * 10^9 m^3 (MWR, 1998a). The mean minimum and maximum annual flow at border gauge are 81 and 6988 m^3 s^{-1} respectively. The lowest daily flow recorded at the border gauge was 67 m^3s^{-1} in May 1965 and a maximum daily flow of 9,308 m^3s^{-1} was recorded in August 1969 (MWR, 1998a)

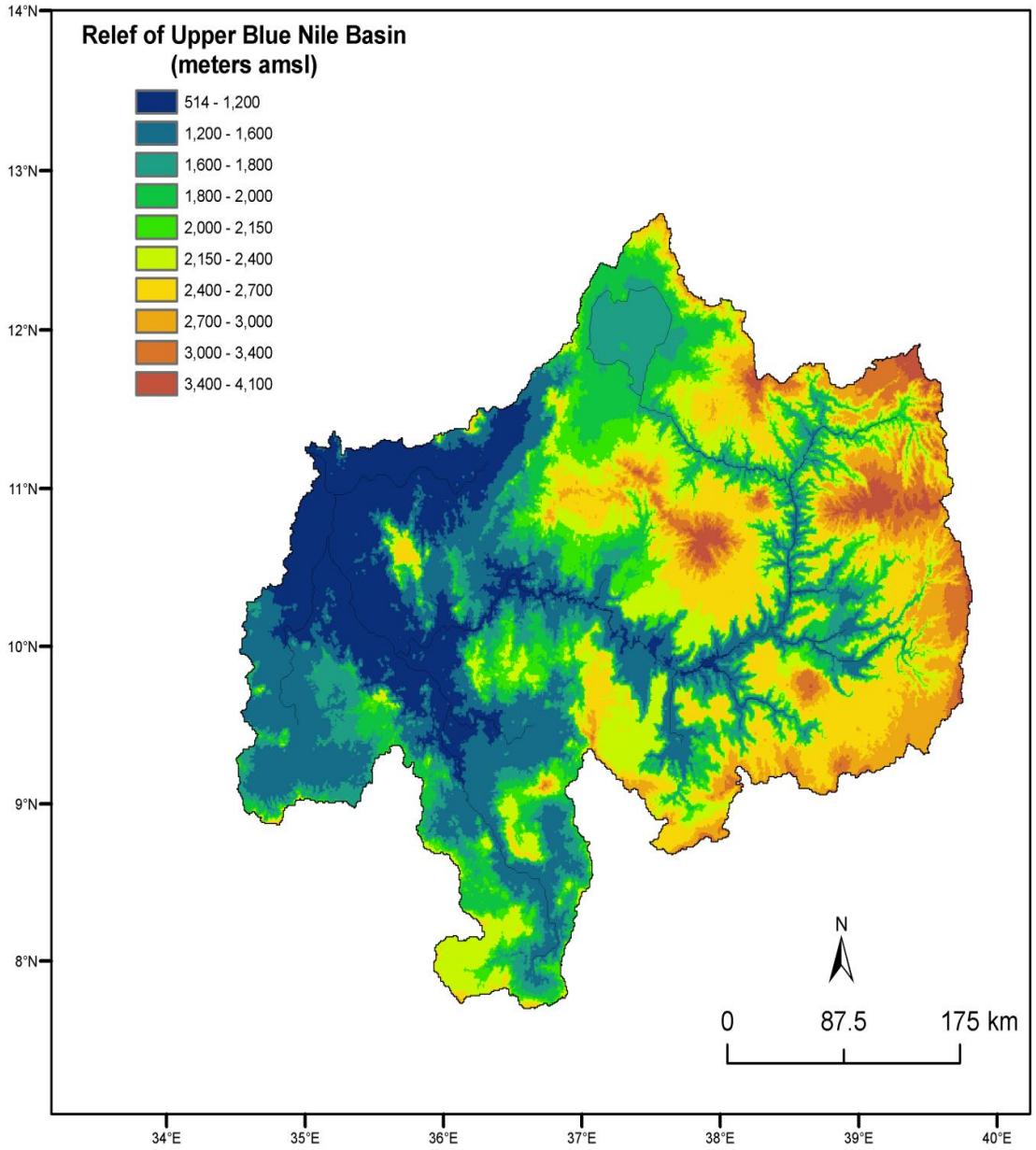

Fig. 6 Relief of the upper Blue Nile basin
(Data source: Jarvis, 2008)

The Didessa River is the largest tributary of the upper Blue Nile River and has high dry season flow. The other three important tributaries which regulate the flow of the upper Blue Nile are Lake Tana, Dabus and Finchaa. Lake Tana affects the flow because of its large

storage capacity (surface area of 3000 km^2) and the restriction at its outlet (MWR, 1998a). The Outflow from the lake peaks two months after maximum rainfall and one month after maximum flow at Roseires (MWR, 1998a). In the headwaters of the Dabus River there is an area of wetlands of approximately 900 km^2 which has a considerable smoothing effect on the runoff distribution (Conway, 2000). As a result peak flow of the Dabus River occurs in September and remain quite high through the following April (Conway, 2000).

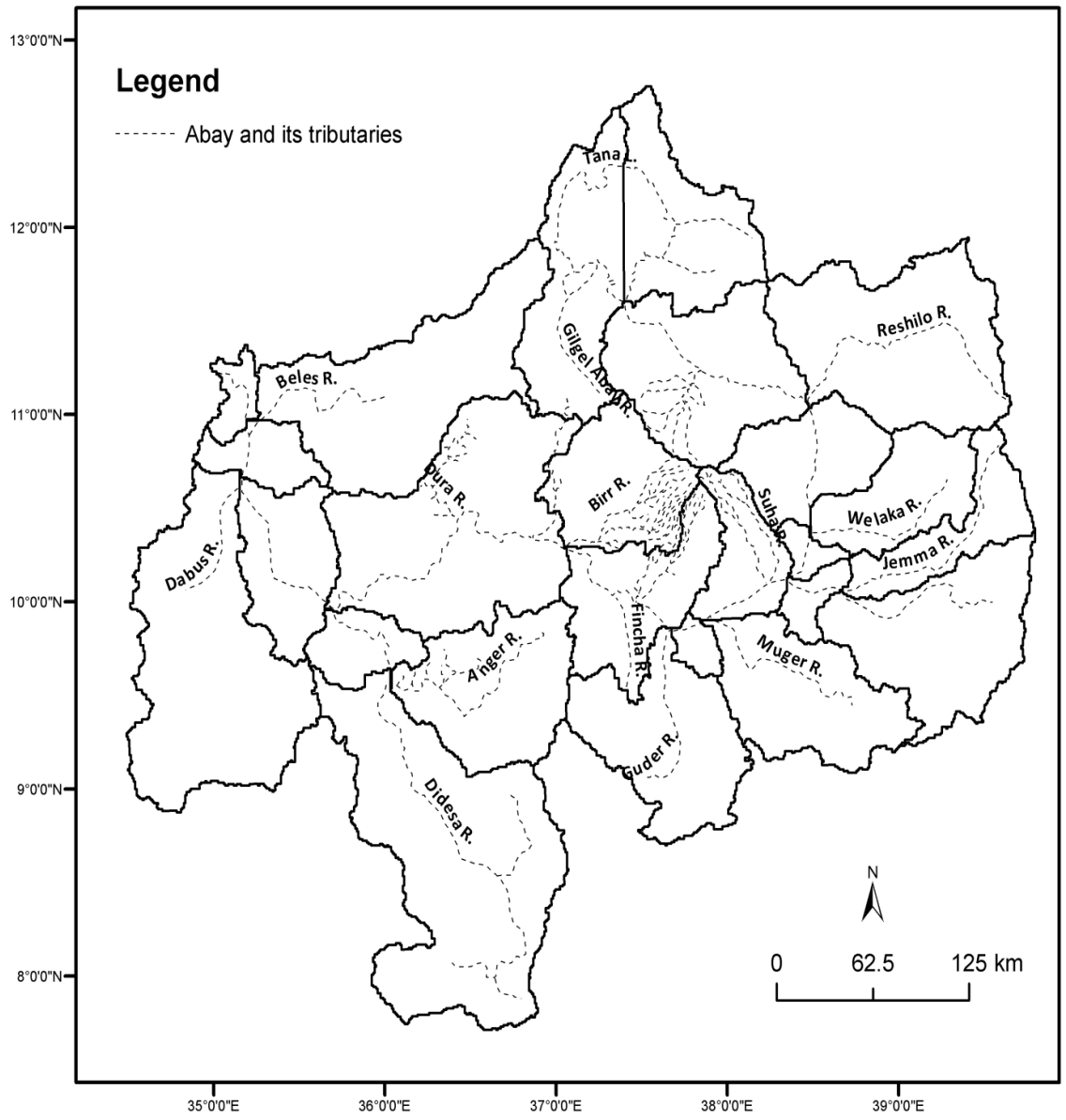

Fig. 7 Abay, its tributaries and sub-basins
(Data source: (MWR, 1999)).

In the headwaters of the Finchaa River there is a small dam which impounds an area of 500-600 km^2, which used to be an area of natural wetlands known as the Chomen Swamps. Both

features have a controlling effect in storing peak season water and releasing it in the following months (MoWR, 1998a).

4.5 Soils

The dominant soil forming processes in the upper Blue Nile basin are the interactions of the soil forming factors of climate, topography, organisms, parent material and time (MWR, 1998b; MWR, 1998d; MWR, 1999). The influence of climate on soil development is by affecting the degree of weathering. Topography plays an important role primarily through modification to the impact of climate. On steep slopes water runs off rapidly retarding soil development. Organisms plays role through the amount of organic matters in the soil. Rocks weather into different soil minerals. Basalts, which are found on the plateaus, are rich in ferromagnesian and break down to clay minerals. Granites and gneisses are rich in quartz and often result into sandy soils (MWR, 1998d).

In the upper Blue Nile basin where the climate is humid, weathering and decomposition are pronounced giving rise to deep and well developed soils such as Alisols, Acrisols and Nitosols. However such soils also occur in the drier, western part of the basin, perhaps reflecting wetter conditions in the past and/or stable land surfaces on which the climate has acted over long periods of time (MWR, 1998d). In the eastern part of the basin where drier climate prevail, less weathering and decomposition have taken place and the soils are shallow and less developed (MWR, 1998d; MWR, 1998b). These soils are Leptosols and Cambisols. Four soil types, Leptosols, Alisols, Nitosols and Vertisols are predominant in the upper Blue Nile basin. The Leptosols are mainly found in the east, north-east and south east portions of the basin. The common occurrence of the Leptosols is along the course of the Abbay River and its main tributaries (MWR, 1998d). Alisols, the second most widely occurring soils, are concentrated in the south, south -west north-west and central parts of the basin. The Nitisols, the third most widely occurring soils are found concentrated in the west of the basin. The Vertisols are found scattered throughout the basin. Other soil types found in the basin are Luvisols, Cambisols, Acrisols, Regosols, Fluvisols, Arenosols and Phaeozems.

The Leptosols mostly occurring in North and South Wello are shallow soils with limited profile development and are prone to drought. The Leptosols are developed on relatively young surfaces and were probably only moderately deep to deep by origin. Most part of the Leptosols is currently cultivated. They have limited agricultural potential but can be used for grazing purposes (MWR, 1998d). The susceptibility of these soils to erosion is one of the reasons which prevent their sustained use for agriculture. Since they occur on steep slopes, they are exposed to a high degree of erosion. The Leptosols are mostly brown/yellowish brown in color, clay loam to clay in texture.

The Alisols are reddish brown in color and have deep profiles usually exceeding 100 cm. Alisols are mainly derived from basalts, granites and granodiorites and possess favorable drainage, structure and workability. Alisols are acid soils and thus may be prone to Aluminum toxicity (MWR, 1998d). The Alisols are dominantly clay and the dominant clay mineral is kaolinite.

Nitosols are the main soil found within the hot, western part of the basin. Nitosols are derived from basalt and tuffs in the central and western highlands or from granites and associated felsic materials. They are reddish-brown in color, clay to clay loam in texture, well drained and very deep. The Nitosols have stable structure, high water holding capacity and permeability (MWR, 1998b Nitosols occur under shrub and wooded grassland and used for cropping and extensive nomadic grazing. They have high fertility and are among the most productive agricultural soils within the basin. Nitosols are moderately prone to sheet erosion (MWR, 1998b).

Vertisols occur on both low, poorly drained plains and on steep rolling highland areas. They are widely distributed in the upper Blue Nile basin. They are characterized by high soil fertility and having swelling clay minerals that create difficulties in working the soils when they are wet or very dry. On the plains these soils have poor internal drainage and are subject to flooding (MWR, 1998b). These soils are dark grayish brown to very dark brown or grey in color, clay to clay loam in texture with deep profiles. The soils are used for cropping,

large scale farming and for extensive grazing in the lowland valleys. They are not easily eroded (MWR, 1998b) (Figure 8).

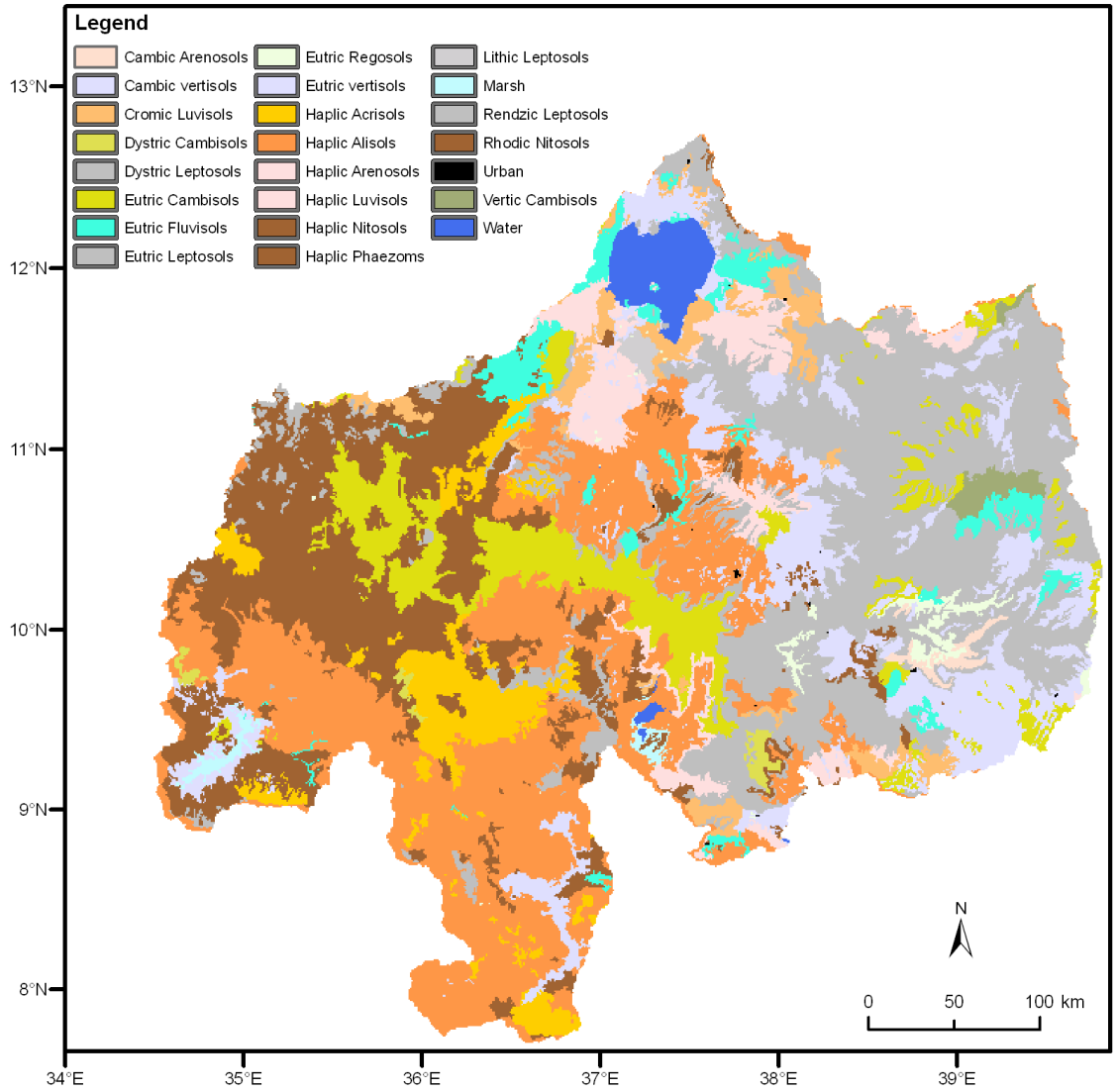

Fig. 8 Distribution of soil types in the upper Blue Nile basin
(Data source: (MWR, 1999)).
NB. Soils were colored following the legend of the soil map of the world by the Food and Agricultural Organization of the United Nations

Most of the remaining soils are deep or very deep soils except Arenosols and Regosols which vary from shallow to moderately deep. The texture of most of the soils consists of clay, clay loam, silt clay, and loam (MWR, 1999).

4.6 Land use and land cover

The three dominant land covers of the basin are cultivation, grassland and woodland (MWR, 1998c). Cultivation is the major land cover of the upper Blue Nile basin occupying about 34% of the basin. Most of the cultivation occurs in the highlands where the elevation is higher than 1500 masl. A variety of annual crops are grown including: wheat, barley, sorghum, tef, maize, finger millet, oil seeds, chick peas and beans (MWR, 1998c).

According to the master plan (MWR, 1998c), grassland covers 23% of the basin. It occurs both in the lowlands and highlands. The low land grasses occupy the lower humid valleys of the Beles, Anger and Didessa valleys. The common grasses are Hyparrhenia spp., digitaria spp. and Panicum spp. The highland grass lands occur above 2,000 masl and include grass species such as Pennisetum, Andropogon, Eragrostis and Cynadon (MWR, 1998c).

Woodland, bush land and shrub land cover 30% of the basin (MWR, 1998c). These are found mainly in the lower western parts of the basin and are associated grassed areas of low woody vegetation. Woody trees/shrubs in these land cover includes Piliostigma thonningii, Stereospermum kunthianum, Combretum spp., Syzygium guineense, Phoenix reclinata.

Forest land covers only about 1.1% of the basin area and is found mostly in the uplands. Most of the forest area is cleared for cultivation or coffee plantation. Remnant forest covers are found in Gera, Setena, Jimma, Komto, Chato and Guangua districts. The dominant species are Podocarpus falcatus and Juniperus procera. Lower slopes contain Aninigeria adolfi-friderici. Plantations mainly include Eucalyptus spp. together with cupressus lusitanica. These plantations are located around villages or in specialized areas set aside for reafforestation. Tree crops covers less than 1% of the basin area (MWR, 1998c). Coffee production is common in Jimma and Illubabor districts of the basin. Patches of mango crop are found in the western parts of the basin (MWR, 1998c).

Bamboo (Oxytenanthera abyssinica and O.borzii) occupies about 4% of the upper Blue Nile basin (MWR, 1999). It occurs in the lower areas of the western part of the basin such as Asosa, Kamashi and Pawe. Afro-alpine vegetation is found in areas above 3,200 masl such as

Mount Guna and Choke. It consists of shrubs, sedges, short woody bushes and trees. Vegetation includes Festuca spp., Giant Lobelia, Erica arborea and hypericum spp. Rock cover accounts about 4% of the UBN. This is mostly consisting of exposed rock on ridges, escarpment sides and the Abay gorge as a result of geologic erosion. Urban areas account for less than 1% of the basin and include towns such as Gondar, Bahir Dar, and Nekemte. (MWR, 1999; MWR, 1998c)

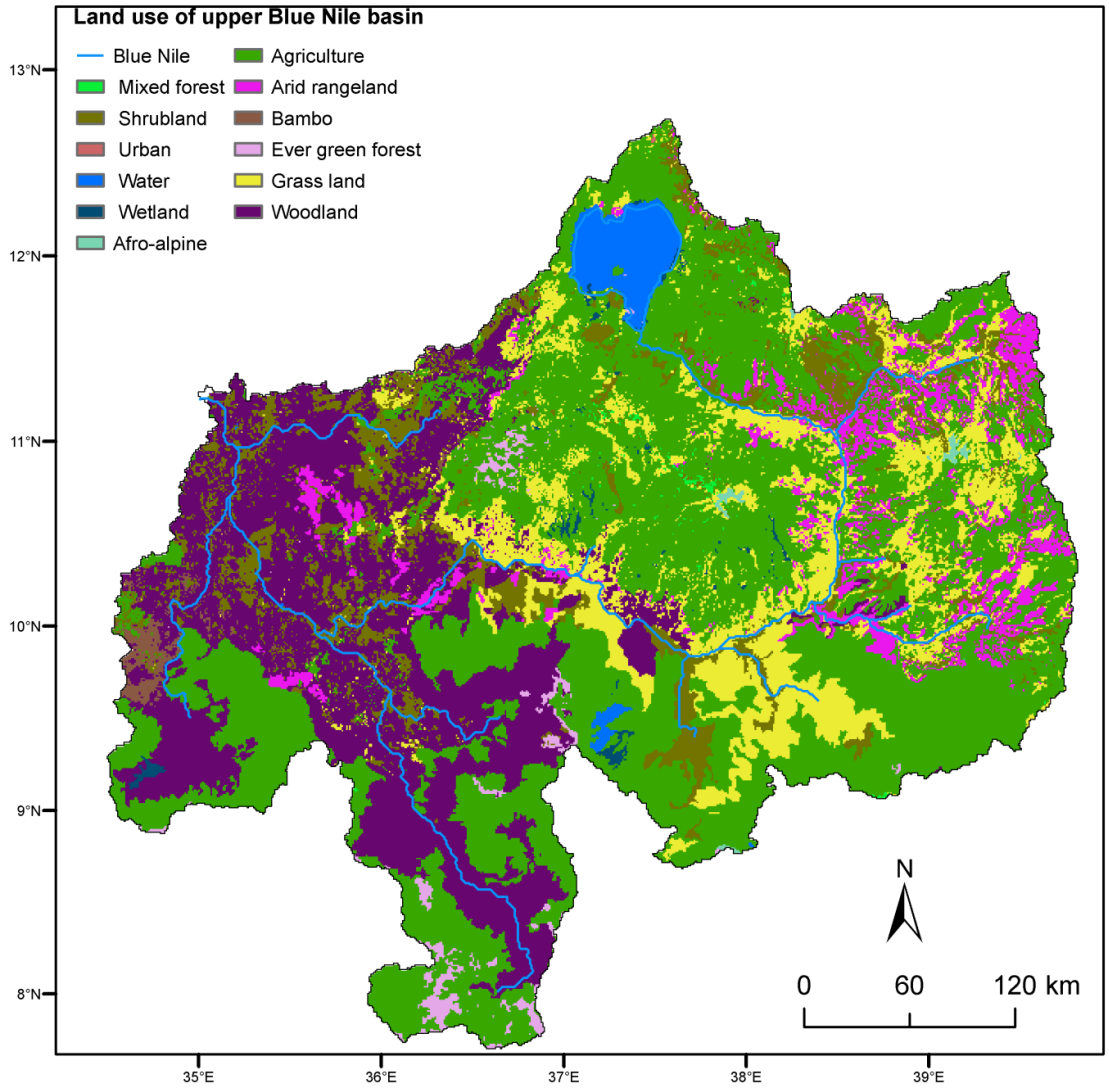

Fig. 9 Land use and land cover of the upper Blue Nile basin
(Data source: WBISPP, 2004).

CHAPTER 5 CLIMATE DOWNSCALING

5.1 Statistical downscaling of rainfall

With the advent of global climate models it is becoming increasingly possible for to study the impact of projected climate change on the availability of water resources. Hydrological models need future projections of precipitation to simulate future flows. However, future projections from GCMs have coarse spatial resolution and cannot be used directly for hydrological modeling, which is usually performed at a catchment scale. Statistical downscaling, which involves developing quantitative relationships between large-scale atmospheric variables (i.e. predictors) and local surface variables, such as rainfall (i.e. predictands), is a widely used approach to overcome the scale mismatch (IPCC-TGICA, 2007).

Downscaling rainfall in the tropics is challenging, both because there is strong ocean atmosphere coupling and because the relationships between large scale predictors and local variables vary strongly within the annual cycle (Wilby et al., 2004). Due to these difficulties and the limited availability of long time series of observed and high resolution climate data, few downscaling models have been developed for the tropics. This section deals with the methods employed in statistical downscaling and the established statistical models for downscaling rainfall in the upper Blue Nile basin.

5.1.1 Selection of climate stations

Five weather stations which have reasonably good quality data for the period of 1961-1990 and are located in the different parts of the basin were selected for the statistical downscaling (Figure 10, table 2). Observed monthly rainfall data for the five stations were obtained from the Ethiopian meteorological agency.

Table 2 Description of meteorological stations used for monthly statistical downscaling

No.	Station	Latitude	Longitude	Altitude (m)	Data availability
1	Assosa	10° 1’ 11.9”	34° 31’12”	1600	1961-1990
2	Gondar	12° 33’ 0”	37° 25’ 12”	1967	1961-1990
3	Combolcha	11° 5’ 6”	39° 49’ 48”	1903	1961-1990
4	Addis Ababa	9° 1’ 48”	38° 46’ 12”	2354	1961-1990
5	Debre Markos	10° 1’ 48”	37° 4’ 12”	2515	1961-1990

(Source: National Meteorology Agency of Ethiopia)

5.1 2 Predictors for statistical downscaling

Candidate predictor variables were selected using existing knowledge of the climate of the tropics and the study basin (Segele et al., 2009). As the tropical region shows a more complex climatic behavior than the mid latitudes, the selected candidate predictor variables include both atmospheric and ocean fields. The selection of predictors was further determined by the availability of variables from the ECHAM5. The candidate predictors used are monthly geopotential height, relative humidity, zonal wind speed, meridional wind speed, mean sea level pressure, sea surface temperature and large scale atmospheric precipitation (Table 3).

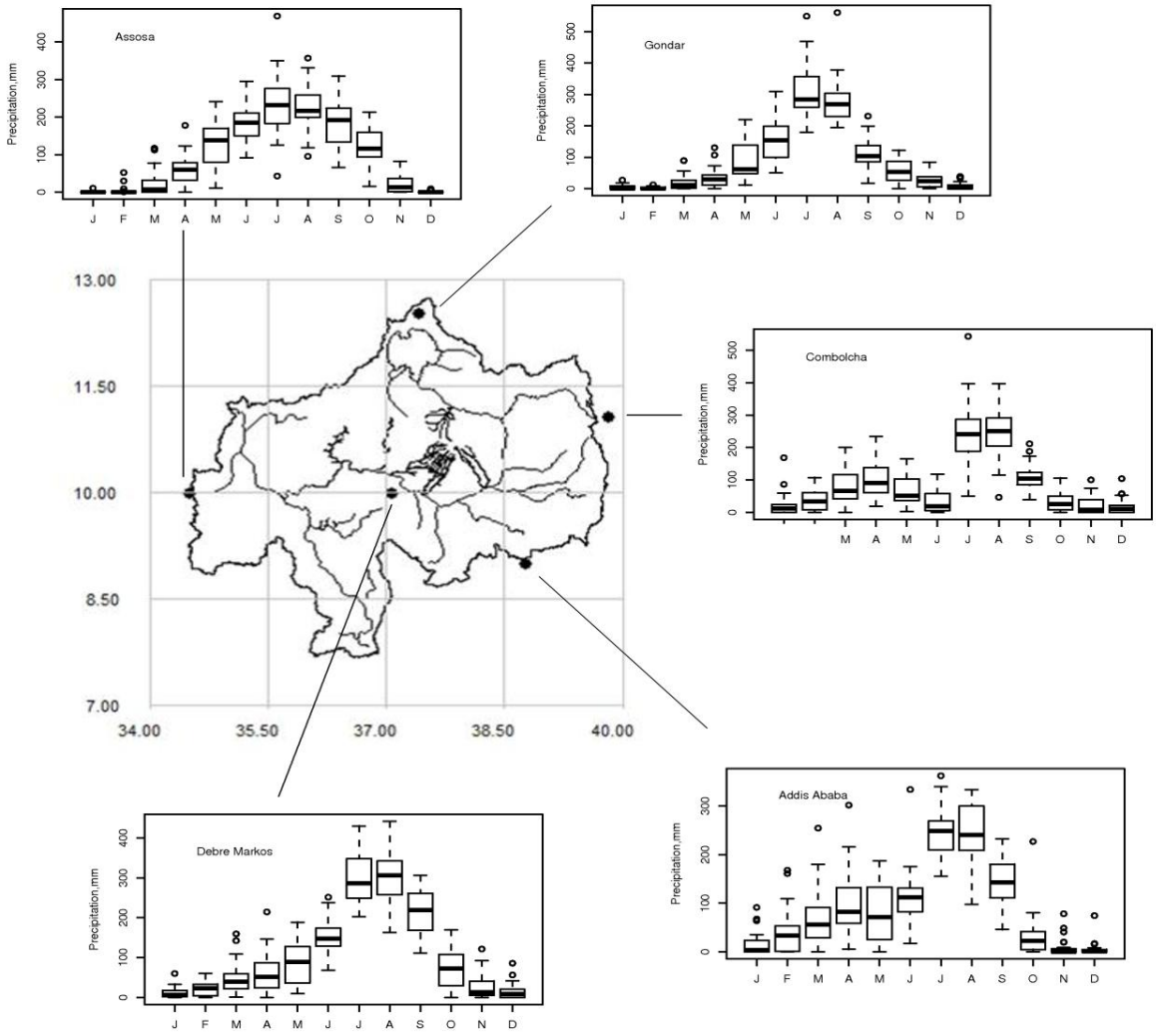

Fig. 10 Map showing the locations of the climate stations in the upper Blue Nile basin; Linked box-plots show the interquartile range of monthly rainfall
(Data source: National Meteorology Agency of Ethiopia)

Observed monthly data of the large scale predictor variables representing the current climatic conditions (1961-1990) were taken from the datasets of the National Centre for Environmental Prediction (NCEP) (Kalnay, 1996). These data are GCM-generated, through assimilation of observations, and have a spatial resolution of 2.5° latitude by 2.5° longitude.

Data for future climate change scenarios for the seven predictor variables selected were taken from the IPCC data distribution centre (Wegner, 2007). It was extracted from the ECHAM5 run 2 simulations from the Max-Plank Institute of Meteorology following the IPCC SRES A1B scenario, with a spatial resolution of 1.9° latitude by 2.5° longitude.

Table 3 Description of predictors for downscaling

Predictors	Unit	Abbreviation	Levels (hP)
Geopotential height	M	Z	500, 850
Relative humidity	%	Rh	500, 850
Zonal wind speed	$m\ s^{-1}$	U	200, 500, 850
Meridional wind speed	$m\ s^{-1}$	V	500, 850
Mean sea level pressure	Mb	MSLP	Surface
Sea surface temperature	K	SST	Surface
Precipitable water	$kg\ m^{-2}$	Precw	Entire atmospheric column

(Source: Own analysis)

5.1.3 Statistical downscaling

The steps used to carry out the statistical downscaling involve: specifying downscaling domains; regriding and standardization of data; multiple regression analysis; evaluation of the statistical downscaling models; application of the Statistical downscaling models and evaluation of the results. The downscaling involved linear multiple regression analysis and was carried out using a number of downscaling and climate data manipulation tools: Clim.pact, CDO, Climate explorer and R.

The accuracy of downscaled values of rainfall has been quantified in terms of the mean absolute error. The absolute errors in simulating rainfall in the upper Blue Nile is provided in

table 4. The accuracy of the selected predictors for the monthly statistical downscaling is measured using the correlation coefficient and results are provided in Figure 14 for Addis Ababa. The accuracy of the domains for the monthly statistical downscaling is measured using the correlation coefficient at 10% significant level. The result of this exercise is provided in figure 12 and 13.

5.1.4 Selection of domains

The selection of domains was based on the climatology of the upper Blue Nile basin and through correlation analysis. First six candidate domains which affect the rainfall amount and pattern in Ethiopia were tested. These include the: Arabian Peninsula (AP), Indian Ocean (IO), Southern Tropical Atlantic Ocean (STAO), North Atlantic Ocean (NAO), Mediterranean and North Africa region (MNA) and upper Blue Nile basin (Figure 11).

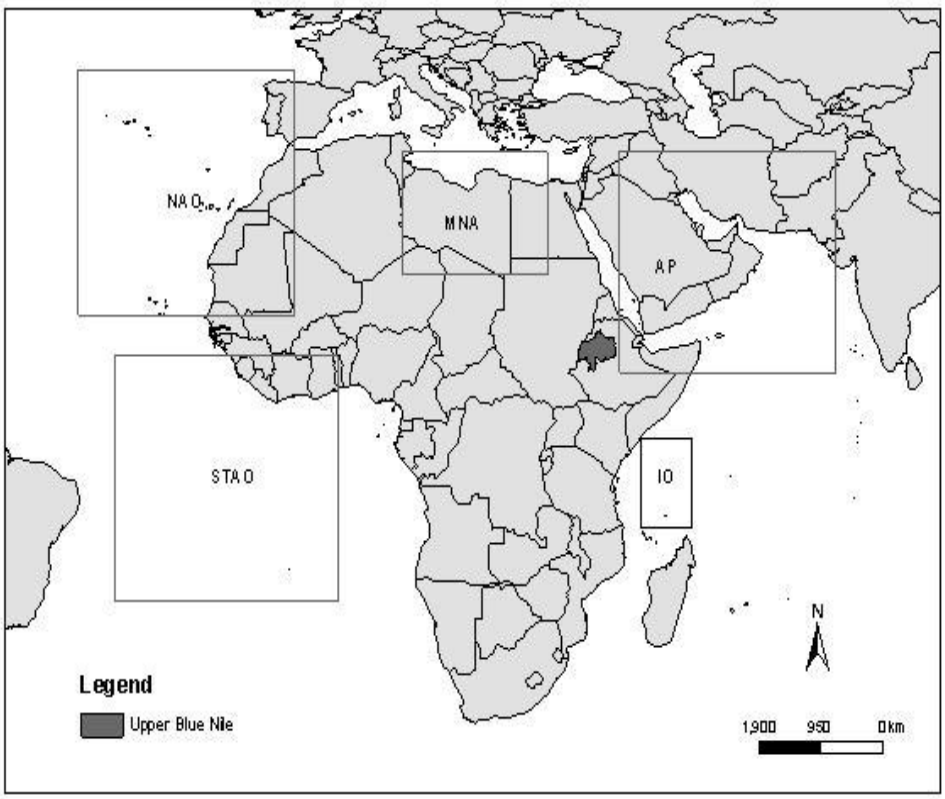

Fig. 11 Location of domains and the upper Blue Nile basin: AP=Arabian Peninsula; NAO=North Atlantic Ocean; STAO = Southern Tropical Atlantic Ocean; MNA=Mediterranean and North Africa; IO = Indian Ocean (Source: Own analysis)

Following the selection of tentative domains, mean sea level pressure which is highly correlated with Ethiopian rainfall (Seleshi and Demaree, 2004) and observed rainfall data

from two test climate stations (Debre Markos and Gondar) were used to explore and select appropriate domains for the whole basin.

After studying the rainfall pattern of the basin, domains identified using Debre Markos climate stations were also used for Addis Ababa. In a similar way domains identified using Gondar climate station were used for Combolcha and Assosa climate stations

Correlation analysis were performed between monthly surface mean sea level pressure taken from the NCEP and observed average monthly rainfall data from the two test stations for the period 1954–1990. The seasonal cycles were removed from the datasets before correlation analysis by subtracting the mean of each month from the monthly values.

The correlation of monthly mean sea level pressure with monthly observed rainfall from the two test stations was not similar during different seasons of the year (Figures 12 and 13). At Debre Markos during the main rainy season (June to September), the correlation was significant at 10% in the Arabian peninsula and in north Atlantic ocean. At Gondar the correlation was significant in the southern tropical Atlantic Ocean, northern Atlantic Ocean, Arabian Peninsula, and Indian Ocean. During the short rainy period both stations show a significant correlation with the northern Atlantic Ocean and southern tropical Atlantic Ocean at 10 % significant level.

After a thorough correlation analysis, visual inspection and examination of the climate of the regions at the Arabian Peninsula, northern Atlantic Ocean, southern tropical Atlantic Ocean and northern Africa were selected to be used for the downscaling rainfall at Addis Ababa and Debre Markos weather stations. In addition, Arabian Peninsula, northern Atlantic Ocean, southern tropical Atlantic Ocean Indian Ocean and Mediterranean, and northern Africa were used for downscaling rainfall at Gondar, Assosa and Combolcha stations.

5.1.5 Effect of combined predictors from different domains

After the selection of the domains, the correlation between the seven predictor variables from each domain and the observed station data was tested on monthly time step. The monthly correlation analysis between area averaged National Centre for Environmental Prediction reanalysis data from these domains and observed station data show mixed results.

When monthly and seasonal correlations were considered all domains were of equal quality. Consequently, a new combined predictor was synthesized from the five domains by extracting the months with the highest correlation from each domain (Table 4). The resultant improvement in the correlation coefficient (R) is shown in figure 14.

The Arabian Peninsula domain was selected for most of the main rainy season. The northern Atlantic Ocean domain was selected for months of December, January, February and March, which corresponds partly to the short rainy period in most parts of the basin. A combination of Arabian Peninsula and northern Atlantic Ocean was considered for June which is one of months with the highest rainfall during the main rainy season. In addition, the southern tropical Atlantic Ocean domain was selected for the months of April and November.

5.1.6 Calibration and validation of statistical downscaling models

Area averaged monthly combined predictors were used to establish a regression model between the National Centre for Environmental Prediction predictors and observed data from the five meteorological stations (Table 2)The period, 1961-1990 was chosen to represent the current climate. A split year approach was followed to calibrate the model for the period 1961-1980 and validate it for the period 1981-1990.

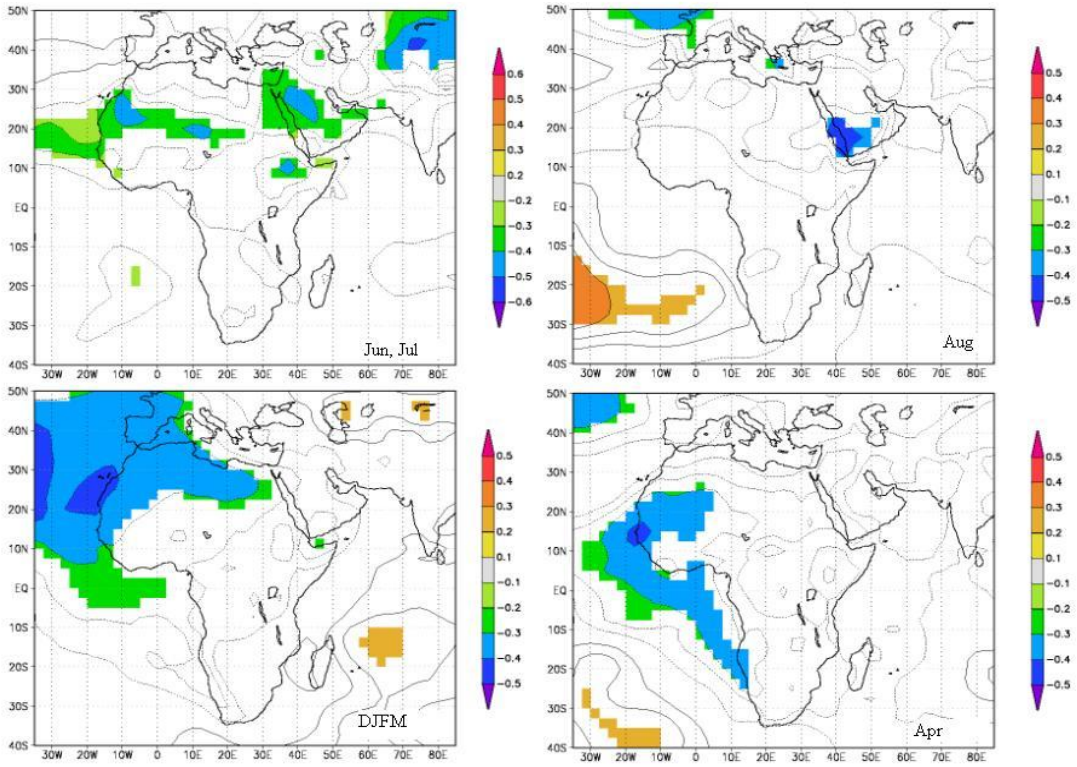

Fig. 12 Monthly correlation between mean sea level pressure and observed rainfall at Debre Markos for a period of 1954-1990 at 10% significant level
(Data Source: KNMI, 2010)

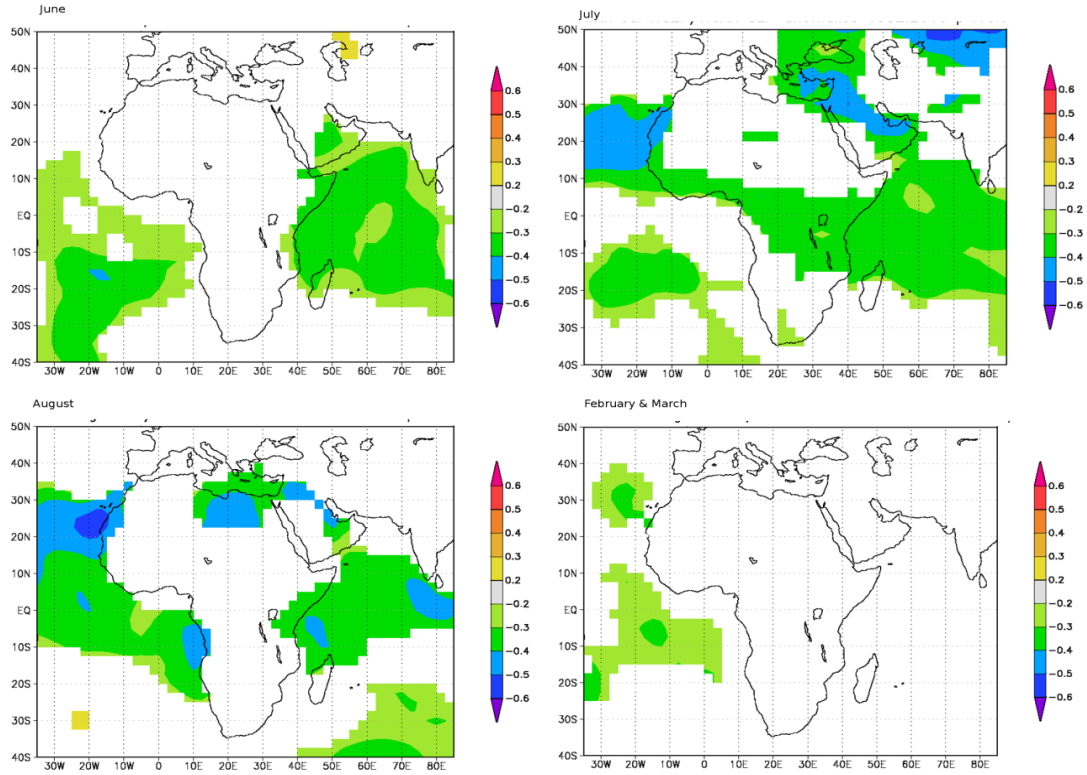

Fig. 13 Monthly correlation between mean sea level pressure and observed rainfall at Gondar for a period of 1954-1990 at 10% significant level
(Data source: KNMI, 2010)

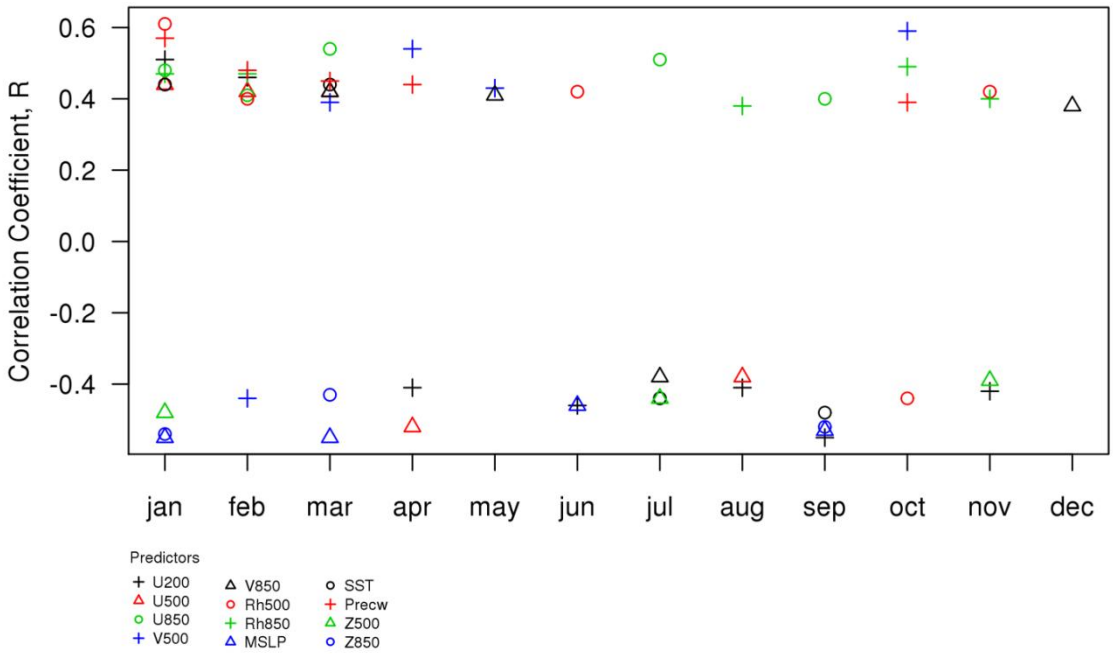

Fig. 14 Monthly correlation between observed data and large scale predictors at Addis Ababa after combining domains and screening of candidate predictors on monthly basis
(Data Source: National meteorological Agency of Ethiopia and kalnay, 1996)

Table 4 Selected domains for the five stations in the basin after correlation analysis of mean monthly observed rainfall with predictors from the National Centre for Environmental Prediction

	Domains for extracting predictors for five meteorological stations	
Months	Debre Markos and Addis Ababa	Gondar, Assosa and Combolcha
January, February, March, December	NAO	NAO
April	NAO and STAO	NAO and STAO
May	AP	AP
June, September	AP and STAO	AP and STAO
July	AP and NAO	IO
August	AP	MNA
October	MNA	MNA

(Source: Own analysis)

Table 5 Mean absolute error of simulated rainfall at the five meteorological stations

Station	Mean absolute error in mean annual rainfall (mm)
Addis Ababa	11
Assosa	25
Combolcha	17
Debre Markos	10
Gondar	12

(Source: Own analysis)

The predictors were standardized using the reference period (1960-1990) before they were subjected to multiple regression analysis with the observed data. Good agreements between the observed and simulated outputs were obtained for most of the stations (Figure 15; Table 5).

As the Mean Absolute Error (MAE) of the annual rainfall varies from 10 to 25 mm and is within the accepted range, the established statistical models were ongoing used for downscaling of ECHAM A1B outputs in the upper Blue Nile basin.

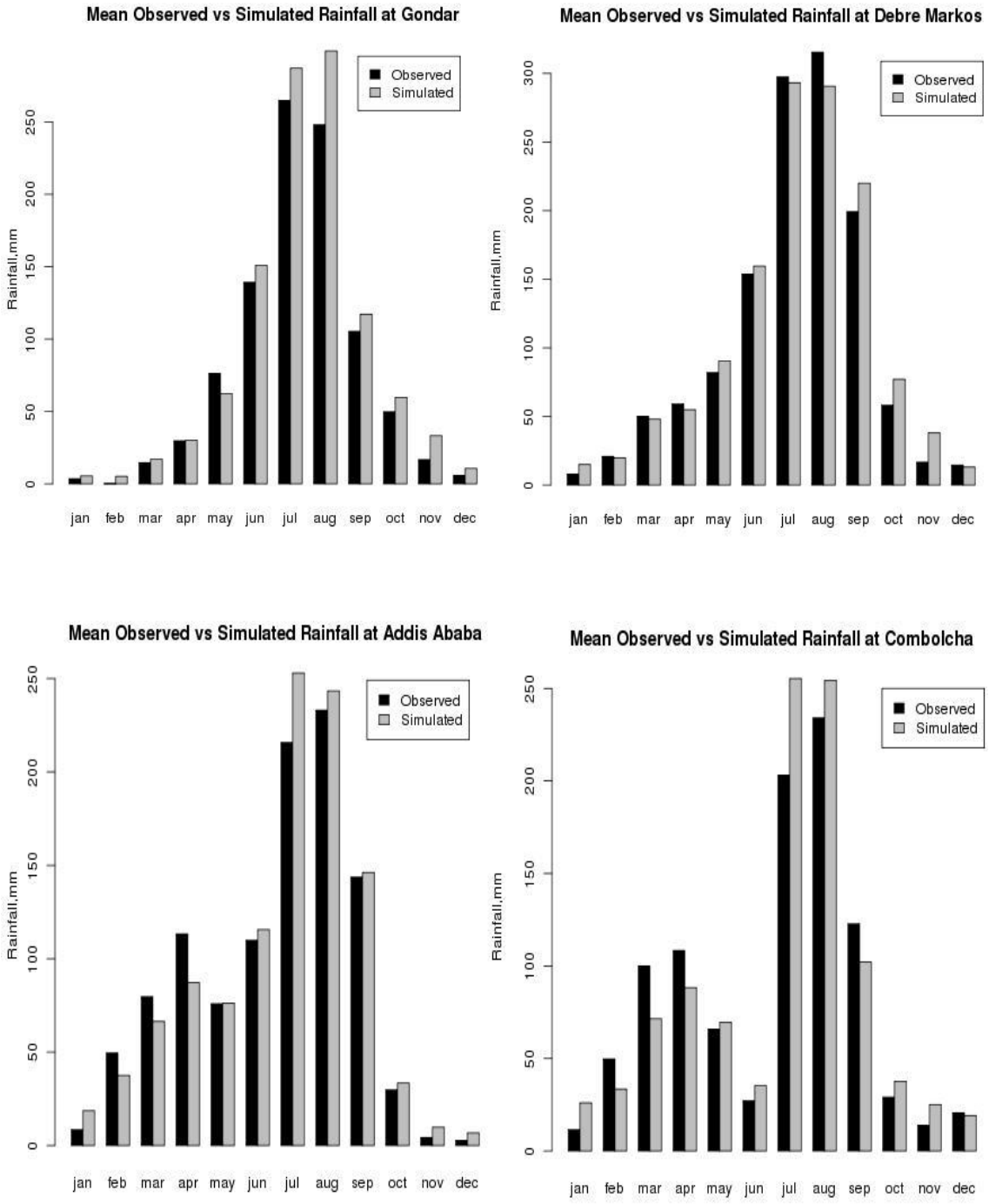

Fig. 15 Validation result of the multiple regression models for four weather stations in the upper Blue Nile basin

(Data source: National Meteorology Agency of Ethiopia)

5.1.7 Simulation of future climate scenarios

To simulate future rainfall in the five locations, data for a future scenario (i.e. from 2041-2070) were extracted from the ECHAM5 A1B global circulation model and used as input to the SDMs.

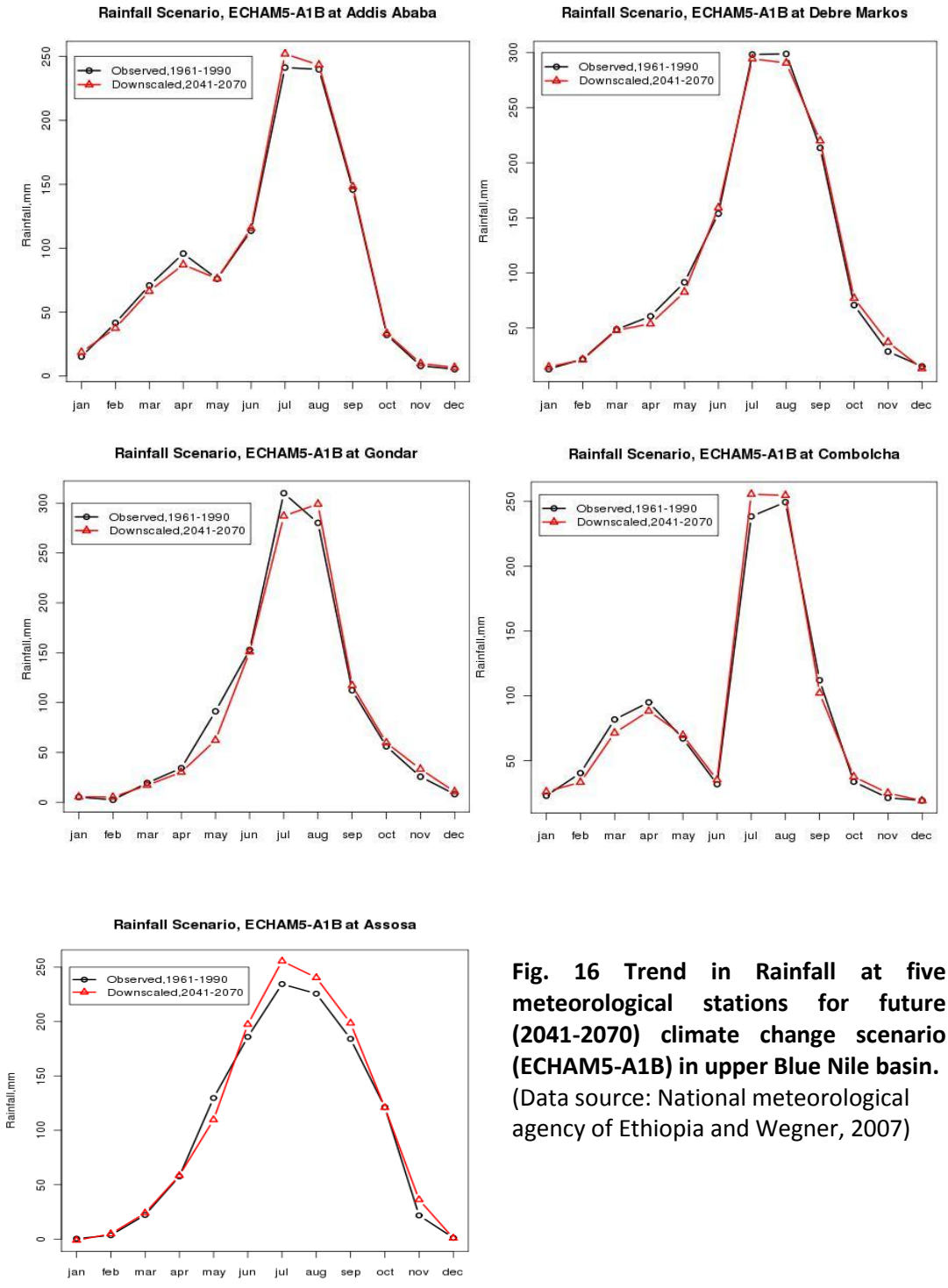

Fig. 16 Trend in Rainfall at five meteorological stations for future (2041-2070) climate change scenario (ECHAM5-A1B) in upper Blue Nile basin. (Data source: National meteorological agency of Ethiopia and Wegner, 2007)

The ECHAM5 run using the validated statistical downscaling models for the A1B scenario shows that in four of the five stations the average monthly rain during the short rainy season decreases by 6-12% (Figure. 16). However, mixed results were obtained for the main rainy season. Compared to the current period an increase of 1-10% was observed at Assosa, Combolcha and Addis Ababa and a decrease of 1-7% at Debre Markos and Gondar dfor the months of June, July and August. However during September, which is the end of the main rainy season, the downscaled monthly rainfall increases by 1-7% for four of the meteorological stations (Assosa, Debre Markos, Gondar and Addis Ababa).

5.2 Dynamical downscaling of temperature and rainfall

Future climate change scenarios from the regional model CCLM and REMO were obtained from the Potsdam Institute of Climate Impact Research through the international water management institute. The regional models were forced with ECHAM5 GCM datasets using the A1B IPCC climate change scenario. These data were used as input in the hydrological model SWAT to simulate water resources availability in 2041-2070 and 2071-2100.

5.2.1 Regional model descriptions

CCLM

The CCLM is a dynamical, non-hydrostatic regional climate model. It is developed jointly by the German Weather Service, the Potsdam Institute of Climate Impact Research, Technical University of Cottbus and Forschungszentrum Geesthacht (GKSS) research center. In 2008 the model became a community model and it is now maintained and further improved by the climate limited-area modeling community (Rockel et al., 2008). The model is based on the primitive thermo-dynamical equations describing the atmospheric motions. The use of a non- hydrostatic form of these equations allows the application of the model in a wide range of spatial scales. The model equations are discretized on a three-dimensional grid based on a rotated geographical coordinate system (Davin et al., 2011). Land surface processes are parameterized by the soil module TERRA_ML (Grasselt et al., 2008).

CCLM is tested in Europe, Asia and Africa. The data used for this study are taken from COSMO_4.0_CLM simulations, which run for the African continent with grid dimensions of 165 x 162 and a grid spacing of 0.5^{o}. It has 32 vertical layers and ten soil layers. The initial

and boundary conditions were taken from the ECMWF Re-Analysis (ERA40). The simulations consist of 30 years daily control runs using ECHAM5-OM (1971-2000) and 100 years transient scenario runs using ECHAM5, A1B climate scenarios (2001-2100) (Hattermann, 2011).

REMO

REMO is a three-dimensional, hydrostatic atmospheric circulation model which solves the discretized primitive equations of atmospheric motion (Jacob, 2001). It is based on the Europa-Model (EM) of the German Weather Service (Majewski, 1991). REMO was developed by the Max Planck Institute for Meteorology in cooperation with German Climate Computing Center, German Weather Service and Forschungszentrum Geesthacht (GKSS). REMO is tested for Africa, Europe, Latin America and Asia (Hattermann, 2011; Paeth, 2005)

REMO has horizontal resolutions between 0.1-1°. For horizontal discretization REMO uses a spherical Arakawa-C grid in which all variables, except the wind components, are defined in the centre of the respective grid box. The grid box centers are defined on a rotated latitude-longitude coordinate system. Vertically, variations of the prognostic variables such as temperature, wind, water vapor content, cloud water content are represented by a hybrid vertical coordinate system (Roeckner et al., 1996). REMO uses ECMWF reanalysis data as lateral boundary forcing for validating simulations. It is coupled with three different hydrology models and three ocean and sea-ice models (Roeckner et al., 1996).

The model output of the REMO regional model for eastern Africa was run in 0.5° horizontal resolution and was nested in to the global coupled climate model ECHAM5 (Hattermann, 2011). The REMO experiment extends from 1951 to 2100 and it has been subject to various scenarios of man-made greenhouse-gas emissions and land cover changes (Roeckner et al., 1996). Each scenario is represented by an ensemble of simulations with different initial conditions in order to account for internal variability in the model (Roeckner et al., 1996).

5.2.2 Observed data

The Climate Research Unit gridded database (CRU TS 2.1) for the period of 1961-1990 was used as observed climate in quantifying the impact of climate change in the upper Blue Nile basin. Temperature and rainfall fields for the upper Blue Nile basin region were obtained from the IPCC data distribution center (Wegner, 2007).

The climate research unit TS 2.1 database includes nine climate elements and extends for the period 1901- 2002 (Mitchell and Jones, 2005). The database is checked for in homogeneities in the station records. It is based on the global network of observed meteorological data and interpolated onto a 0.5° grid covering the global land surface excluding Antarctica (Mitchell and Jones, 2005).

5.2.3 Bias correction

The CCLM and REMO regional model outputs were first bias corrected before they produce future scenarios and used for the hydrological modeling. The CCLM temperature data were corrected first by obtaining the difference between observation and the scenario data. Subsequently the difference was added onto the CCLM scenario data. For rainfall bias correction ratios between observation and scenario data were used and added to the scenario data.

The REMO data were bias corrected using a probabilistic approach called CDF-transform (Michelangeli et al., 2009). It is based on the assumption that there exists a transformation T allowing to translate the cumulative distribution functions (CDF) of a large scale variable (here REMO output), into the CDF representing the local-scale climate variable, i.e., predictand, at a given climate station. The CDF-t is an extension of Q-matching approach and it directly deals with and provides CDFs (Michelangeli et al., 2009). Although CDF-t and Q-matching have similarities, the CDF-t approach takes into account the change in the large-scale CDF from the historical to the future time period, while Q-matching only projects the simulated large-scale values onto the historical CDF to compute and match quantiles. In addition, Q-matching cannot provide local quantiles outside the range of the historical observations (Michelangeli et al., 2009; Wood et al., 2004).

Daily rainfall and temperature time series from sixteen climate stations in upper Blue Nile basin were used for the bias correction of REMO downscaled temperature and rainfall fields (Table 6). Observed data from 1961-1980 were used for calibration and from 1981-1990 for validation. Projected CDF were estimated for 1981-2100. The result of the bias correction was evaluated by using mean and variance during the validation period. The result of the bias correction of a typical station is provided in Appendix 3.

Table 6 Description of weather stations used for bias correction and hydrological modeling (Source: Ethiopian Meteorological Agency)

No.	Station	Latitude	Longitude	Altitude (m)	Data availability
1	Alem Ketemb	10° 1’ 48”	39° 1 48”	2280	1961-1990
2	Assosa	10° 1’ 12”	34° 31 12”	1600	1961-1990
3	Bahir Dar	11° 35’ 60”	37° 25 12”	1770	1961-1990
4	Debre Markos	10° 1’ 48”	37° 4’ 12”	2515	1961-1990
5	Debre Zeit	8° 43’ 48”	38° 57’	1900	1961-1990
6	Fiche	9° 48’	38° 42’	2750	1961-1990
7	Majete	10° 29’ 56”	39° 51’	2002	1961-1990
8	Makele	13° 30’	39° 28’ 48”	2070	1961-1990
9	Nefas Mewcha	11° 43’ 48”	38° 27’	3000	1961-1990
10	Shambo	9° 34’ 12”	37° 6’	2430	1961-1990
11	Addis Ababa	9° 1’ 48”	38° 45’	2408	1961-1990
12	Combolcha	11° 7’ 12”	39° 43’ 48”	1903	1961-1990
13	Bedele	8° 26’ 60”	36° 19’ 48”	2030	1961-1990
14	Jimma	7° 4’ 12”	36° 49’ 48”	1725	1961-1990
15	Nekemt	9° 4’ 48”	36° 28’ 12”	2080	1961-1990
16	Shola Gebeya	9° 3’	38° 46’ 12”	2500	1961-1990

5.2.4 Changes in rainfall and temperature at basin level

Results for the future scenarios were summarized into three periods (2011–2040, 2041–2070, and 2071–2100). Average annual temperature changes for the upper Blue Nile basin were 2011-2040: 1.5, 2041-2070: 2.6, and 2071-2100: 4.5 °C relative to the historical climate

based on the CCLM. Temperature changes based on REMO downscaling followed similar pattern with warming of 2011-2040: 1.5, 2041-2070: 2.8 and 2071-2100: 4.8 °C. REMO produced greater warming during 2041-2070 than during 2071-2100 as compared to CCLM (Table 7). The spatial distribution of temperature changes (Figure 17) in the upper Blue Nile basin based on the two regional models indicates that, in all the three periods of this century the models show both an increase and decrease in temperature with some areas showing constant temperature as compared to the historical mean (1961-1990). CCLM produced a much larger range of temperature change than the REMO regional model. The temperature ranges were 14.2, 14.4 and 14.5 °C for CCLM for 2011-2040, 2041-2070 and 2071-2100 respectively.

The CCLM downscaling resulted in less rain in the upper Blue Nile as compared to the REMO simulation (Table 8). Basin-average annual rainfall based on the CCLM downscaling were 1.8, -6.6 and -6.4% of observed historical rainfall (1961-1990) for future periods of 2011-2040, 2041-2070 and 2071-2100. These results are in contrast to the results of REMO downscaling, which showed a consistent increase of 9.2, 11.8 and 22.3% for 2011-2040, 2041-2070 and 2071-2100. The CCLM results showed a north-south bias, up to the middle of the century i.e. broadly wetter in the south and west and drier in the north and east. During the second half of the 21st century the pattern of the rain is less clear with possible wetter conditions in the west than east of the upper Blue Nile basin. Generally the CCLM scenario shows drier conditions in the second than the first half of the 21st century. The REMO result shows dry condition in the central part of the upper Blue Nile basin and wet conditions in the north-west and eastern parts of the basin for the 21st century (Figure 18).

Table 7. Changes of mean temperature under SRES A1B scenario under different downscaling techniques from 2071-2100 to 1961-1990 in the upper Blue Nile basin

Downscaling technique	Mean temperature (˚C)								
	2011-40			2041-70			2071-100		
	mean	SD	PI	mean	SD	PI	mean	SD	PI
COSMO-CCLM	20.1	2.7	8.0	21.5	2.8	13.8	23.4	2.8	23.9
REMO	20.4	3.1	8.0	21.7	3.1	14.9	23.7	3.0	25.5

SD=Standard deviation, PI=Percent increase

(Data source: Hattermann, 2011)

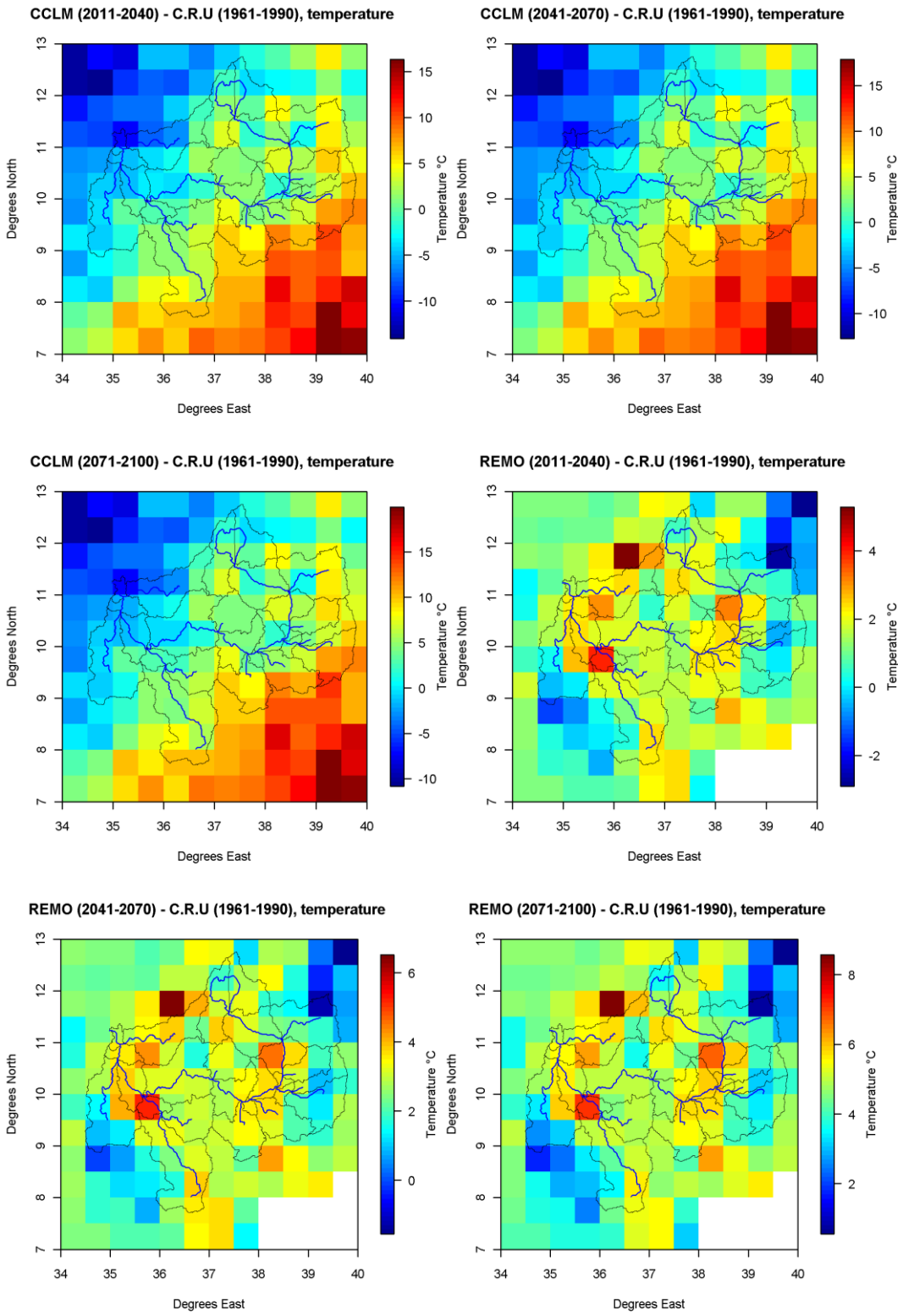

Fig. 17 Change in temperature in three time periods (2011-2040, 2041-2070, 2071-2100) as compared to observed CRU 2.1 temperature of ECHAM5 forced with CCLM and REMO
(Data source: Hattermann, 2011 and Mitchell, 2005)

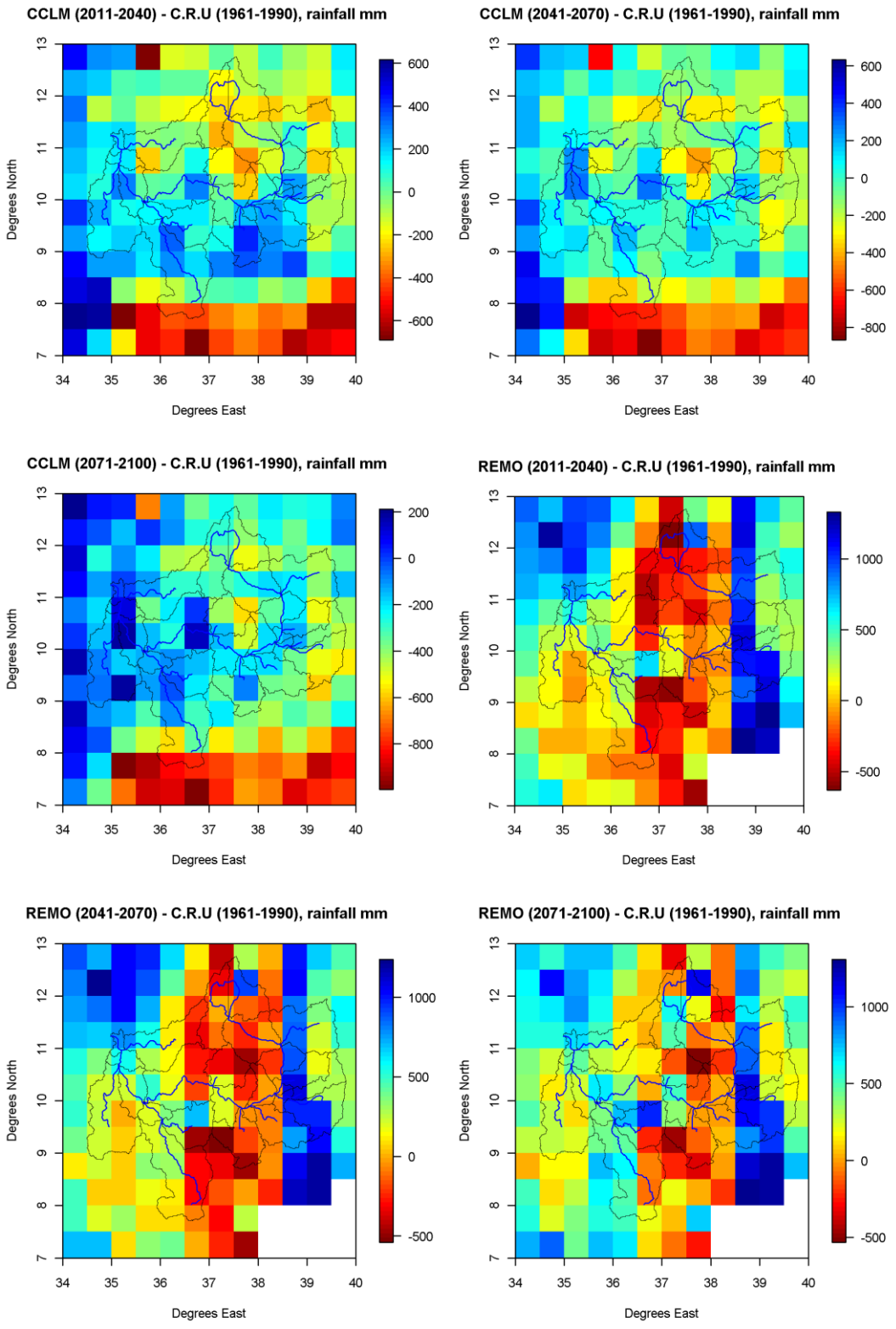

Fig. 18 Change in rainfall in three time periods (2011-2040, 2041-2070, 2071-2100) as compared to observed CRU 2.1 temperature of ECHAM5 forced with CCLM and REMO
(Data source: Hattermann, 2011 and Mitchell, 2005)

Table 8. Changes of mean precipitation under SRES A1B scenario under different downscaling techniques from 2071-2100 to 1961-1990 in the upper Blue Nile basin

	Rainfall (mm)								
	2011-40			2041-70			2071-100		
	Mean	SD	PI	mean	SD	PI/PD	mean	SD	PD
COSMO-CCLM	1340	263	1.8	1230	231	-6.6	1232	241	-6.4
REMO	1437	403	9.2	1472	356	11.8	1610	381	22.3

SD=Standard deviation, PI=Percent of increase, PD=Percent of decrease

(Data source: Hattermann, 2011)

5.2.5 Changes in rainfall and temperature at sub basin level

According to the Ministry of Water Resources of Ethiopia, the upper Blue Nile basin consists of fourteen sub-basins. The basins were delineated by considering the left and right bank tributaries separately and aggregating smaller sub-basins for development and planning purposes (MWR, 1998a). These are Tana, north Gojam, Beshilo, Welaka, Jemma, south Gojam, Muger, Guder, Finchaa, Dedesa, Anger, Wonbera, Dabus and Beles (Figure 19).

The sub basin level CCLM seasonal temperature scenarios for the upper Blue Nile basin are reported in three periods: 1983-2011, 2051-2070 and 2071-2100. Considering to period 1983-2011, which is a current climate scenario, Muger, Beles, and Welaka are the three warmest sub-basins with the mean annual temperature of 22.9, 22.4, and 22.4 °C respectively (Table 9). According to the CCLM current scenarios, the highest seasonal mean temperature was 25°C and it was from the Muger sub basin during *Belg* season while the lowest temperature of 15.9 °C was for the Fincha sub basin during *Bega* season. For the period of 2021-2051, Muger continues to be warm with a seasonal mean temperature of 26.5 °C during the *Belg* season. The lowest temperature for the same time period reported totals 16.8 °C during *Bega* in the Jemma sub basin. During the period, 2071-2100, Muger is expected to be warmer with an increase in temperature by 19% as compared to the temperature for the 1983-2011 period. North Gojam is expected to have the lowest temperature in the period2071-20100 even with an increase of 21% of during 1983-2011. Based on CCLM simulations in all the three periods and for all the seasons except *Kiremet*; Muger, Beles and Welaka are the three warmest sub basin in the upper Blue Nile basin.

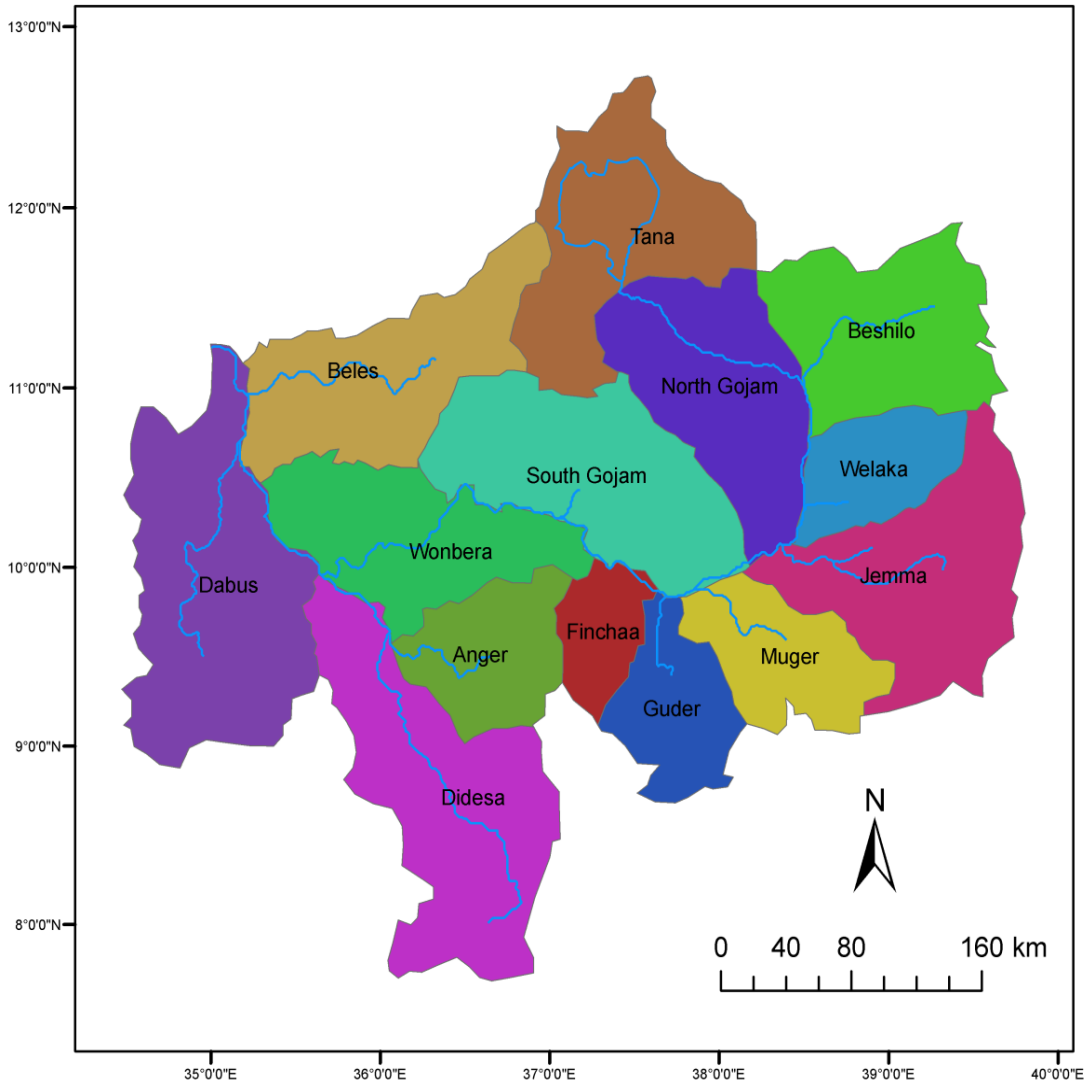

Fig. 19 the upper Blue Nile basin and its sub-basins based on the Ethiopian water resource basin delineation.
(Data source: Ministry of Water Resources of Ethiopia)

CCLM estimates a rise in seasonal mean temperature in the three periods mentioned above and for all the seasons. Generally, the changes in temperature during the *Belg* season are larger than during the other seasons for all sub-basins of the upper Blue Nile basin. This has a serious implication on food production especially in the eastern sub-basins such as North Gojam, Beshelo, Jemma and Welaka were the agriculture is commonly practiced during the season. The increase in temperature ranges from 0.7 to 0.9 °C for *Tseday*, 0.9 to 1 °C for *Bega*, 1.3 to 1.8 °C for *Belg* and 0.8- 1 °C for *Kiremt* between 1938-2011 and 2051-2070. Similarly the increase in temperature is highest during *belg* when periods 1983-2011 and

2071-2100 are compared. The increase in temperature reached to about 5°C for Beshelo, Welaka, Dabus sub-basins during the *Belg* season. An increase in temperature during the *Belg* season has an enormous effect on the flow of the upper Blue Nile as most of the flow during this period is from ground water flow rather than direct runoff as the distribution of the *Belg* rain is restricted to small portion of the watersheds. The increase in temperature in the sub-basins during the *Tseday* season is about 3.3, in *Bega* season is 3.8, *Bleg* 4.7 and during *Kiremet* 4.2 when the period 1983-2011 and 2051-2070 are compared.

Table 9 Mean seasonal CCLM current and future temperature scenarios, for the MoWR sub-basins of the upper Blue Nile River basin based on ECHAM5 A1B IPCC scenario.

ID	Sub basin	1983-2012				2021-2050				2071-2100			
		TSE	BEG	BEL	KIR	TSE	BEG	BEL	KIR	TSE	BEG	BEL	KIR
1	Tana	18.9	19.6	20.9	19.1	19.8	20.6	22.5	19.9	22.0	23.5	25.8	23.1
2	North Gojam	16.1	16.7	18.5	17.2	17.0	17.6	20.1	18.1	19.5	20.6	23.3	21.2
3	Beshilo	19.5	20.5	21.9	19.4	20.4	21.5	23.7	20.2	22.6	24.3	27.0	23.4
4	Welaka	21.6	22.1	24.3	21.5	22.4	23.1	26.0	22.4	24.7	25.9	29.3	25.9
5	Jemma	16.0	15.9	18.6	17.9	17.0	16.8	19.9	18.8	19.6	19.7	23.0	22.2
6	South Gojam	16.4	16.2	18.9	18.4	17.3	17.1	20.2	19.2	19.9	20.1	23.1	22.6
7	Muger	22.0	22.9	25.0	21.7	22.8	23.9	26.5	22.6	25.1	26.5	29.7	26.3
8	Guder	16.2	16.5	18.9	17.2	17.2	17.4	20.5	18.1	19.7	20.5	23.7	21.4
9	Finchaa	16.2	15.9	18.6	18.2	17.1	16.8	20.0	19.1	19.8	19.7	23.0	22.6
10	Didesa	18.4	18.2	21.2	18.8	19.3	19.2	22.8	19.7	21.7	21.9	25.9	23.3
11	Angar	17.7	18.4	20.6	18.0	18.6	19.4	22.3	18.9	20.9	22.2	25.4	22.1
12	Wonbera	17.1	17.8	19.3	17.5	18.0	18.7	21.0	18.3	20.4	21.8	24.2	21.3
13	Dabus	17.6	18.7	20.0	17.7	18.6	19.6	21.8	18.6	20.8	22.6	25.0	21.6
14	Beles	21.5	22.1	24.7	21.5	22.2	23.0	26.3	22.5	24.5	25.7	29.5	26.5

*TSE= Tsedey (Sep,Oct,Nov); BEG=Bega (Dec,Jan,Feb); BEL=Belg (Mar, Apr,May); KIR= Kiremt (June,July,August)
(Data source: Hattermann, 2011)

CHAPTERS 6 LAND USE CHANGE SCENARIOS IN THE UPPER BLUE NILE BASIN

6.1 Description of land use and land cover based on field investigation

A field trip was conducted in the upper Blue Nile basin in January 2010 to obtain firsthand information about the basin. Five sub-basins of upper Blue Nile basin namely Tana, Beles, Finchaa, Didessa and Dabus were the focus of the trip.

In most of the areas along the Addis-Bahir Dar-Gondar road, rainfed crop production is the main land use system with different kinds of crops and cropping patterns. Tef, niger seed, sorghum, maize, finger millet, wheat, lupine, check pea, lentil are commonly cultivated in these areas. There are also patches of plantation forest especially near Debre Markos planted during the Derg times (Figure 20b; Figure 20c)

Complex cropping patters are found in the basin. During the field trip, in places where the agro climatology is seems to be similar some portions of the farmers' land were having mature crops ready for harvest as the other parcels where cultivated for planting crops during the short (B*elg)* rain at the end of January. Such cases were seen in places near Debre Markos where the climate is locally classified as *Dega* and in the highlands of Finchaa sub basin.

The Bambo forests which are commonly found in the south western part of the upper Blue Nile basin is cover extensive area especially in the south western lowlands and it are also found in areas near Nekemte (Figure 20a). Widespread mango plantations are found in Ginbi area (Figure 20e). The Fincha area is of a particular interest in modelling the water resource of upper Blue Nile basin as wetlands are abundant in basin, which might regulates the Blue Nile flow (Figure 20f). Abay berha is the gorge where the Abay River descends to the south western lowlands from Lake Tana in the central highlands.

a) Bamboo forest near Assosa

d) Abay Berha and Blue Nile Gorge

b) Juniperous plantation near Debre Markos

e)Mango plantation at Gimbi

c) Eucalyptus plantation near Debre Markos

f) Wetlands at Fincha

Fig. 20 Typical land use and land cover of the upper Blue Nile basin
(Source: Photos taken by Michael Menker Girma)

It is covered by bushes and is prone to wild fire. The climate in this area is arid with very hot temperature and its incisions at some points reaches up to a kilometre (Figure 20d). Farmers who live at the edge of Abay bereha are facing difficulties in farming due to mass movements. Landscapes without clear surface drainage outlets near these areas are abundant as result of land subsidence.

6.2 Land use change scenarios

Future time land use change scenarios were developed in consultation with soil and water experts and through the review of watershed management project documents..Foreign direct investment and past trends in the basin was considered. Discussions with small holder farmers in different parts of the basin were also held and contributed in constructing climate change scenarios..

The likely future scenarios in the basin in the near future (2015-2030) would be an expansion of large scale irrigation following the tributaries of the upper Blue Nile particularly Beles, Koga, Fincha, Rib and Birr; upland area afforestation particularly near existing or proposed dam locations and expansion of private large scale irrigation schemes in the lowlands through foreign direct investment (Figure 21). Future land use change scenario was formulated by assessing planed projects in the basin for the expansion of irrigation (Table 10), considering the area allocated for foreign direct investment and considering present day afforestation activities and future plans.

The government of Ethiopia is attracting foreign direct investment by preparing cultivable land mostly in the Gambela, Benshangul Gumuz and Southern Nations and Nationalities regions of Ethiopia. The Federal Ministry of Agriculture of Ethiopia delineated around 3 million hectares of land for investment in the three regions of Ethiopia. About 1 million hectares of the prepared land is expected to be in Benshangul Gumuz region and in the upper Blue Nile basin of Ethiopia. Consequently, the future land use change scenario is prepared taking into account at least half of this area (500,000 ha) will be cultivated and converted into agricultural land in the future.

Recently many irrigation projects in the upper Blue Nile basin made watershed management a top priority. Some of the projects are IFAD special country program II, African development bank supported Koga large scale irrigation projects and ENTRO's fast-track watershed project in three major watersheds of the Blue Nile Basin: Rib, Jema and Gumera (Haileslassie et al., 2008).

Table 10 Summary of planned irrigation expansion projects in the upper Blue Nile basin

	Projects	Expected change in land use
1	Koga irrigation project	At koga area to be irrigated is 7000 ha but at the moment only 1000 ha is irrigated (NBI, 2010).
2	Tana Beles project	The Tana Beles Dam will be used for power generation and irrigation and will connect artificially the Tana and Beles sub-basins. The project is also expected to help irrigate 140,000 ha.
3	Fincha irrigation expansion project	The Fincha irrigation scheme existing irrigable area is about 8,700ha, which is located at west bank of Finchaa River. After accomplishment of the ongoing sugar cane expansion project located at east bank it will upgrade its capacity by 7,000ha cane field with expected cane production of 735,000 TC/year (WWDSE, 2011)
4	Rib irrigation project	The Rib dam is expected to irrigate a total of 20,000 ha in the Fogera plain.
5	Megech irrigation project	The proposed Megech dam and reservoir project will develop more than 7300 hectares of irrigated agriculture.

(Source: Indicated in the table and personal communication with the Ministry of Water Resources of Ethiopia)

Environmental bureaus of regional governments are also engaged on the afforestation efforts. For example the rural land administration and land use proclamation of the Amhara regional state encourages lands with a slope of higher than 60% to be put under conservation (Haileslassie et al., 2008). In formulating the future land use scenarios lands which are located in uplands and where some soil conservation activities have been already started were considered and allocated to the expansion of reforestation areas (Table 11).

Another land use change expected in the upper Blue Nile basin is the coverage of water bodies. As a result of the current trend of building dams in Ethiopia, it is expected that the area of the basin covered by water will increase in the near future. The grand millennium dam and the completion of the dams at Megech, Rib and Birr dam are expected to create large reservoirs in the basin. The grand millennium dam is expected to create an artificial lake of 40km width. It will be the largest hydropower dam in Africa and the 10th largest on Earth and will be twice the size of Ethiopia's largest natural Lake Tana.

Table 11 Existing and future land use change scenarios for the upper Blue Nile basin

	Land use type	Abbreviation	Existing coverage (km^2)	Future coverage (km^2)	PI/PD*
1.	Afroalphine	AFR	256.32	256.32	0.00
2	Arid rangeland	SWRN	8207.62	8207.62	0.00
3	Agriculture	AGRL	71975.60	76278.00	5.98
4	Grassland	RNGE	20151.50	19948.70	-1.01
5	Bamboo	BAMB	1072.03	1019.26	-4.92
6	Forest evergreen	FRSE	1614.84	1614.84	0.00
7	Forest mixed	FRST	252.55	558.63	121.20
8	Shrub land	SHRL	15428.40	13844.50	-10.27
9	Urban	URBN	9.80	9.80	0.00
10	Water	WATR	3139.21	5017.90	59.85
11	Wetland	WETL	651.36	635.53	-2.43
12	Wood land	WODL	34719.70	30087.80	-13.34

*PI=Percentage increase; PD=Percentage decrease

(Source: Own analysis, Data source: WBISPP, 2004)

For the design of the future land use scenarios the area coverage by water bodies is increased by 2000 km^2 taking into account the increasing trend in the reservoirs.

The increase of area coverage by agricultural land in the upper Blue Nile basin is expected to be at the same extension of wood land and shrub land. A small decline of the covered by

Bamboo forest and wetlands in the western lowlands is expected and formulated in the future land use scenario (Table 10).

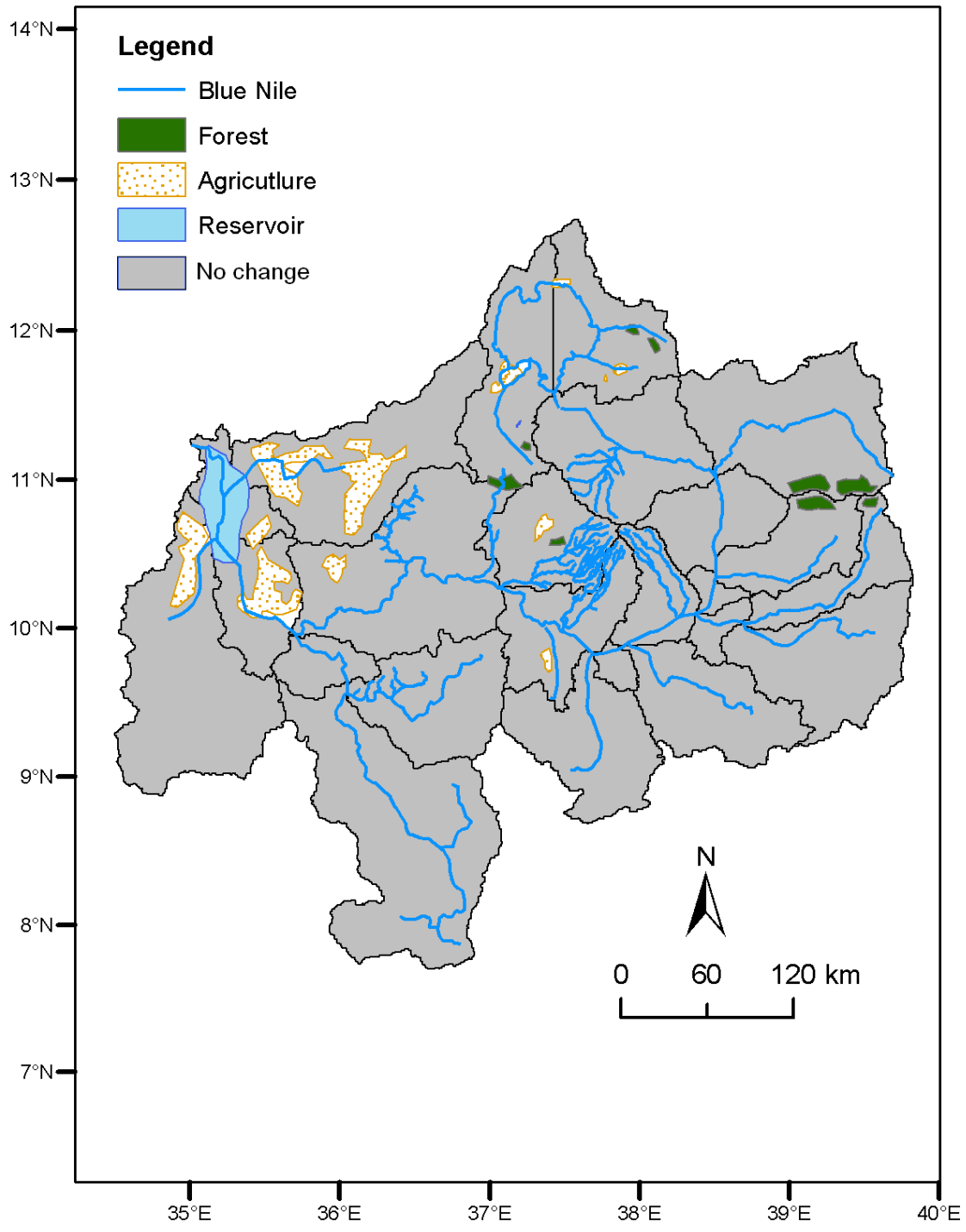

Fig. 21 Future land use scenario for the upper Blue Nile basin
(Source: Own analysis)

CHAPTER 7 IMPACT OF CLIMATE AND LAND USE CHANGE ON WATER RESOURCES

7.1 Soil and water assessment tool

7.1.1 Model description

The Soil and Water Assessment Tool (SWAT2009) was used to study the impact of climate and land use change on the water resources of the upper Blue Nile basin. SWAT is a river basin or watershed scale model developed to predict the impact of land management practices on water, sediment and agricultural chemical yields in large complex watersheds. The model is able to consider varying soils, land use and management conditions over long time period (Figure 22). The model is physically based and computationally efficient; it uses readily available inputs and allows users to study long-term impacts. SWAT is a continuous time model. The model is not designed to simulate detailed, single-event flood routing (Arnold et al., 1998).

SWAT requires the division of a watershed into sub watersheds. Each sub watershed is connected through a stream channel and further divided into Hydrologic Response Units (HRU). Hydrologic Response Units are unique combinations of soil and vegetation types in a sub watershed. SWAT simulates hydrology, vegetation growth, and management practices at the Hydrologic Response Unit level. Water, nutrients, sediment, and other pollutants from each Hydrologic Response Units are summarized for each sub watershed and then routed through the stream network to the watershed outlet.

The hydrological cycle in SWAT is simulated using the following water balance equation:

$$\boldsymbol{SW_t = SW_o + \sum_{i=1}^{t}(R_{day} - Q_{surf} - E_a - W_{seep} - Q_{gw})}$$ **----------eq. 1**

Where SW_t is the final soil water content (mm H_2O)

SW_0 is the initial soil water content on day i (mm H_2O)

t is the time (days)

R_{day} is the amount of precipitation on day i (mm H_2O)

Q_{surf} is the amount of surface runoff on day i (mm H_2O)

E_a is the amount of evapotranspiration on day i (mm H_2O)

Q_{gw} is the amount of return flow on day i (mm H_2O)

W_{seep} is the amount of water entering the vadose zone from the soil profile on day i (mm H_2O)

The following is a description of key processes and algorithms used in SWAT during the set up of the model for the upper Blue Nile basin. The description is taken from SWAT theoretical manual (Neitsch et al., 2011).

7.1.2 Climate input and climate data generation

The climate variables required by SWAT are daily precipitation, maximum and minimum air temperature, solar radiation, wind speed and relative humidity. Climate data are handled in SWAT2009 in two ways: First the user prepares average monthly weather indices to be used by SWAT climate generator and input the available observed daily data into SWAT.

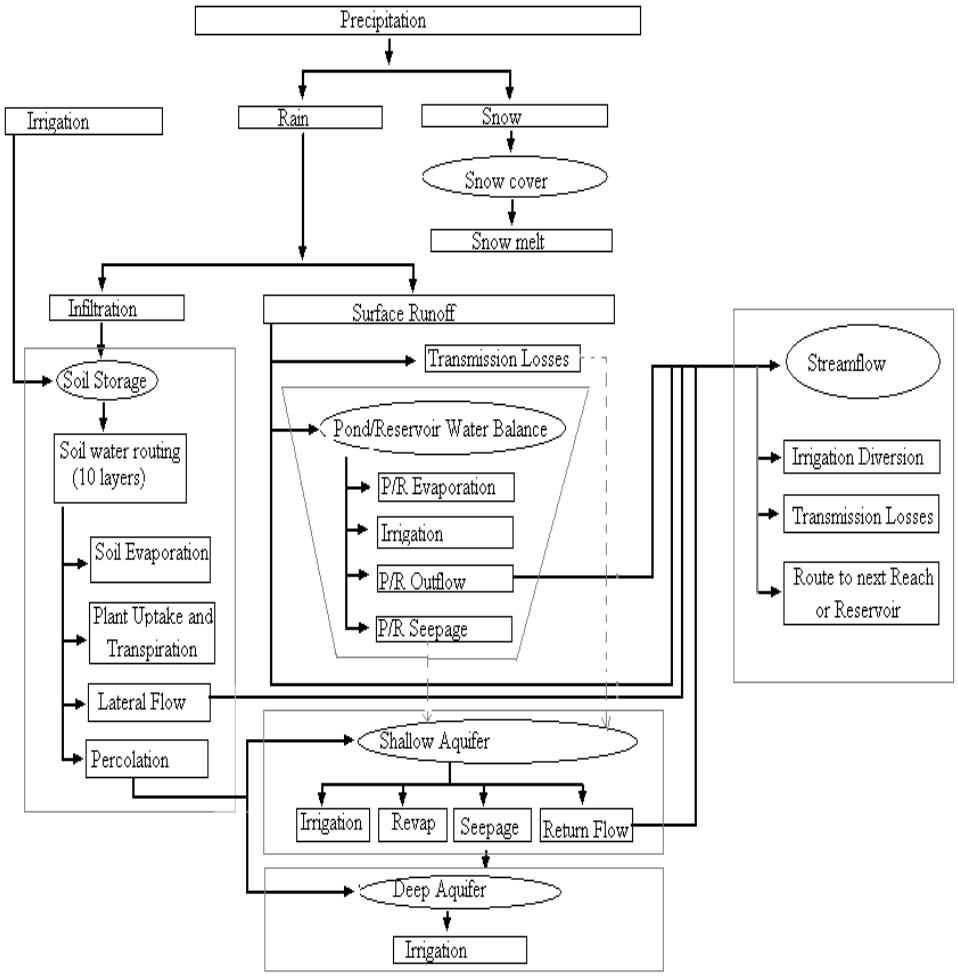

Fig. 22 Main components and processes in SWAT hydrological modeling (Neitsch et al., 2011).

Second, in case observed weather data are not available or missing values occur in the measured datasets, the average monthly weather generator information will be utilized to generate climate data.

SWAT uses a first-order Markov chain model developed by Nicks (1974) to generate daily precipitation by comparing a particular day with the monthly wet-dry probabilities of the weather generator monthly input data and defining the day as wet or dry. If a day is classified as wet, the amount of precipitation is generated from a skewed distribution or a modified exponential distribution (Neitsch et al., 2011).

Maximum and minimum air temperatures and solar radiation are generated from a normal distribution. A continuity equation is incorporated into the SWAT weather generator to account for temperature and radiation variations caused by dry vs. rainy conditions. A modified exponential equation is used to generate daily mean wind speed using the mean monthly wind speed. The relative humidity model uses a triangular distribution to simulate the daily average relative humidity from the monthly average. As with temperature and radiation, SWAT uses the continuity equation to adjust the mean daily relative humidity to account for wet- and dry-day effects (Neitsch et al., 2011).

7.1.3 Surface runoff

Surface runoff is calculated using a modified soil conservation service curve number method (Soil Conservation Service, 1972). The curve number varies non-linearly with the moisture content of the soil. The curve number drops as the soil approaches the wilting point and increases to near 100 as the soil approaches saturation. The lower the curve number, the more permeable the soil is (Neitsch et al., 2011).

$$Q_{surf} = \frac{(R_{day} - I_a)^2}{(R_{day} - I_a + S)} \quad \text{(eq. 2)}$$

Where Q_{surf} is the accumulated runoff or rainfall excess (mm),

R_{day} is the rainfall depth for the day (mm);

I_a is the initial abstractions which includes surface storage, interception and infiltration prior to runoff (mm) and

S is the retention parameter (mm).

The retention parameter varies spatially due to changes in soil, land use, management and slope and temporally due to changes in soil water content. The retention parameter is defined as (Neitsch et al., 2011):

$$S = 25.4\left(\frac{1000}{CN} - 10\right)$$ …… (eq. 3)

Where, CN is the curve number for the day;
I_a is the initial abstractions

Canopy interception is the function of plant type and cover (Neitsch et al., 2011) . It affects infiltration, surface runoff and evapotranspiration. When the soil conservation curve number method is used for the calculation of runoff, the canopy interception is included in the term for initial abstractions that also includes surface storage and infiltration and is estimated as 20% of the retention parameter value for a given day. Thus the above equation becomes (Neitsch et al., 2011):

$$Q_{surf} = \frac{(R_{day} - 0.2S)^2}{(R_{day} + 0.8S)}$$ …….. (eq.4)

Runoff occurs when $R_{day} > I_a$.

The Curve number is a function of the soil's permeability, land use and antecedent soil water conditions(Neitsch et al., 2011). The daily curve number value adjusted for moisture content is calculated by rearranging the above equation and inserting the retention parameter calculated for that moisture content:

$$CN = \frac{25400}{(S + 254)}$$……(eq.5)

Where, CN is the curve number on a given day and S is the retention parameter calculated for the moisture content of the soil through the streambed. Swat is capable of adjusting curve numbers for slope. It uses an equation developed by Williams(1995).

Some portion of the surface flow can be lost via leaching through the streambed. These losses are known as transmission losses. It occurs in ephemeral or intermittent streams where groundwater contribution occurs only at certain times of the year, or not at all

(Neitsch et al., 2011). SWAT uses Lane's method to estimate transmission losses. Both runoff volume and peak rate are adjusted when transmission losses occur in tributary channels (Neitsch et al., 2011).

7.1.4 Evapotranspiration

Evapotranspiration includes evaporation from the plant canopy, transpiration, sublimation and evaporation from the soil (Neitsch et al., 2011). SWAT has three methods. One of them, the Priestley-Taylor method requires solar radiation, air temperature and relative humidity input variables (Neitsch et al., 2011).

$$\lambda E_o = \alpha_{pet} \times \frac{\Delta}{\Delta+\gamma}(H_{net} - G) \quad \text{.....(eq. 6)}$$

Where λ is the latent heat of vaporization (MJ kg^{-1}),
Eo is the potential evapotranspiration (mm d^{-1}),
α_{pet} is a coefficient,
Δ is the slope of the saturation vapor pressure-temperature curve, de/dT (kPa $°C^{-1}$),
γ is the psychrometric constant (kPa $°C^{-1}$),
Hnet is the net radiation (MJ m^{-2} d^{-1}),
G is the heat flux density to the ground (MJ m^{-2} d^{-1}).

Actual evaporation is calculated in SWAT, first by evaporating rainfall intercepted by the plant canopy and then by calculating the maximum amount of transpiration and the maximum amount of sublimation/soil evaporation (Neitsch et al., 2011).

7.1.5 Soil water

Water may be removed from the soil by plant uptake or evaporation. It can percolate below the bottom of the soil profile and ultimately become aquifer recharge. The water may move laterally in the profile and contribute to stream flow (Neitsch et al., 2011).

Percolation is calculated for each soil layer of the profile. Water is allowed to percolate if the water content exceeds the field capacity water content for that layer and the layer below is not saturated (Neitsch et al., 2011). The amount of water that moves from one layer to the underlying layer is calculated using storage routing methodology. Water that percolates out of the lowest soil layer enters the vadose zone (Neitsch et al., 2011). Lateral subsurface flow,

or interflow is stream flow contribution which originates below the surface but above the zone where rocks are saturated with water (Neitsch et al., 2011). A kinematic storage model is used to predict lateral flow in each soil layer. The model accounts for variation in conductivity, slope and soil water (Neitsch et al., 2011).

7.1.6 Ground water

Water enters into the groundwater storage primarily by infiltration/percolation. Water leaves groundwater storage primarily by discharge into rivers or lakes (Neitsch et al., 2011). Return flow or base flow is the volume of stream flow originating from groundwater (Neitsch et al., 2011). SWAT partitions groundwater into two aquifer systems: a shallow, unconfined aquifer which contributes return flow to streams within the watershed and a deep, confined aquifer which contributes return flow to streams outside the watershed (Neitsch et al., 2011). Water percolating past the bottom of the root zone is partitioned into two fractions-each faction becomes recharge for one of the aquifers. In addition to return flow, water stored in the shallow aquifer may replenish moisture in the soil profile in very dry conditions or be directly removed by plant (Neitsch et al., 2011).

An exponential decay weighting function of precipitation /groundwater response model is utilized in SWAT to account for the time delay in aquifer recharge once the water exits the soil profile. The steady-state response of groundwater flow to recharge is given by (Neitsch et al., 2011):

$$Q_{gw} = \frac{8000 * K_{sat}}{L_{gw}^2} \times h_{wtbl} \quad \text{……(eq. 7)}$$

Where Q_{gw} is the ground water flow into the main channel on day i
K_{sat} is the hydraulic conductivity of the aquifer (mm/day)
L_{gw} is the distance from the ridge or sub basin divide for the groundwater system to the main channel (m)
H_{wtbl} is the water table height (m)

Water table fluctuations due to no steady state response of groundwater flow to periodic recharge is calculated in SWAT following the method of Smedema and Rycroft (1983).

7.1.7 Land cover/plant growth

The plant growth component of SWAT is based on the cropping systems simulation model, EPIC. Phenological plant development is based on daily accumulated heat units. Potential biomass is calculated based on a method developed by Monteith. According to the model used by SWAT temperature, water and nutrients can inhibit plant growth (Neitsch et al., 2011). The growth cycle of a plant is controlled by plant attributes in the plant growth database and by the timing of operations provided in the management database.

The heat unit concept is based on the theory that plants have heat requirements that can be quantified and linked to time to maturity (Neitsch et al., 2011). According to this theory the only portion of the mean daily temperature that contributes towards plant development is the amount that exceeds the base temperature (Neitsch et al., 2011). To measure the total heat requirements of a plant, the accumulation of daily mean air temperatures above the plant's base temperature is recorded over the period of the plant's growth and expressed in terms of heat units. The heat unit accumulation for a given day is calculated with the equation (Neitsch et al., 2011):

$HU = T_{av} - T_{base}$ When $T_{av} > T_{base}$ ……(eq. 8)

Where, HU is the number of heat units accumulated on a given day (heat units),
T_{av} is the mean daily temperature (°C), and
T_{base} is the plant's base or minimum temperature for growth (°C).

The total number of heat units required for a plant to reach maturity is calculated : (Neitsch et al., 2011)

$\mathrm{PHU} = \sum_{d=1}^{m} \mathrm{HU}$……(eq. 9)

Where PHU is the total heat units required for plant maturity (heat units), HU is the number of heat units accumulated on day d where d=1 on the day of planting and m is the number of days required for a plant to reach maturity.

SWAT allows management operations to be scheduled by day or by fraction of potential heat units.

7.1.8 Management practices

SWAT allows management practices to be defined at Hydrological Response Units level. This can be done by defining the beginning and the ending of growing season. At the end of the growing season, the biomass may be removed from the Hydrological Response Units as yield or placed on the surface as residue. Other options are harvest operations, grazing, harvest and kill operations, and kill and end of growing season(Neitsch et al., 2011) .

7.1.9 Flood routing

SWAT provides two methods to simulate water routing in stream network. These are variable storage routing method and (flow continuity equation) (Neitsch et al., 2011) and the Muskingum routing method (wedge and prism storage) (Neitsch et al., 2011). In this research the variable storage method is employed.

7.1.10 SWAT calibration parameters

Five of the SWAT calibration parameters which are used for the calibration of the SWAT model are discussed below (Neitsch et al., 2010)..

Surface runoff lag coefficient (SURLAG)

In large sub-basins with a time of concentration greater than 1 day, only a portion of the surface runoff will reach the main channel on the day it is generated. SWAT incorporates a surface runoff storage feature to lag a portion of the surface runoff release to the main channel (Neitsch et al., 2010). The surface runoff lag coefficient controls the fraction of the total available water that will be allowed to enter the reach on any one day. For a given time of concentration, as The surface runoff lag coefficient decreases in value more water is held in storage. The delay in release of surface runoff will smooth the stream flow hydrograph simulated in the reach (Neitsch et al., 2010).

Time of concentration is defined as the time needed for water to flow from the most remote point in a watershed to the watershed outlet. It is a function of the topography, geology, and land use within the watershed (Neitsch et al., 2010)

Groundwater delay time (GW_DELAY)

Water that moves below the lowest layer of the soil profile by percolation or bypass flow enters and flows through the vadose zone before becoming shallow aquifer recharge (Neitsch et al., 2010). The lag between the time that water exits the soil profile and enters the shallow aquifer will depend on the depth to the water table and the hydraulic properties of the geologic formations in the vadose and groundwater zones (Neitsch et al., 2010). The delay timecannot be directly measured (Neitsch et al., 2010). It can be estimated by simulating aquifer recharge using different values for δgw and comparing the simulated variations in water table level with observed values. It was noted that monitoring wells in the same area had similar values for delay time, so once a delay time value for a geomorphic area is defined, similar delay times can be used in adjoining watersheds within the same geomorphic province (Neitsch et al., 2010).

Base flow alpha factor (ALPHA_BF)

The base flow recession constantis a direct index of groundwater flow response to changes in recharge. Values vary from 0.1-0.3 for land with slow response to recharge to 0.9-1.0 for land with a rapid response (Neitsch et al., 2010). Although the base flow recession constant may be calculated, the best estimates are obtained by analyzing measured stream flow during periods of no recharge in the watershed. It is common to find the base flow days reported for a stream gauge. This is the number of days for base flow recession to decline through one log cycle. When base flow days are known, the alpha factor can be calculated (Neitsch et al., 2010):

$$\alpha_{gw} = \frac{1}{N} ln \left[\frac{Q_{gw,N}}{Q_{gw,O}}\right] = \frac{1}{BFD} \times \ln [10] = \frac{2.3}{BFD} \quad \text{(eq. 10)}$$

Where α_{gw} is the base flow recession constant, and BFD is the number of base flow days for the watershed.

Deep aquifer percolation fraction (RCHRG_DP)

RCHRG DP is the fraction of percolation from the root zone which recharges the deep aquifer. The value for RCHRG_DP should be between 0.0 and 1.0.

SWAT simulates two aquifers in sub-basins. The shallow aquifer is an unconfined aquifer that contributes to flow in the main channel or reach of sub-basin. The deep aquifer is a confined aquifer. Water that enters the deep aquifer is assumed to contribute to streamflow outside of the basin (Neitsche et al, 2009).

The amount of water that will be diverted from the shallow aquifer due to percolation to the deep aquifer on a given day is:

$W_{deep} = \beta_{deep} * W_{rchrg}$ .....(eq 11)

Where, W_{deep} is the amount of water moving into the deep aquifer on day I,
β_{deep} is the aquifer percolation coefficient (Deep aquifer percolation fraction)
W_{rchrg} is the amount of recharge entering both aquifers on day i

Initial Soil Conservation Service (SCS) runoff curve number for moisture condition II (CN2)

The SCS curve number is a function of the soil's permeability, land use and antecedent soil water conditions. Typical curve numbers for moisture condition II are given in SCS Engineering Division (1986). These values are appropriate for a 5% slope. The curve number may be updated in plant, tillage, and harvest/ kill operations. If the SCS runoff curve number for moisture condition II (CNOP) is never defined for these operations, the value set for initial SCS runoff curve number for moisture condition II i.e. CN2 will be used throughout the simulation. If the SCS runoff curve number for moisture condition II is defined for an operation, the value for CN2 is used until the time of the operation containing the first SCS runoff curve number for moisture condition II value. From that point on, the model only uses operation the SCS runoff curve number for moisture condition II values to define the curve number for moisture condition II. Values for Initial Soil Conservation Service (SCS) runoff curve number for moisture condition II and the SCS runoff curve number for moisture condition II should be entered for pervious conditions. In Hydrological Response Units with

urban areas, the model will adjust the curve number to reflect the impact of the impervious areas (Neitsch et al., 2010).

7.2 SWAT setup for the upper Blue Nile basin

SWAT2009 is used to study the impact of climate change on the water resources of upper Blue Nile basin. The major steps employed were watershed delineation, determination of hydrological response units, preparation of climate and weather generation data, development of soil, land use and plant growth databases, and processing of input files. A two way hierarchal chart shows the steps followed in setting up the input files for swat model in the upper Blue Nile. These are mainly spatial data and climate parameters used latter to run the model.

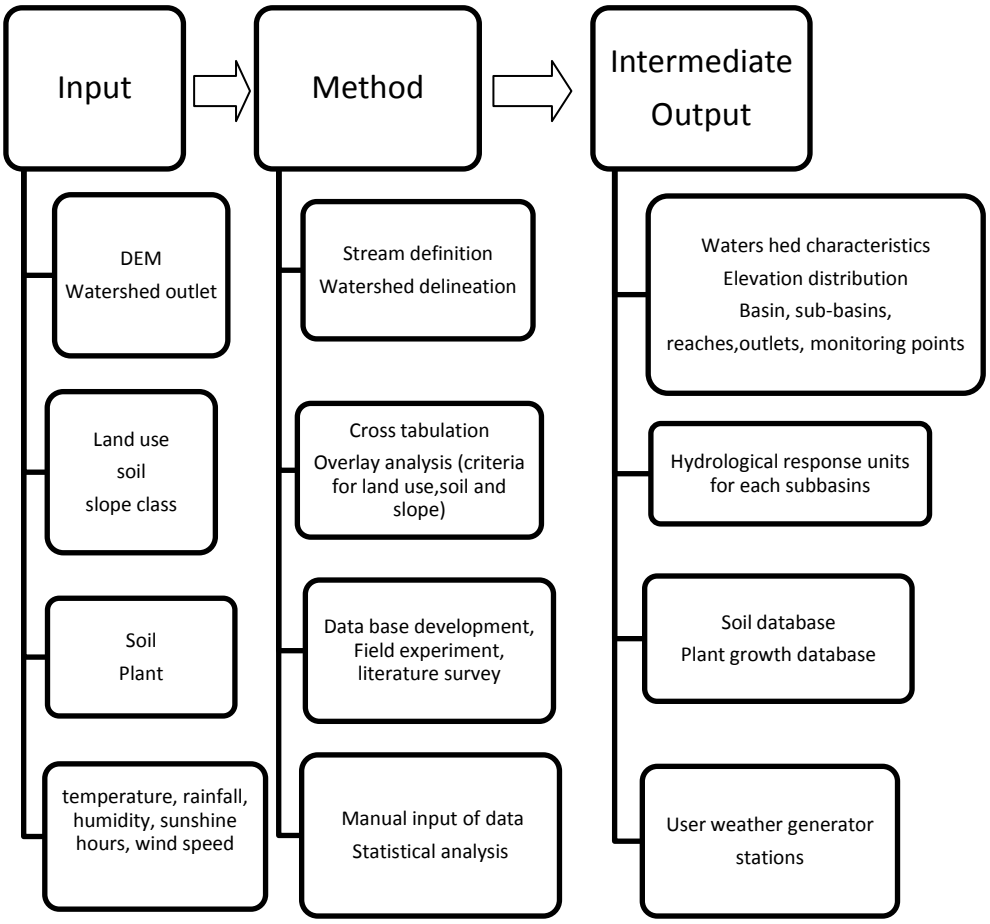

Fig. 23 Flow chart of inputs, methods and intermediate outputs used in setting up a model for the upper Blue Nile basin.

Based on the intermediate outputs (Figure 23), the initial watershed input values were prepared for the simulation of the runoff using SWAT. The initial inputs files created include

soil data, weather generator data, sub basin general data, hydrological response unit general data, main channel data, groundwater data, management data, watershed general data, master watershed file and configuration file.

7.2.1 Model inputs

The model inputs used were:

- SRTM digital elevation model with a horizontal resolution of 90 m (Jarvis et al., 2008);
- A detail land use from the Ethiopian woody biomass project with a scale of 1:250,000 (WBISPP, 2004);
- Soil map and data from the Abay master plan project with a scale of 1:250,000 (MWR, 1999);
- Daily temperature, precipitation, solar radiation, and wind speed from the Ethiopian meteorological agency;
- Plant and soil management databases based on literature survey and field survey and
- Discharge data from the Ethiopian ministry of water resources.

7.2.2 Watershed delineation

ArcGIS with ArcSWAT extension was used to delineate the upper Blue Nile basin. In ArcSWAT the upper Blue Nile river basin was delineated using SRTM DEM up-stream of El Diem gauge (latitude 11.23, longitude 34.99; See Figure 3). Due to the large size of the basin, limited capacity of the available computing machine (dual core, 2GB) and software for delineation, the resolution of the SRTM DEM was reduced to 800m. Based on an area threshold of 60,000 km^2, the ArcSWAT interface was used to delineate 25 sub-basins within the upper Blue Nile basin. Satellite maps and topographic maps were employed in order to identify basin outlet and to extract the river network for watershed delineation.

After the watershed delineation the total area of the upper Blue Nile basin is found to be 157,941.1 km^2. During the watershed delineation process it was noted that the area of upper Blue Nile depends on the type of geographical information system software used. The total area delineated by ArcHydro of ArcGis 9.3 was smaller than the area delineated by raster software IDRISI which resulted in about 170,000 km^2 while both software used the same horizontal resolution and type of DEM and outlet points. The difference in area was

considered as a software issue and the output from ArcGIS was used as the ArcSWAT version of the SWAT model is preferred for modeling stream flow in the basin.

7.2.3 Hydrologic response units

In order to account for differences in evapotranspiration and other hydrologic conditions, hydrologic response units were created for the upper Blue Nile basin based on differences in land use, soil and slope. After overly analysis of the three data layers, the sub-basins of the upper Blue Nile basin were divided into 244 hydrologic response units.

In SWAT, the distribution of hydrologic response units within the watershed is defined by the HRUs definition command. Using this command one or more unique land use/soil/slope combinations can be created for each sub-basin. If a single hydrologic response unit per sub-basin is selected, the hydrologic response unit is determined by the dominant land use category, soil type and slope class within each watershed. If multiple hydrologic response units are selected, the user specify sensitivities for the land use, soil and slope data that will be used to determine the number and kind of HRUs in each watershed (Winchell et al, 2007). In this study multiple HRUs were assigned to each sub-basin. For the definition of multiple hydrologic response units, a land use threshold of 5%, a soil threshold of 20% and a slope threshold of 20% were used. Finally, runoff was predicted separately for each hydrologic response unit and routed to obtain total runoff for the entire watershed.

Soil

Soil data provided by the Ethiopian Abay basin master plan document are available at a scale of 1:25000 is used for the above purpose. In the basin there are eleven soil types with twenty soil classes. The major soil types are Leptosols, Alisols, Nitosols, and Vertisols (Figure 24). Haplic alisols, eutric leptosols, haplic nitosols, eutric vertisols and eutric cambisols constitutes about 61% of the area of the basin.

Table 12 Soil classes of the upper Blue Nile basin used as input in SWAT

No.	Soil class	Description	Area (km^2)
1	HAPACR	Haplic Acrisols	7030.04
2	HAPALI	Haplic Alisols	36699.45
3	CAMARE	Cambic Arenesols	566.93
4	HAPARE	Haplic Arenesols	637.79
5	DYSCAM	Dystric Cambisols	659.66
6	EUTCAM	Eutric Cambisols	11516.45
7	VERCAM	Vertic Cambisols	968
8	EUTFLU	Eutric Fluvisols	4746.5
9	DYSLEP	Dystric Leptosols	2118.44
10	EUTLEP	Eutric Leptosols	30555.24
11	LITLEP	Lithic Leptosols	548.08
12	RENLEP	Rendzic Leptosols	4774.4
13	CHRLUV	Chromic Luvisols	4473.59
14	HAPLUV	Haplic Luvisols	6474.42
15	MARSH	-	700.37
16	HAPNIT	Haplic Nitosols	14805.68
17	RHONIT	Rhodic Nitosols	10383.35
18	HAPPHA	Haplic Phaezoms	73.13
19	EUTREG	Eutric Regosols	1136.11
20	URBAN	-	42.22
21	CAMVER	Cambic Vertisols	2015.15
22	EUTVER	Eutric Vertisols	14054.05
23	WATER	-	2923.59

(Data source: Ministry of Water Resources of Ethiopia)

The soil classes together with their corresponding codes for swat database were Haplic Acrisols (HAPACR), Haplic Alisols (HAPALI) , Cambic Arenosols (CAMARE), Haplic Arenosols (HAPARE), Dystric Cambisols (DYSCAM), Eutric Cambisols (EUTCAM), Vertic Cambisols (VERCAM), Eutric Fluvisols (EUTFLU), Dystric Leptosols (DYSLEP), Eutric Leptosols (EUTLEP), Lithic Leptosols (LITLEP), Rendzic Leptososls (RENLEP), Cromic Luvisols (CROLUV), Haplic Luvisols (HAPLUV), Haplic Nitosols (HAPNIT), Rhodic Nitosols (RHONIT), Haplic Phaezoms (HAPPHA), Eutric Regosols (EUTREG), Cambic Vertisols (CAMVER), Eutric Vertisols (EUTVER).

Land use

Land use data from the Ethiopian Woody Biomass Project are used for the hydrological modeling. The detailed dataset is generalized into twelve main land use classes for the hydrological modeling (Figure 25). Agriculture (AGRL), afro-alpine (AFRA), shrub land (SHRL), water (WATR), wood land (WODL), wetland (WETL), forest ever green (FRSE), forest mixed (FRST), bamboo (BAMB), grassland (RNGE), arid rangeland (SWRN) and urban (URBN). About 45 % of the basin is cultivated with different kinds of annual and perennial crops. Wood land together with grass land consists of 35% of the basin. The coverage of forest is low with only 1.1% of the basin.

Table 13 Land use classes of the upper Blue Nile basin used as input in SWAT

No.	Land use classes	Description	Area (km^2)
1	AFRA	Afro-alpine	256.32
2	SWRN	Arid rangeland	8207.62
3	AGRL	Agriculture	71975.60
4	RNGE	Grassland	20151.50
5	BAMB	Bambo	1072.03
6	FRSE	Evergreen forest	1614.84
7	FRST	Mixed forest	252.55
8	SHRL	Shrub land	15428.40
9	URBN	-	9.80
10	WATR	-	3139.21
11	WETL	Wetland	651.36
12	WODL	Wood land	34719.70

(Source: Own analysis; Data source: WBISPP, 2004)

Slope

Slope for the upper Blue Nile basin is generated from the SRTM Digital Elevation Model after projecting the data into equal area projection. The slopes of the basin range from flat to 58% inclination. Most of the eastern part of the basin is mountainous with slopes ranging from 10-58% inclination. The flat lands are located in the north east particularly in the Beles and Tana basins and in the south west, Dabus sub basin. Five slope classes were used for the purpose of hydrologic response unit definition in SWAT. The classes were 0-3%, 3-12%, 12-24%, 24-45% and 45-58%.

7.2.4 Soil, land cover and plant growth database

SWAT uses six databases to store information required for soil, plant growth, urban land characteristics, tillage, fertilizer components and pesticide properties (Neitsch et al, 2002). Among these the soil and plant growth databases were developed to simulate runoff in the upper Blue Nile basin.

The user soils database is used to store custom soil data. Providing data using this database is required for projects which do not use the US Soil Database included in SWAT (Neitsch et al, 2002). The soil database for the upper Blue Nile basin was developed based on the soil types of the upper Blue Nile basin, information from project documents and measured and calculated infiltration and hydraulic conductivity values from the major soils of the upper Blue Nile basin.

The soil data were input into the SWAT model based on soil layers. Depending on the availability of data from different profiles in the basin, depths ranging from 0.8 to 2 m were used in providing the soil data. The major soil parameters used in SWAT user soil database were soil hydrologic group, maximum root zone, hydraulic conductivity, percent of clay, silt, sand and rock; soil bulk density, and soil electrical conductivity.

The land cover/plant growth database for the upper Blue Nile basin was established through modification of the available plant growth parameters in the land cover/plant growth database of SWAT using literature (WBISPP, 2004; WWDSE, 2011; NBI, 2010) on plant parameters in Ethiopia and through the introduction of special crop types such as Bamboo and Afro alpine. The types of land covers used in the plant cover database are provided under the chapter 4.5. For each of the land cover types, the following major parameters were used in the SWAT: plant cover database; base temperature, leaf area development, energy biomass conversion, stomatal conductance, canopy height, root depth, plant nutrient content, and harvest indexes.

7.2.5 Climate and weather generator data

Observed daily climate data for the period of 1961-1990, from sixteen climate stations (Table 6) in and around the upper Blue Nile basin were prepared to be used for the hydrological modeling. The climate variables include minimum temperature, maximum temperature, rainfall, humidity, sunshine hours, and wind speed. R program codes were developed and used to produce the weather generator data and to prepare the climate datasets in SWAT format (Appendix 1). All climatic parameters were used in preparing the monthly weather generator data. Due to missing data and short records, only daily precipitation and temperature time series were used as direct input for SWAT, other parameters such as solar radiation and humidity were generated using the weather generator. Out of the fifteen stations SWAT automatically selected eight stations (Assosa, Alem ketema, Bahir Dar, Bedele, Debre Markos, Fiche, Nefas Mewcha and Shambo) and assigned to each sub-basin based on proximity.

Climate projections from CCLM and REMO were obtained in grids of 0.5° x 0.5° horizontal resolution. Future climate change scenarios for SWAT were extracted by superimposing the locations of the eight stations used to simulate historical runoff over the grids of the regional models.

7.3 Model calibration and validation results

The SWAT2009 model was calibrated and validated using measured stream flow data collected at El Diem located on the main Blue Nile River in Sudan near the Ethiopian border. A split year approach was followed during the calibration. The total available historical discharge data (1961-1990) were divided into two sets: 20 years (1961-1980) for calibration and 10 years for validation (1981-1990).

SWAT2009 was run for historical and future periods in order to study the impact of climate change. First, the model was calibrated using observed discharge data. Then using the calibrated model, SWAT was run for two future period climate change scenarios (2041-2070 and 2071-2100). The climate change data used were dynamically downscaled temperature

and rainfall time series of ECHAM5 global circulation model outputs based on the IPCC SRES-AR4 A1B scenario.

7.3.1 Parameter estimation software

Parameter ESTimation (PEST) software developed by Doherty (2004) was used for automatic calibration of SWAT parameters. It is a model independent parameter estimator with advanced predictive analysis and regularization features. Its model independence relies on its ability to communicate with a model through the model's input and output files, which allows easy calibration setup with different models. PEST implements a variant of the Gauss-Marquardt-Levenberg method of parameter estimation (Watermark Numerical Computing, 2010).

PEST "calibrates" a model by reducing the discrepancies between model outputs and field observations to a minimum in the weighted least squares sense. The differences between field measurements and model outputs are encapsulated in an "objective function" defined as the weighted sum of squared deviations between field observations and corresponding model outputs. As PEST executes, it progressively reduces this objective function until it can reduce it no more (Watermark Numerical Computing, 2010).

7.3.2 Sensitivity analysis

Model sensitivity analysis assesses the relative sensitivity of the model output with respect to the changing of model parameters. Sensitivity analysis was performed using PEST (Watermark Numerical Computing, 2010). It calculates a figure related to the sensitivity of each parameter with respect to all observations based on the Jacobian matrix (Watermark Numerical Computing, 2010). The "composite sensitivity" of parameter i is defined as;

$$S_i = \frac{(J^t Q J)_{ii}{}^{1/2}}{m} \quad \text{.....(eq. 11)}$$

Where, J-is the Jacobian matrix;

Q- is the "cofactor matrix"; a diagonal matrix whose elements consist of the squared observation weights;

m- is the number of observations with non-zero weights.

Thus, the composite sensitivity of the i^{th} parameter is the normalized value with respect to the number of observations (Watermark Numerical Computing, 2010). The relative composite sensitivity of a parameter is obtained by multiplying its composite sensitivity by the magnitude of the value of the parameter. It is thus a measure of the composite changes in model outputs that are incurred by a fractional change in the value of the parameter.

Composite parameter sensitivities are useful in identifying those parameters which may be degrading the performance of the parameter estimation process through lack of sensitivity to model outcomes (Watermark Numerical Computing, 2010). The use of relative sensitivities in addition to normal sensitivities assists to compare the effects that different parameters have on the parameter estimation process when these parameters are of different type, and possibly of very different magnitudes (Watermark Numerical Computing, 2010).

7.3.3 Calibration

Parameters which are relatively important in determining runoff in tropical regions and results of the SWAT manual sensitivity analysis were used for the calibration (Table 11). The range of parameter values were taken from the SWAT user's manual (Neitsch et al., 2002). First, the water balance and stream flow of the upper Blue Nile basin was calibrated for average annual conditions followed by manual daily stream flow calibration. SWAT parameters from the manual calibration were later used as initial values during automatic calibration using PEST. The first year (1961) is utilized as a 'warm-up' period to stabilize the simulation runs for SWAT.

7.3.4 Calibration criteria

Four efficiency criteria were used to evaluate the model predictions. These are sum of squared weighted residual (Watermark Numerical Computing, 2010), correlation coefficient (Watermark Numerical Computing, 2010) Nash-Sutcliffe efficiency (Nash and Sutcliffe, 1970) and relative volume error (Krause et al, 2005).

Table 14 Parameters and their range used during calibration of the SWAT model in the upper Blue Nile basin.

Symbol	Description	Unit		Values
GW DELAY	Groundwater delay time	days	0	500
GW _REVAP	Revap coefficient		0.02	0.2
SURLAG	Surface lag	days	1	24
GWQMN	Depth of water in shallow aquifer	mm	0	5000
ALPHA BF	Base flow recession constant	days	0	1
CN2	Initial SCS runoff curve number for moisture condition II		35	98
RCHRG DP	Deep aquifer percolation fraction	fraction	0	1.0
REVAPMN	Threshold depth of water in the shallow aquifer for revap	mm	0	500
SHALLST	Initial depth of water in the shallow aquifer	mm	0	1000
DEEPST	Initial depth of water in deep aquifer	mm	0	3000
REVAPMN	Threshold depth of water in the shallow aquifer for revap or percolation to the deep aquifer to occur	mm	0	500
GWHT	Initial ground water height	m	0	25
GW_SPYLD	Specific yield of the shallow aquifer	m^3/m^3	0	0.4
ESCO	Soil evaporation compensation factor.	-	0	1
EPCO	Plant uptake compensation factor	-	0	1

Sum of squared weighted residual

When used for parameter estimation, PEST aims to lower the objective function as far as it can be lowered and hence adjust model parameters until the fit between model outputs and field observations is optimized in the weighted least squares. The extent to which model outputs are in agreement with observation is apparent from the value of the objective function.

Correlation coefficient

Unlike the objective function, the correlation coefficient is independent from the number of observations involved in the parameter estimation process and from the absolute levels of

uncertainty associated with those observations (Watermark Numerical Computing, 2010). In addition, the use of the correlation coefficient allows tom compare directly the results of different parameter estimation exercises. A correlation coefficient of > 0.9 is usually expected for a fit (significance level of 0.05 is defined as narf!) between model outputs and observations (Watermark Numerical Computing, 2010).

The correlation coefficient R is calculated as

$$R = \frac{\sum(w_i c_i - m)(w_i c_{oi} - m_o)}{[\sum(w_i c_i - m)(w_i c_i - m)\sum(w_i c_{oi} - m_o)(w_i c_{oi} - m_o)]^{1/2}} \quad \text{(eq. 12)}$$

Where:-

- c_i is the i^{th} observation value,
- c_o i is the model-generated counterpart to the i^{th} observation value,
- m is the mean value of weighted observations,
- m_o is the mean of weighted model-generated counterparts to observations, and
- w_i is the weight associated with the i^{th} observation (or "rotated observation" if a covariance matrix is used to specify observation uncertainty instead of individual observation weights).

Nash–Sutcliffe coefficient

The Nash-Sutcliffe model efficiency coefficient is used to assess the predictive power of hydrological models (Nash and Sutcliffe, 1970). It ranges from -∞ to 1. An efficiency of 1 corresponds to a perfect match of modeled discharge to the observed data. An efficiency of 0 indicates the model predictions are as accurate as the mean of the observed data (Nash and Sutcliffe, 1970). Efficiency less than 0 occur when the observed mean is a better predictor than the model. The closer the model efficiency is to 1, the more accurate the model is.

$$NS = 1 - \frac{\sum_{t=1}^{T}(Q_0^t - Q_m^t)^2}{\sum_{t=1}^{T}(Q_0^t - \overline{Q_0})^2} \quad \text{(eq. 13)}$$

Where, NS is the Nash-Sutcliffe model efficiency coefficient

Q_0 is observed discharge

Q_m is modeled discharge

Q_0^t is observed discharge at time t

Relative volume error

Relative volume error (RV_E) is used for quantifying the volume errors. It can vary from ∞ and -∞. A model performs well when the RV_E approaches zero from both sides. A relative volume error between +5 or -5% indicates that a model performs well while relative volume errors between +10 and -10% indicate a model with reasonable performance (Krause et al, 2005).

$$RV_E = \left[\frac{\sum(Q_{sim}-Q_{obs})}{\sum Q_{obs}}\right] \times 100\% \quad \text{.....(eq. 14)}$$

7.3.5 Sensitivity test results

SWAT was sensitive to deep aquifer percolation fraction (), groundwater delay time (GW_DELAY), initial soil conservation service runoff curve number for moisture condition II (CN2), surface lag (SURLAG), base flow recession constant (ALPHA_BF), soil evaporation compensation factor (ESCO) and plant uptake compensation factor (EPCO) in decreasing order. The detail sensitivities are presented in Table 15. SWAT was found to be more sensitive to groundwater parameters such as recharge depletion fraction and ground water delay. Since the upper Blue Nile basin is mostly characterized by a wet season of four months followed by about six months of dry season, the contribution of groundwater to dry season river flow in the basin is significant. The results from the sensitivity study indicate that the sensitivity of the SWAT parameters varies during high flow and low flow conditions. SWAT was more sensitive to deep aquifer percolation fraction, revap coefficient, groundwater delay time and soil evaporation compensation factor under low stream flow and to initial soil conservation service runoff curve number for moisture condition II, deep aquifer percolation fraction and surface lag during high flows. Simulated water yield was sensitive to depletion fraction. A slight decrease in depletion fraction results in a large increase in the water yield of the basin. The water yield was also more sensitive to soil evaporation compensation factor and initial soil conservation service runoff curve number for moisture condition II as compared to other SWAT parameters.

The shape of the hydrograph under low flow conditions was sensitive to groundwater delay. When the groundwater delay is increased the width of low flow increases simultaneously. An increase in soil evaporation compensation factor generally increased the volume of low

flow during the calibration. Peak flow radically increases when depletion fraction is decreased and initial soil conservation service runoff curve number for moisture condition II is increased. Peak flow was found to be sensitive to surface lag during calibration as reported in other studies (Cibin et al., 2010), however an increase in surface lag resulted in an expected spikes during the calibration, as result it was kept at a minimum.

7.3.6 Calibration results

The calculated water yield of the upper Blue Nile upstream of El Diem gauge totals 287.0 mm based on observed data and a drainage area of 160,000 km^2.

Table 15 Sensitivity of SWAT parameters

PARAMETER		Sensitivity	Rank	Values
SHALLST	Initial depth of water in the shallow aquifer	0.22	9	0.39
DEEPST	Initial depth of water in deep aquifer	0.00	10	1000.00
GW_DELAY	Groundwater delay time	40.24	2	52.10
ALPHA_BF	Base flow recession constant	12.51	5	0.40
GWQMN	Depth of water in shallow aquifer	0.41	8	15.00
GW_REVAP	Revap coefficient	0.00	10	0.02
REVAPMN	Threshold depth of water in the shallow aquifer for revap	0.00	10	300.00
RCHRG_DP	Deep aquifer percolation fraction	76.84	1	0.66
GWHT	Initial ground water height	0.00	10	20.00
GW_SPYLD	Specific yield of the shallow aquifer	0.00	10	0.003
CN2	Initial SCS runoff curve number for moisture condition II	32.28	3	55.00
ESCO	Soil evaporation compensation factor	3.57	6	0.83
EPCO	Plant uptake compensation factor	3.45	7	0.91
SURLAG	Surface lag	13.43	4	1.00

The simulated water yield for the calibration period totals 299.8 mm. The largest contribution to the water yield was from the shallow ground water flow (213.1 mm). Lateral flow and surface runoff contributed 61.6 mm and 29.0 mm respectively.

The calibrated flows match observed flows well (Figure 24). The Relative Volume Error, Nash-Sutcliffe simulation efficiency and correlation coefficient values computed are2.57%, 0.82 and 0.90 for the calibration period, showing a reasonably good agreement between observed and simulated stream flows. The year showing the largest error is 1972, which is known for drought in Ethiopia (DPPC, 2000). In this year the magnitude of the simulated peaks is over estimated as compared to observed peak flow. Generally,the calibrated flow matched well the low flows as compared to peak flows. This is in contrast to other works which report difficulties in simulating low flow using SWAT (Van Liew and Garbrecht, 2003; Sudheer et al., 2007)

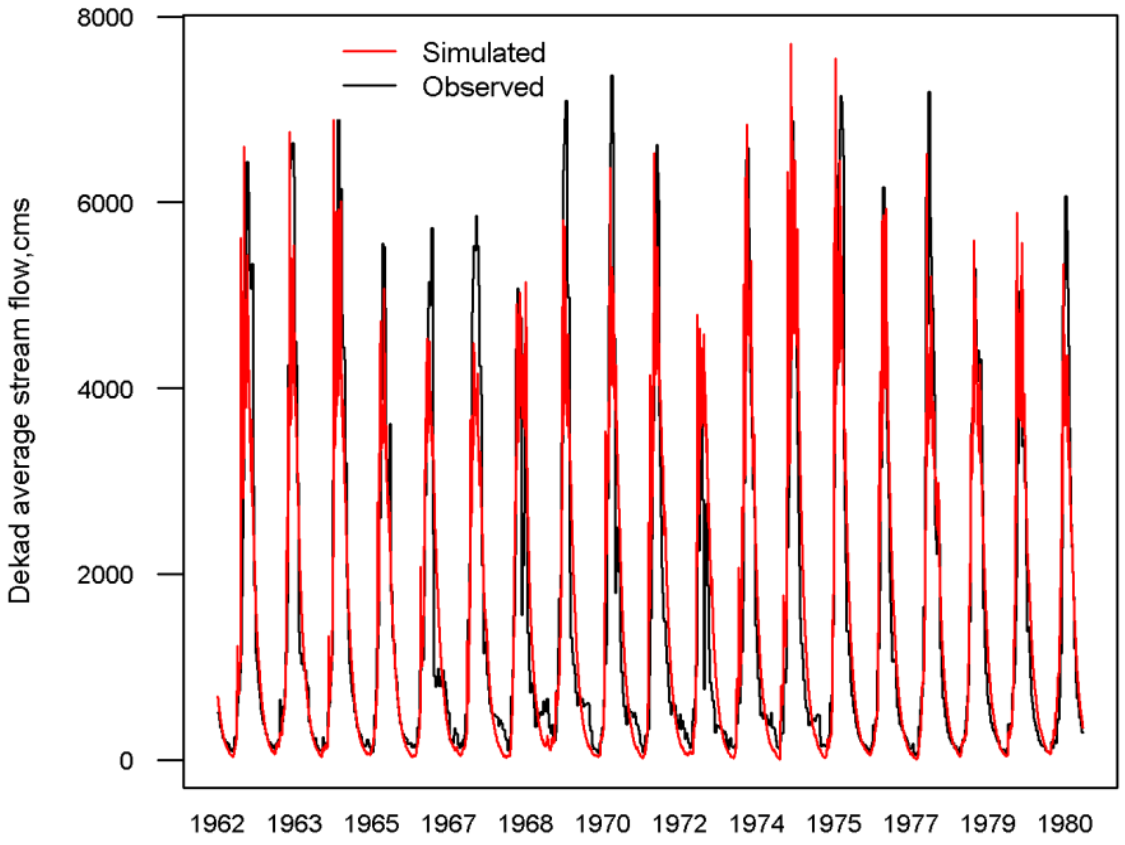

Fig. 24 Observed and simulated dekad mean discharge at El Diem in the calibration period.
(Data source: International Water Management Institute)

7.3.7 Model verification

Model verification is essential in order to examine the validity of a model over the intended domain and get feedback if refinement of the model is needed (Neitsch et al, 2002)Model verification was performed for the years 1981-1990. The calibrated SWAT model was used

to simulate the daily stream flows for validation and climate change scenarios. The simulation results were compared with the corresponding observed values at dekad time steps.

The simulation during validation matches well with the measured data in most of the cases (Figure 25. Generally, the model simulates well low flows as compared to peak flows. The year showing the largest error is 1990. Statistical evaluation reveales that the model is able to explain most of the variability in the measured stream flow with NS coefficient of 0.81, RVE of 11.5 and correlation coefficient of 0.9.

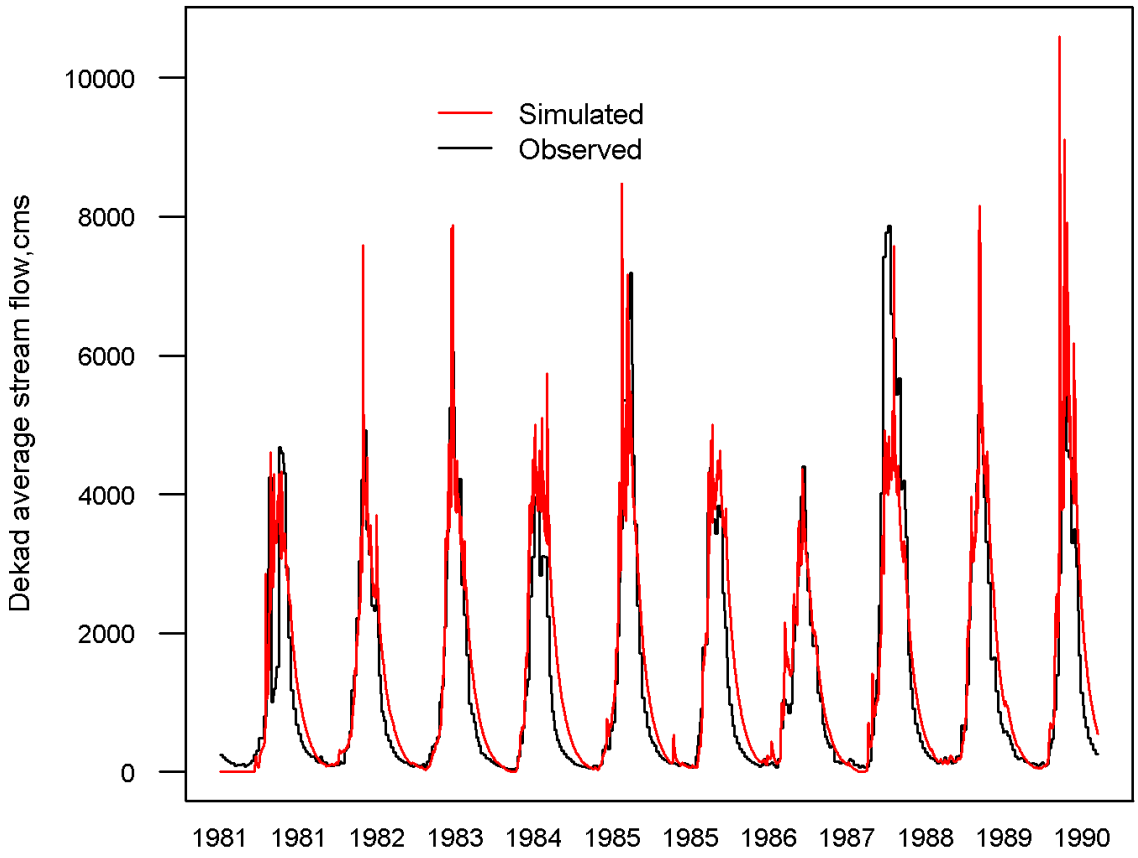

Fig. 25 Observed and simulated dekad average mean discharge at El Diem during the verification period.
(Data source: International Water Management Institute)

7.4 Model simulation corresponding to future climate and land use change

7.4.1 Climate change impacts

Two periods of thirty years were used to compare the hydrological impact of climate change on the water resources of the upper Blue Nile basin using the two regionally downscaled climate scenarios (REMO and CCLM) and a calibrated SWAT model. Periods compared are from 2041-2070 and 2071-2100.

The impact of climate change on the hydrology of upper Blue Nile based on ECHAM5 A1B simulation as downscaled by the two regional models shows mixed results. Downscaled climate scenarios based on REMO consistently resulted in an increase in mean annual runoff by the mid of the century and last quarter of the century (Table 16). However, the CCLM scenarios resulted in an increase from 2041- 2070 and a decrease in flow from 2071-2100. In both cases, it is predominantly during second period that greater changes in runoff occurred. Future projection of total water yield in the upper Blue Nile basin generally showed an increase, except the CCLM future projection during 2041-2070. Based on CCLM simulation the water yield at El Diem is expected to increase by 13% during 2041-2070 despite a decrease in basin average rainfall by 100mm and slight decrease (-5.6%) during 2071-2100 (Table 17).

Table 16 Changes of mean annual runoff under SRES A1B scenario using two downscaling techniques at El Diem in the upper Blue Nile basin

Downscaling technique	**Runoff (m^3 sec^{-1})**	
	2041-70	2071-2100
	PI/PD	PI/PD
CCLM	9.2	-10.0
REMO	102.8	141.4

PI=Percent of increase, PD=Percent of decrease

(Source: own analysis, Data source: Hattermann, 2011)

Table 17 Basin averaged climatic and hydrological variables for two periods 2041-2070 and 2071-2100

	Rainfall (mm)	Potential Evapotranspiration (mm)	Actual Evapotranspiration (mm)	Total water yield (mm)
Observed, 1961-1980	1391.3	1319.9	672.3	287.0
CCLM, 2041-2070	1290.5	1441.9	566.5	325.6
CCLM, 2071-2100	1146.9	1526.2	550.7	270.7
REMO, 2041-2070	1996.1	1377.0	665.5	619.6
REMO, 2071-2100	2096.5	1437.8	667.2	696.4

(Source: own analysis, Data source: Hattermann, 2011)

The REMO simulation agrees with CCLM indirection of change of water yield during 2041-2070 but the magnitude is much higher with REMO with an increase of 116%, which is a result of significant increase in rainfall in REMO rainfall projections. During 2071-2100 the water yield based on the REMO simulation was higher with 143%.

A close look into the mean simulated monthly flow (Figure 26) revels that during 2041-2070, CCLM based monthly simulated runoff results in a decrease by 13-51%, however REMO based simulated runoff shows consistent increase by 2-185% (data not shown). During 2071-2100, the CCLM based simulated monthly runoff shows consistent decrease by 5-51% from January to September, followed by an increase of 18-45% in the remaining months. In contrast, REMO based simulation shows consistent increase by 6-279% throughout the year. The wide range in the flow of REMO based runoff simulation can be associated with an increased rainfall in REMO rainfall projections.

In general, the REMO based runoff simulation shows larger increase in runoff as compared to the CCLM based runoff simulation. This result shows that even by employing climate change data (temperature and rainfall) from a single global climate model (ECHAM5), using one climate change scenario (A1B) and the same initial condition (ERA40) during downscaling, it is possible to get inconsistent results on the impact of climate change on the

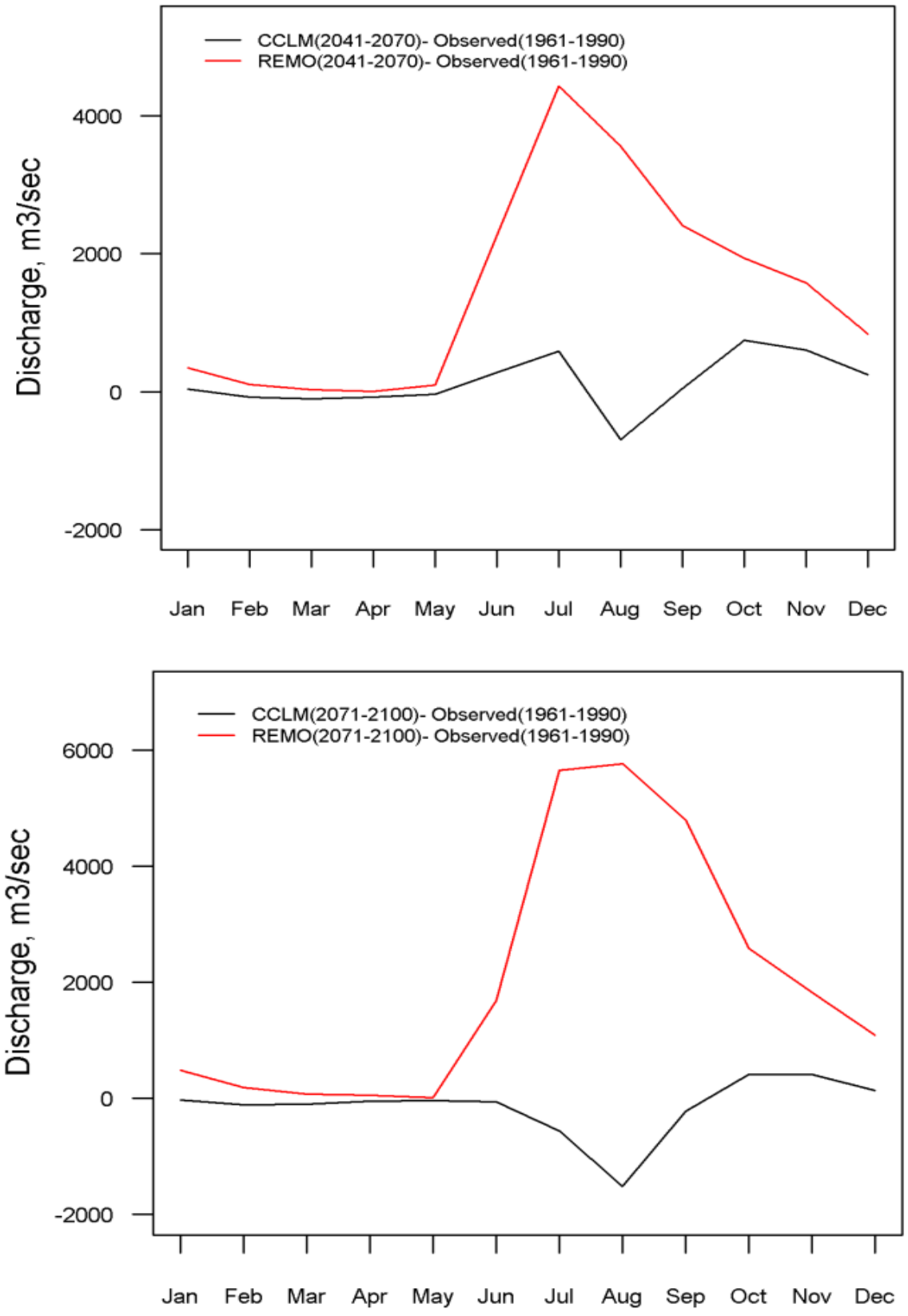

Fig. 26 Anomalies of mean monthly discharge a) for 2041- 2070 and b) for the 2071-2100
(Source: own analysis, Data source: Hattermann, 2011)

water resources. This is probability due to differences in the representation of the physical processes in the regional models employed for downscaling. This finding is not unique to this study, Karambiri et al. (2011) found out an increasing trend of the discharge of Nakambe River in Volta basin by up to 156% during the period of 2031-2040 for RACMO and 68% during 2011-2020 for REMO based on ECHAM5 A1B scenario data. Soliman et al., (2009) using ECHAM5 A1B scenario and downscaled by RegCM3 reports future increase in Blue Nile flow at El Diem by about 1.5% annually.

The reason for inconsistent impact of the regional models on the water resources of the upper Blue Nile basin can be due to limited skill of the regional models in simulating the upper Blue Nile rainfall. Although many regional models claim that they reproduce African climatological patterns, it should be recognized that there are limitation in simulating African monsoon system (Paeth et al., 2011),, the seasonal cycle of temperature and precipitation, inter-annual variability and the small rainfall over East Africa(Hulme et al., 2001).

7.4.2 Land use change impact

A summary of the annual water balance in the Blue Nile River basin for the baseline simulation and for the future use conditions is provided in Table 18. Results suggest that future land use/land cover change from expansion of agricultural land through foreign direct investment, an increase in water bodies through the constriction of dams and a minor increase in forest cover may have minimal effects on the annual water balance in the basin. Under the future scenario, water yield decreased slightly from 299.7 to 299.33 mm. Average annual runoff showed decrease by 1% and average annual ET decreased slightly. The slight decrease might be due to the large size and complex hydrology of the upper Blue Nile basin. Spatially disaggregated multi site runoff calibration approach at sub-basin level might show the hydrological impact more clearly.

Table 18 Land use impact on the drainage basin hydrology of the upper Blue Nile basin during 2015-2030 period

	Average annual basin values (mm)	
	Present land use	Future land use scenario
Surface runoff	30.03	29.72
Total aquifer recharge	624.87	624.48
Total water yield	299.70	299.33
Evapotraspiration	662.2	662.1
Potential ET	1326.4	1326.4

(Source: own analysis, Data source: WBISPP, 2004).

CHAPTER 8 CONCLUSIONS

Future climate projections downscaled by the regional models REMO and CCLM and land use change scenarios based on expected development trends are used to assess impacts on the hydrology of the upper Blue Nile River Basin. The major interest is to evaluate if the downscaled climate projections provide consistent hydrological impact on the upper Blue Nile basin. Calibrated SWAT model is applied to simulate future runoff under future climate and land use scenarios.

The impact of ECHAM5 A1B scenario as downscaled by the two regional climate models shows mixed results. Even if the two regional models predict an increase in runoff in most of the cases, the magnitude of change is wide and the projected impact results seems highly uncertain. The uncertainty observed in the impact analysis of mean discharge is mainly due to uncertainty in regional downscaling. The performance of the hydrological model for the historical period (1961-1990) is good.

The impact of future land use change based on an increase in agriculture, forest and water bodies does not show significant impact in the river discharge. A more detailed modeling and calibration at sub basin scale might be important to capture changes in land use. The finding of this study signifies the importance of capturing uncertainties in regional downscaling before pursing impact studies and the need for improving regional climate models in reproducing East Africa climatological patterns.

The limitations of this study are that it is based on a single GCM (ECHAM5) and the SRES A1B scenario, which represents a mid range climate change scenario, which assumes a balance between fossil intensive and non-fossil energy sources. A greater range of rainfall and temperature changes would be obtained by including other SRES scenarios.

Downscaling rainfall in the upper Blue Nile basin is not straight forward. The use of more than one testing climate stations to determine the location of downscaling domains is found to be essential. Due to significant variation in monthly correlation between predictors (atmospheric and ocean variables) and predictand (rainfall) within the annual cycle in

different domains, rainfall downscaling in upper Blue Nile basin should consider combining predictors from different domains rather than using a particular domain to obtain better statistical downscaling models.

The result of future climate change simulation using ECHAM5-A1B outputs as input to statistical downscaling models developed for the basin shows: i) a decrease in rainfall by 6-12% during the small rainy period and ii) mixed results for the main rainy season. Future research in downscaling rainfall in the upper Blue Nile should consider different IPCC emission scenarios and use of multiple GCMs. In addition the effect of domain size on model performance, uncertainties in the statistical downscaling and the data used should be evaluated.

REFERENCES

Arnold, J.G., Srinivasin, R, Muttiah, R.S Williams, J.R (1998) Large area hydrologic modeling and assessment:Part I. Model development. JAWRA 34(1):73-89.

Arsano Y., Tamrat I., (2005). Ethiopia and the Eastern Nile Basin. Aquat. Sci 67: 15-27.

Bewket, W. Sterk, G (2004) Dyanmics in land cover and its effect on stream flow in the Chemoga watershed, Blue Nile basin, Ethiopia. Hydrological Processes 19:445-458.

Beyene, T., Dennis, P.L kabat, P (2010) Hydrologic impacts of climate change on the Nile River Basin: implications of the 2007 IPCC scenarios. Climate Change 100 (3-4):769-815.

Cibin, R., Sudheer, K.P Chaubey, I (2010) Sensitivity and identifiability of stream flow generation parameters of the SWAT model. Hydrological Process DOI:10.1002/hyp.7568:.

Collins, W.J., Bellouin, N, Doutriaux-Boucher, Gedney, N, Hinton, T Jones, C.D (2008) Evaluation of the HadGEM2 model. :.

Conway, D. Hulme, M (1993) Recent fluctuations in precipitation and runoff over the Nile sub-basins and their impact on main Nile discharge. Climatic Change 25:127-151.

Conway, D. Hulme, M (1996) The impacts of climate variability and future climate change in the Nile basin on water resource in Egypt. Water resources development 12:277-296.

Conway, D. (2000) The Climate and Hydrology of the upper Blue Nile River. The Geographical Journal 166:49-62

Conway, G. (2009) The science of climate change in Africa: impacts and adaptation. :.

Davin, E.L., Stoeckli, R, Jaeger, E.B, Levis, S Seneviratne, S.I (2011) COSMO-CLM2: A new version of the COSMO-CLM model coupled to the Community Land Model. Climate Dynamics doi: 10.1007/s00382-011-1019-z:.

DPPC (Disaster Prevention and Preparedness Committee of Ethiopia) (2000). Country Report on the State of Drought Early Warning Systems in Ethiopia, Ethiopia, Addis Ababa

Doherty, J. (2004) PEST: Model-Independent Parameter Estimation User Manual. :.

Doty, B. Kinter , J.L (1992) The Grid Analysis and Display System (GrADS): A practical tool for earth science visualization. Eighth international conference on interactive information and processing systems :.

Downing, T., Ringius, L, Hulme, M Waughray, D (1997) Adapting to climate change in Africa. Mitigation and adaptation strategies for global change 2(1):19-44.

(EEPCo) Ethiopian Electric Power Corporation (2012). List of electric power stations. http://www.eepco.gov.et/projectcat.php?pcatid=2#. (Accessed February 2013).

ERG [Ethiopian Resource Group]. 2009. Diversity and security for the Ethiopian power system, A preliminary assessment of risks and opportunities for the power sector. Forum for Environoment and Heinrich Boll Foundation.52.

Fowler, H., Blenkinsop, S Tebaldi, C (2007) Linking climate change modeling to impact studies: recent advances in downscaling techniques for hydrological modeling. International Journal of climatology 27:1547-1578.

Grasselt, R., Schuettemeyer, D, Warrach-Sagi, K, Ament, F Simmer, C (2008) Validation of TERRA-ML with discharge measurements. Meteorology Z 17(6,SI):763-773.

Haileslassie, A., Hagos, F, Mapedza, E, Sadoff, C, Awulachew, S.B, Gebreselassie, S Peden, D (2008) Institutional settings and livelihood strategies in the Blue Nile Basin: Implications for upstream/downstream linkages. IWMI working paper 132:.

Hattermann, F.F. (2011) Re-Thinking Water Storage in Subsaharan Africa, report on generation of regional climate scenarios.

Hulme, M. (1994) Global climate change and the Nile basin. In: The Nile Sharing a Scarce Resource, Edition (P.P. Howell and J.A. Allan, ed), p 139-162.

Hulme, M., Doherty, R, Ngara, T, New, M Lister, D (2001) African climate change:1990-2100 . Climate Research 17:145-168.

Hurni, H., Tato, K Zeleke, G (2005) The implications of changes in population, land use, and land management for surface runoff in the Upper Nile Basin areas of Ethiopia . Mountain research and development :147-154.

IFRCRCS (International Federation of Red Cross and Red Crescent Societies). (2006), Ethiopia: Floods

IPCC (2007) IPCC fourth assessment report. :104.

IPCC-TGICA (2007) General Guidelines on the Use of Scenario Data for Climate Impact and Adaptation Assessment. Version 2:66.

Jacob, D. (2001) A note to the simulation of the annual and inter-annual variability of the water budget over the Baltic Sea drainage basin. Meteorology and Atmospheric Physics 77(1-4):61-73.

[Jarvis 2008] Hole-filled 90m SRTM for the globe . http://srtm.csi.cgiar.org.

[John 2010] The R project for statistical computing. http://www.r-project.org/.

[KNMI2010] Climate explorer. http://climexp.knmi.nl/.

Kalnay (1996) The NCEP/NCAR 40 year reanalysis project. American Meteorological Society 77:437-470.

Karambiri, H., Garcia Galliano, S.G, Yacouba, H, Ibrahim, B, Barbier, B Polcher, J (2011) Assessing the impact of climate variability and climate change on runoff in West Africa: the case of Senegal and Nakambe River basins. Atmospheric science letters 12(1):109-115.

Krause, P., Boyle, D. P., Base, F. (2005). Comparison of different efficiency criteria for hydrological model assessment. Advances in Geosciences 5:89-97.

MWR (Ministry of Water Resources) (1998a) Abbay river basin integrated development master plan project. III water resources:142.

MWR (Ministry of Water Resources) (1998b) Abbay River basin integrated development master plan project. XII environoment:140.

MWR (Ministry of Water Resources) (1998c) Abbay River basin integrated development master plan project, land cover/land use. X land resources development:83.

MWR (Minstry of Water Resources) (1998d) Abbay River basin integrated development master plan project. VIII Reconnaissance soil survey:206.

MWR (Ministry of water Resources of Ethiopia) (1999) Abbay river basin integrated development master plan project: Semi-detail soils survey, Phase 2. 8

Majewski, D. (1991) The Europa model of the Deutscher Wetterdienst. ECMWF Seminar on numerical methods in atmospheric models 2:147-191.

Michelangeli, P.A., Vrac, M Loukos, H (2009) Probabilistic downscaling approaches: Application to wind cumulative distribution functions. Gophysical Research Letters 36:L11708.

Mitchell, T.D. Jones, P.D (2005) An improved method of constructing a database of monthly climate observations and associated high resolution grids. International Journal of Climatology 25:693-712.

NBI (Nile Basin Initiative) (2010) Effect of land use/land cover management on koga reservoir sedimentation. Nile basin capacity building network :41.

Nash, J.E. Sutcliffe, J.V (1970) River flow forecasting through conceptual models part I- A discussion of principles. Journal of Hydrology 10 (3):.

Neitsch, S.L., Arnold, J.G, Kiniry, J.R Williams, J.R (2011) Soil and water assessment tool: Theoretical Documentation, Version 2009. :.

Neitsch, S.L., Arnold, J.G, Kiniry, J.R, Srinivasan, R Williams, J.R (2002) Soil and water assessment tool user's manual. Soil and water research laboratory, Agricultural Research Service Version 2000:472.

Neitsch, S.L., Arnold, J.G, Kiniry, J.R, Srinivasan, R Williams, J.R (2010) Soil and water assessment tool input/output file documentation. Texas Water resources Institute Version 2009:620.

Nicks, A.D. (1974) Stochastic generation of the occurrence, pattern and location of maximum amount of daily rainfall. Proc. Symp. Statistical Hydrology :.

Paeth, H., Hall, N.M.J, Gaertner, M.A Alonso, M.D (2011) Progress in regional downscaling of West African precipitation. Atmospheric science letters 12(1):75-82.

Paeth, H., Born, K., Podzun, R., Jacob, D. (2005). Regional dynamical downscaling over West Africa: model evaluation and comparison of wet and dry years. Meteorologishe Zeitschrift, 14: 349-367.

Rasmus, E. (2010) Climate analysis and empirical-statistical downscaling (ESD) package for monthly and daily data. :.

Rockel, B., Will, A Hense, A (2008) The regional climate model COSMO CCLM editorial. Meteorol Zt 12(4):347-348.

Roeckner, E., Arpe, K, Bengtsson, L, Christoph, M, Claussen, M, Dumenil, L, Esch, M, Giorgetta, M, Schlese, U Schulzweida, U (1996) The atmospheric general circulation model ECHAM-4: Model description and simulation of the present day climate. Report No. 218:.

Roeckner, E., Brokopf, M.E, Giorgetta, M, Hagmann, S Kornblueh, L (2006) Sensitivity of simulated climatee to horizontal and vertical resolution in ECHAM5 atmosphere model. American meteorological Society :3771-3791.

Segele, Z.T., Lamb, P.J Leslie, L.M (2009) Large-scale atmospheric circulation and global sea surface temperature associations with Horn of Africa June–September rainfall. International Journal of Climatology 29:1075-1100.

Seleshi, Y. Demaree, G.R (2004) Rainfall variability in the Ethiopian and Eritrean highlands and its links with the Southern Oscillation Index. Journal of Biogeography 22:.

Single, J. (2009) Aggreko commissions 30MW power rental project in Ethiopia. http://africa.aggreko.com/news-events/press-releases/30-mw-power-to-ethiopia/ (Accessed February 2013)

Smedema, L.K. Rycroft, D.W (1983) Land drainage planning and design of agricutlural drainage systems. Cornell University press:.

Soil Conservation Service (1972) Hydrology. in National Engineering Handbook, Edition (ed.), pp . SCS.

Soliman, E.S., Sayed, M, Nour, E Samy, G (2009) Integration of NFS with regional climate model to simulate the Nile basin hydro-climatology. Nile Basin Water Engineering Scientific Magazine 1:75–85.

Sudheer, K.P., Chaubey, I, Garg, V Migliaccio, K.W (2007) Impact of time scale of the calibration objective function on the performance of watershed models. Hydrological processes 21(25):3409-3419.

Taye, M.T., Ntegeka, V, Ogiramoi, N.P Willems, P (2010) Assessment of climate change impact on hydrological extremes in two source regions of the Nile River Basin. Hydrology and Earth System Sciences 7:5441-5465.

[University_of_Oxford2009] Country-level climate data summaries. http://country-profiles.geog.ox.ac.uk/.

Schulzweida,U. Kornblueh, L.Quest, R. (2009) Climate Data Operators. MPI for Meteorology and Brockmann Consult :.

Van Liew, M.W. Garbrecht, J.D (2003) Simulation of the impacts of flood retarding structures on streamflow for a watershed in southwestern Oklahoma. Journal of soil and water conservation society 58(6):340-348.

WBISPP Woody Biomass Inventory and Strategic Planning Project in Ethiopia (2004) Land use and land cover database. :.

WWDSE (2011) Finchaa sugar factory expansion project: Sailent features. Water Works Design and supervision enterprise :2.

[Watermark_numerical_computing2010] Pest model independent parameter estimation. 2010.

Wegner (2007) IPCC DDC AR4 ECHAM5/MPI-OM SRESA1B run2: CERA-DB "EH5_MPI_OM_SRESA1B_2". :.

Wilby, R.L., Charles, S.P, Zorita, E, Timbal, B, Whetton, P Mearns, L.O (2004) Guidelines for use of climate scenarios developed from statistical downscaling methods. . :27.

Williams, J.R. (1995) Chapter 25: The EPIC model. In: Computer models of watershed hydrology., Edition (V.P. Singh, ed), p 909-1000.

Winchell, M. ,Srinivasan, R., Di Luzio, M., Arnold, J. (2007). ArcSWAT interface for SWAT 2005 user's guide. USDA agricultural research service. Texas. 436

Wing, H., Cheung, G, Gabriel, B.S Singh, a (2008) Trends and spatial distribution of annual and seasonal rainfall in Ethiopia. International journal of climatology 28(13):1723-1734.

Wood, A.W., Leung, L.R, Sridhar, V Lettenmaier, D.P (2004) Hydrologic implication of dynamical and statistical approaches to downscaling climate model outputs. Climate Change 62:189-216.

World Resources Institute (2000) World Resources 2000-2001, People and Ecosystems: The faying web of life. :.

APPENDIX 1

The following R program functions were prepared for the preparation of the SWAT weather generator climate input data for the hydrological modeling. The weather generator generates climate input for SWAT or filling missing values of station records.

1. Dew point temperature

```
tmx <- read.table("stationtmx",sep="",header=T)
tmi <- read.table("stationmin",sep="",header=T)
rh <- read.table("stationrh",sep="",header=T)
dew <- function(tmx,tmi,rh){
eomax <<- 0.6108 * exp((17.27 * tmx)/(tmx+237.3))
eomin <<- 0.6108 * exp((17.27 * tmi)/(tmi+237.3))
es <<- (eomax + eomin)/2
ea <<- es * (rh/100)
tdew <<- 237/17.27 * log(ea/0.6108)/ (1-0.057904* log(ea/0.6108))}
dew(tmx,tmi,rh)
tdew
write.table(tdew,file="stationdew",sep="",col.names="tdew_ave",row.names=F,quote=F)
```

2. Average wind speed

```
files <- list.files(pattern="^station")
for( i in files){
station.every <- read.table(i,sep="",header=F)
month <- station.every[,2]
wind <- station.every[,4]
wndav <- tapply(wind,month,mean,na.rm=T)
wndav <- round(wndav,digits=2)
write.table(wndav,paste(i,"wnd",sep=""), sep="\t",row.names=T,col.names=F,quote=F)}
```

3. Probability of a wet day following a dry day

```
station.data <- read.table("stationx",sep="",header=F);
months <- station.data[,2];
raindata <- station.data[,4];
ea <- split(raindata,months);
ajan <- ea[1]; ajan <- data.frame(ajan);
afeb <- ea[2]; afeb <- data.frame(afeb);
amar <- ea[3]; amar <- data.frame(amar);
aapr <- ea[4]; aapr <- data.frame(aapr);
amay <- ea[5]; amay <- data.frame(amay);
ajun <- ea[6]; ajun <- data.frame(ajun);
ajul <- ea[7]; ajul <- data.frame(ajul);
aaug <- ea[8]; aaug <- data.frame(aaug);
asep <- ea[9]; asep <- data.frame(asep);
aoct <- ea[10]; aoct <- data.frame(aoct);
anov <- ea[11]; anov <- data.frame(anov);
adec <- ea[12]; adec <- data.frame(adec);
rm(ea,a,months,raindata);
all <- list(ls())
alla <- all[[1]]
for (i in alla){
xb <- get(i)
xa <- unlist(xb);
xa <- as.numeric(xa);
x <- replace(xa,xa > 0,1);
x[is.na(x)] <- -99
for(j in 1:length(x)-1){
y <<- 0
y <<- diff(x)
wetfdry <<-length(y[y==1])
dry <<- length(x[x==0])
```

```
PRW <<- wetfdry/dry
PRW <<- round(PRW,digits=3)}
cat(paste(i,PRW))}
```

4. Probability of a wet day following a wet day in a month

```
station.data <- read.table("station01",sep="",header=F);
months <- station.data[,2];
raindata <- station.data[,4];
ea <- split(raindata,months);  # ea is rain data splited by month
ajan <- ea[1]; ajan <- data.frame(ajan);
afeb <- ea[2]; afeb <- data.frame(afeb);
amar <- ea[3]; amar <- data.frame(amar);
aapr <- ea[4]; aapr <- data.frame(aapr);
amay <- ea[5]; amay <- data.frame(amay);
ajun <- ea[6]; ajun <- data.frame(ajun);
ajul <- ea[7]; ajul <- data.frame(ajul);
aaug <- ea[8]; aaug <- data.frame(aaug);
asep <- ea[9]; asep <- data.frame(asep);
aoct <- ea[10]; aoct <- data.frame(aoct);
anov <- ea[11]; anov <- data.frame(anov);
adec <- ea[12]; adec <- data.frame(adec);
rm(ea,a,months,raindata);
all <- list(ls())
alla <- all[[1]]
for (i in alla){
xb <- get(i)
xa <- unlist(xb); xa <- as.numeric(xa);
x <- replace(xa,xa > 0,1);
x[is.na(x)] <- -99
for(j in 1:length(x)-1){
y <<- 0
```

```
y <- filter(x,rep(1/1,2),side=2)
ys <<- na.omit(y)
wetfdry <<-length(ys[ys==2])
wet <<- length(x[x==1])
PRW <<- wetfdry/wet
PRW <<- round(PRW,digits=3)}
cat(paste(i,PRW))}
```

APPENDIX 2

The following R programming language codes were use for bias correcting the REMO regional model outputs which latter used for the impact studies. The procedure is using the CDF-transform method (Michelangeli et al., 2009). To verify the result of the bias correction the Kolmogorovsmirnov test was used.

```
setwd("c:/futureswat/obsbias/rain")
library(foreign)
library(CDFt)   # the CDFT library for the bias correction

obs <- read.dbf("DEBMAR.dbf")    # Station observed data
obs[obs == -99] <- NA
ObsRp <- obs[as.Date(obs[,1]) <= "1980-12-31",]
ObsRp <- ObsRp[,2]
ObsRp <- as.numeric(ObsRp)

sim <- read.delim("GP_076_044.kli",header=TRUE, sep="")    # Raw REMO output data
Sim <- sim[,c(3,7)]
Sim[Sim== -999] <- NA
DataGp <-  Sim[Sim[,1] < 1981,]
DataGp <- DataGp[,2]
DataGp <- as.numeric(DataGp)

DataGf <- Sim[Sim[,1] > 1980,]
DataGf <- DataGf[,2]
DataGf <- as.numeric(DataGf)
DataGf.1 <- na.omit(DataGf)

VerRp <- obs[which(as.Date(obs[,1]) >= "1981-01-01"),]   #for verification

obsdata <- cbind(ObsRp,DataGp)
```

```
obsdata.1 <- na.omit(obsdata)
ObsRp.1 <- obsdata.1[,1]
DataGp.1 <- obsdata.1[,2]
ct <- CDFt(ObsRp.1,DataGp.1,DataGf.1,dev=2)
x <- ct$x
FGp <- ct$FGp
FGf <- ct$FGf
FRp <- ct$FRp
FRf <- ct$FRf
ds <- ct$DS
par(mfrow=c(1,2))
plot(x, FGp,type="l",lty=2,ylim=c(0,1),xlab="x",ylab="CDF(x)")    # for plotting the output
lines(x,FGf,type="l",lty=2,col=2)
lines(x,FRp,type="l")
lines(x,FRf,type="l",col=2)
plot(DataGf.1,ds,xlab="Large-scale data", ylab="Downscaled data")

all <- cbind(DataGf.1,ds)
t <- seq(as.Date("1981-01-01"),as.Date("1990-12-31"),by="days")
ds.v <- ds[1:3652]
ver <- cbind(VerRp,ds.v)
matplot(ver,type="l",col=c(1,2))
ds.v1 <- ds.v
ds.v1[ds.v1 < 0.99] <- 0
Gf.v <- DataGf[1:3652]
ver.1 <- cbind(VerRp,ds.v1,Gf.v)
matplot(ver.1,type="l", col=c(1,2,3))
KolmogorovSmirnov(VerRp[,2],ds.v1)  # Statistical test to verify the result
KolmogorovSmirnov(VerRp[,2],Gf.v)
vernames <- ver.1[,-1]
legend(2,60,names(vernames),col=c(1,2,3),lty=1)
```

APPENDIX 3

Bias correction result of REMO out. The figure below shows aggregated monthly REMO rainfall and observed rainfall at Debre Markos for three years (1961, 1962, 1963)

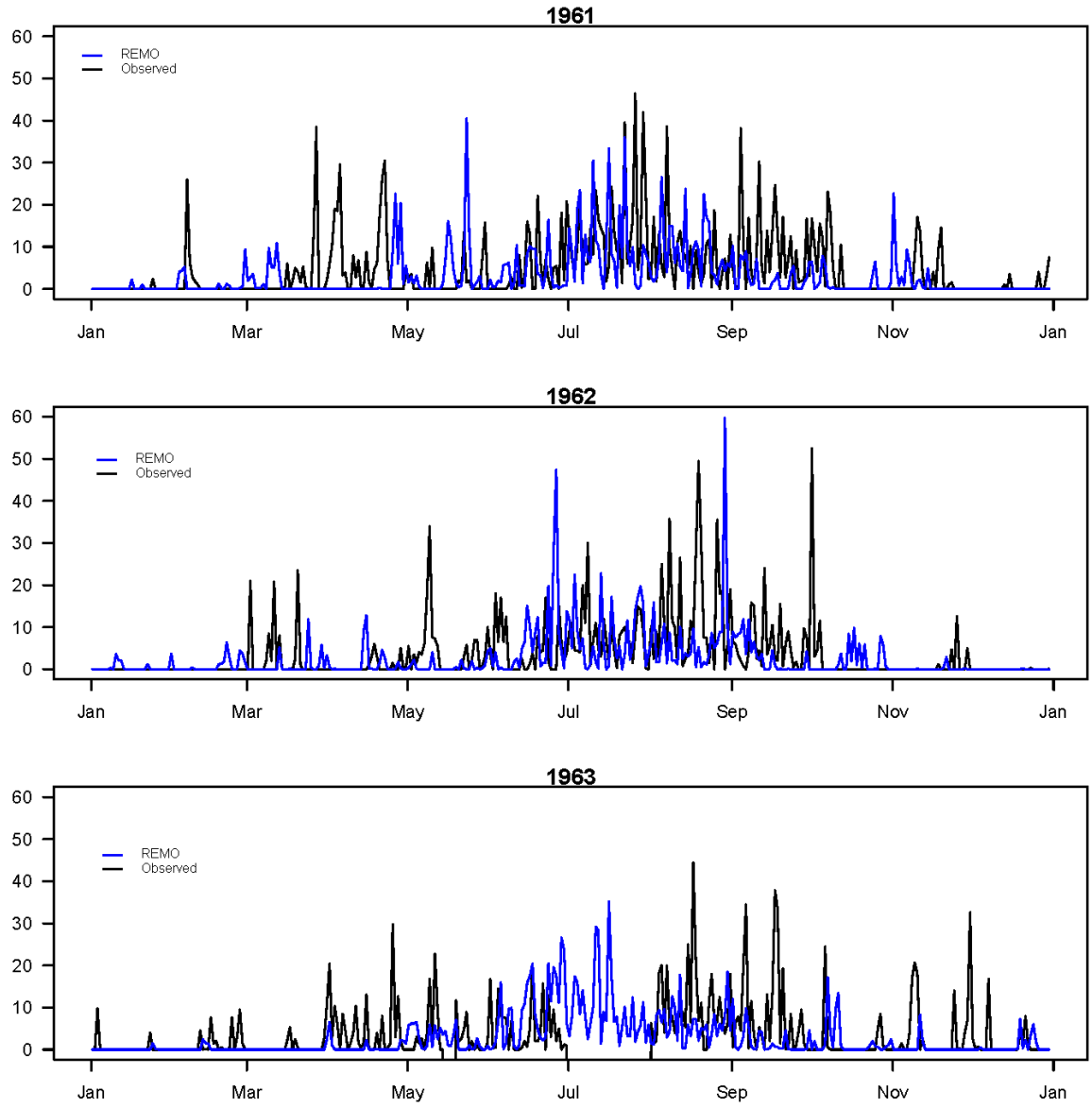

ERKLÄRUNG

Hiermit erkläre ich, dass ich die Dissertation 'Potential Impact of Climate and Land Use Change on the Water Resources of Upper Blue Nile Basin' selbständig angefertigt und keine anderen als die von mir angegebenen Quellen und Hilfsmittel verwendet habe.

Ich erkläre weiterhin, dass die Dissertation bisher nicht in dieser oder anderer Form in einem anderen Prüfungsverfahren vorgelegen hat.

Berlin, 24 April 2012. _____

(Michael Menker Girma)